Fluorescent Detection of Chromatin using Functionalized Magnetic Beads on a Digital Microfluidic Device

by

Yaas Bigdeli

Department of Electrical and Computer Engineering
Duke University

Date: _____

Approved:

_____
Richard B. Fair, Supervisor

_____
Nan M. Jokerst

_____
Adrienne Stiff-Roberts

_____
Aaron D. Franklin

_____
Tuan Vo-Dinh

Dissertation submitted in partial fulfillment of
the requirements for the degree of Doctor
of Philosophy in the Department of
Electrical and Computer Engineering in the Graduate School
of Duke University

2022

ABSTRACT

Fluorescent Detection of Chromatin using Functionalized Magnetic Beads
on a Digital Microfluidic Device
by

Yaas Bigdeli

Department of Electrical and Computer Engineering
Duke University

Date: _____
Approved:

_____
Richard B. Fair, Supervisor

_____
Nan M. Jokerst

_____
Adrienne Stiff-Roberts

_____
Aaron D. Franklin

_____
Tuan Vo-Dinh

An abstract of a dissertation submitted in partial
fulfillment of the requirements for the degree
of Doctor of Philosophy in the Department of
Electrical and Computer Engineering in the Graduate School of
Duke University

2022

Abstract

Epigenetics is the study of inheritable mechanisms and factors that regulate gene expression. Although the underlying genetic sequence is the same in every cell, it is the epigenome that controls the expression of these genes and accounts for differences in phenotype. Epigenetic controls have clinical ramifications from cancer to autoimmune disorders to psychiatric pathologies. The main tool to study epigenetics is chromatin immunoprecipitation (ChIP), which probes the relationship between the underlying DNA and its structural histone proteins. Standard benchtop ChIP has five major drawbacks: (1) it requires a large input volume of cells, (2) it is very time consuming, work intensive, and low throughput, (3) it suffers from poor chromatin yield and sensitivity, (4) ChIP antibodies can be non-specific, vary by batch, and have low sensitivity, (5) and ChIP performs bulk tissue analysis which loses the granularity necessary to detect cell-to-cell variations.

Digital microfluidic biochips (DMFBs) have proven successful at utilizing small volumes of reagents and samples to perform high throughput analyses using a variety of assaying techniques, making them an ideal platform for ChIP adaptation. Droplet manipulation using electrowetting-on-dielectric, in conjunction with magnetic bead control using magnetic field gradients generated by a current running through a wire on the device, provide all the necessary functionality to successfully run ChIP more efficiently on a DMFB.

Translation of the benchtop ChIP protocol onto a DMFB addresses the issues facing epigenetic study workflow. The smaller volumes reduce reaction time, decrease reagent and sample use, and increase sensitivity and granularity towards single-cell resolution. Automation makes ChIP less labor consuming. DMFB platforms can be expanded for parallel operation and

multiplexing thus increasing throughput. Finally, streamlining all the steps of ChIP onto one device greatly reduces sample loss, thereby expanding the type of studies possible.

Herein, specifically modified nucleosomes and human chromatin were detected in a new semi-quantitative fluorescent immunoassay on a DMFB. Furthermore, chromatin was immunoprecipitated using a new targeted biotinylated technique. Successful chromatin capture and detection is a powerful tool for ChIP protocol development. This approach provides a rapid method to screen for antibody specificity and sensitivity as well as a confirmatory check point in the overall ChIP protocol to ensure that the target analyte has been isolated prior to any downstream analyses. Finally, a new modified 'pull-through' DMFB design was introduced to enhance the capture and detection of analyte-bound magnetic beads.

The contributions from the studies described in this dissertation have provided the first steps towards ChIP implementation on a DMFB:

1) Developed new fluorescent confirmatory chromatin and nucleosome immunoprecipitation assays.

2) Demonstrated that the immunoprecipitation assays were detectible on-chip without any complex downstream analyses nor specialized fluoroscopy instrumentation.

3) Demonstrated that the immunoprecipitation assays performed at higher sensitivity than traditional benchtop ChIP.

4) Developed a single-channel pixel intensity measurement system for semi-quantitative analysis of chromatin and post-translationally modified nucleosomes directly on-chip.

5) Designed a new DMFB for improved capture of magnetic beads with twice the measured signal intensity using a new pull-through droplet scan method with on-chip embedded magnetic controls.

Dedication

In loving memory of my grandfather.

Contents

List of Tables

List of Figures

Acknowledgements

First, I would like to thank my advisor Professor Richard Fair for his unfailing kindness and patience. From listening intently when I dashed excitedly into his office to share a new result to keeping in touch almost every week of the past five years, he has been a source of constant support and guidance for which I am beyond grateful.

Thank you to Professor Nan Jokerst, Professor Adrienne Stiff-Roberts, Professor Franklin, and Professor Vo-Dinh for agreeing to be on my committee and whose guidance from the qualifying exam through the preliminary exam is reflected in this dissertation.

Thank you to Kirk Bryson, Jay Dalton, Talmage Tyler, and Dr. Walters at the Shared Material Instrumentation Facility at Duke. Without their training, instruction, and help this project would not be possible.

Thank you to my lab mates Shruti Preetam and Shu Huang for all the time spent training me and for answering my endless questions. You made transitioning into this program much easier. Shruti, each of our conversations was a source of comfort and camaraderie that helped me keep going.

Thank you to Dr. Kristen C. Scott, Dr. Tun-Che Liang, Dr. Zhanwei Zhong, Dr. Bridget Crawford, Dr. Callie Woods, Sehwa Oh, and Alberto Ruiz La Riva for their expertise.

Thank you to Callie and Kavita for reading every document and listening to every presentation. If it weren't for our conversation one afternoon around Callie's dining room table, I would not have had the confidence to pursue a Ph.D.

A special thank you to my teachers at Moravian Academy. Thank you to Mrs. Overdorf, Mrs. McCambridge, Mr. Strohl, Mrs. Vorhees, Mr. Ballard, Dr. Dee, and Mr. Bross for laying the math and science foundations that have gotten me through my entire academic career. Thank you

to Mrs. Beck-Briggs for teaching me to explore and to develop new ideas, and for helping me find a voice with which to express them.

Thank you to the friends I've made from Pennsylvania to New York to North Carolina. Your friendship, visits, phone calls, and Zooms, have made graduate school less lonely.

Thank you to my grandmother, uncles, aunts, and cousins for their unending love and support from across the globe.

Maman and Baba you have encouraged me every step of the way and given me the push I needed whenever my feet have wandered of course or faltered. You are with me everywhere I go.

Lastly, thank you to my late-night work companion, Albaloo.

1. Introduction

1.1 Understanding Epigenetics

Human cells all share the same genotype, or DNA sequence. However, the differences in phenotype, or cell type and function, manifest from the expression or suppression of particular genes [1]. Epigenetics is the study of the mechanisms and environmental factors that control gene expression in both healthy and diseased states without altering the underlying nucleotide sequence. Epigenetic studies contribute to our understanding of biological systems from the molecular level to the tissue level, within an organism, across a population, and over generations [2]–[4]. Epigenetic behavior is inheritable but also highly variable. Therefore, there can be clinically significant variations within a single sample of cells even though epigenetic controls and structures are passed to daughter cells during mitosis and generationally from parent to offspring [5]. However, since external environmental factors can alter an individual's epigenome within a single lifetime, it is important to probe the epigenome at great granularity. This has ramifications when searching for cell-to-cell variability in cancer analysis, but also when looking at the broader effects of the vast medications, products, and therapies currently available [1], [5]–[8].

Fundamentally, the study of epigenetics is linked with DNA structure, how it is packaged, stored, and utilized in the cell nucleus. DNA is a very specific sequence of deoxyribonucleic acids, or nucleotide bases, held together in a strand by a phosphodiester bond. Two such strands match up to form base pairs in the commonly depicted double helix structure. Every 147 base pairs, the helix wraps around a nucleosome, an octameric structure consisting of four pairs of protein monomers, namely the histones H2A, H2B, H3, and H4. The nucleosomes form 'beads on a string', as shown in Figure 1, and are the building blocks of chromatin, which can be further folded to form chromosomes [1], [9].

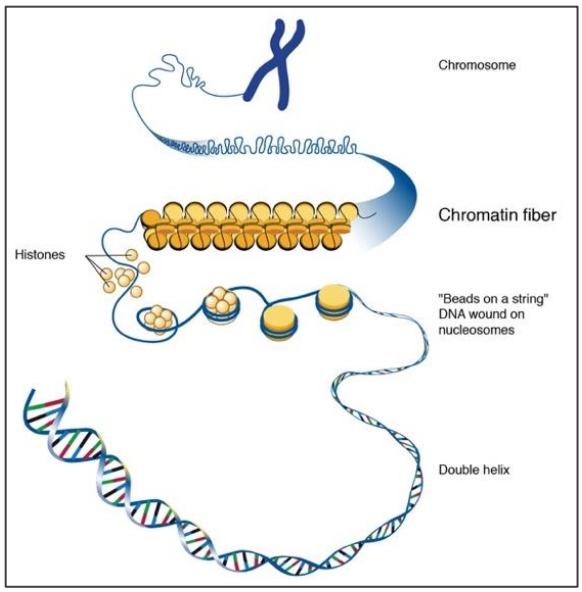

Figure 1: DNA structural hierarchy [9].

Nucleosomes are held together by hydrogen bonds and salt bridges that can be modified to either more tightly or loosely bind the chromatin. This can open a particular region of underlying DNA for transcription or replication. Epigenetic control happens mainly at this level of DNA organization. The arrows in Figure 2 indicate the areas of interest when studying epigenetic features such as DNA methylation, histone modification, chromatin accessibility, nucleosome occupancy, and the three-dimensional chromosomal conformation [10], [11].

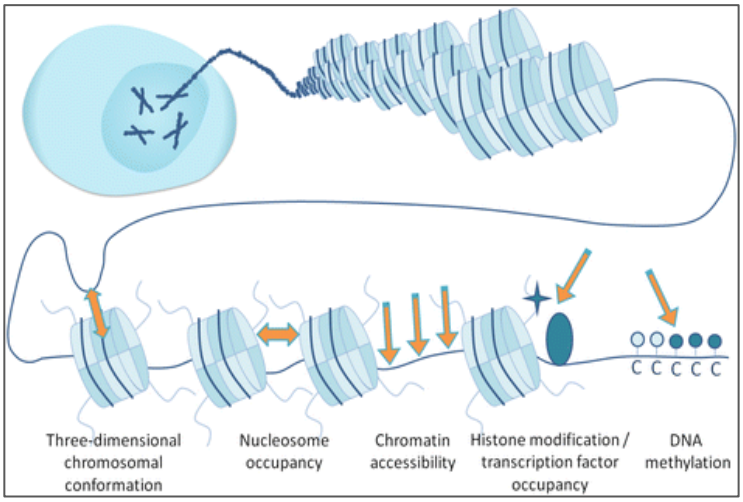

Figure 2: Location of epigenetic controls [10].

There are four main epigenetic control mechanisms: cytosine methylation [12]–[14], post translational modification of histones [4], [15]–[17], non-coding RNA, and finally, further packaging of chromatin into higher-level structures. Cytosine methylation, usually done to suppress gene expression, occurs at the DNA level by adding a methyl group onto cytosine, one of the base pair nucleotides [1]. Posttranslational modifications (PTMs), as shown in Figure 3, involve the addition of methyl, acetyl, phosphoryl, or ubiquitin groups to one or several of the amino acids that comprise histone proteins to alter the tightness of chromatin packing [15], [18][19][20]. Non-coding RNA works to regulate both cytosine methylation and post translational modification. Finally, the chromatin can be bundled into chromosomes with the addition of other structural proteins [1]. The focus of this thesis will be the detection of whole chromatin and specific PTMs of histones of isolated nucleosomes.

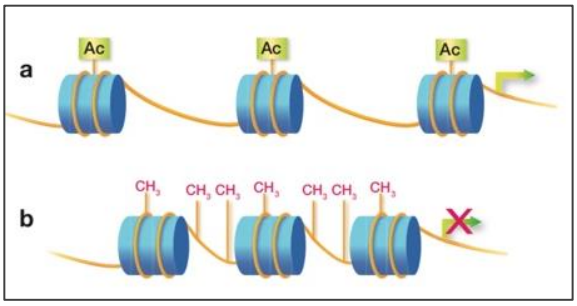

Figure 3: Posttranslational modification examples. The yellow lines represent DNA wrapped around the blue nucleosomes. A) The acetyl groups (Ac) cause the chromatin to be more loosely packed and more translationally available. B) DNA methylation results in more condensed chromatin and silences the gene [1].

Each of the above mechanisms control whether specific parts of the DNA are accessible for transcription and translation into RNA and proteins, respectively. Thus, chromatin can exist in three 'transcriptional states': (1) euchromatin, which is more open and ready for translation, (2) constitutive heterochromatin, which is generally closed off, and (3) facultative heterochromatin,

which is repressed but can be activated [1], [21], [22]. The downstream macromolecules, RNAs and proteins, determine cellular behavior, regulate enzymatic processes, and contribute to the functionality (or dysfunctionality) of cells, tissues, organs and organisms [1], [12].

One specific motivation to study PTMs of histones is for the role that they play in cancer biology. Enzymes that alter histones can do so either locally or globally and have historical patterns of modification that can consist of either a single location or large regions. For example, heterochromatin, which is largely inactive, has a low degree of acetylation and is associated with high representation of histone H3K9me2/3 (the H3 protein is di-or-trimethylated on the ninth lysine). Conversely, euchromatin is a more active region of the genome and has higher amounts of acetylation and can be identified with high amounts of histone H3K4me2 (the H3 protein is dimethylated on the fourth lysine) [23]. Alterations of promoter-specific epigenetic patterns can result in the incorrect repression or activation of genes that can lead to cellular aberrations, carcinogenesis, or to the progression of cancer.

Understanding PTMs of histones not only reveals how some cancers develop but can also help predict cancer prognosis. One method is to measure the enzymes that catalyze PTMs, but it is also possible to use dyes and histological staining to look at the amount of the modifications within the nuclei of the cells in a tissue sample [24]. More recently, the focus has shifted towards the study of circulating nucleosomes within the bloodstream. As some cancers progress and cause cells to die and rupture, nucleosomes are released into the bloodstream. By studying the prevalence of certain histones within a patient's plasma, the hope is to detect cancers at an earlier stage and without expensive or invasive diagnostic testing (e.g., colonoscopy) [25]. Volition's Nu.Q® system uses a double-antibody dye capture of plasma nucleosomes (Figure 4A) in a well-plate format [26].

A similar approach uses magnetic bead-bound antibodies to pull the nucleosomes from plasma. Then, liquid chromatography and mass spectroscopy are used to detect and differentiate endogenous PTMs [27]. Figure 4 shows the platform used to capture the nucleosomes (Figure 4A) and to detect them (Figure 4B).

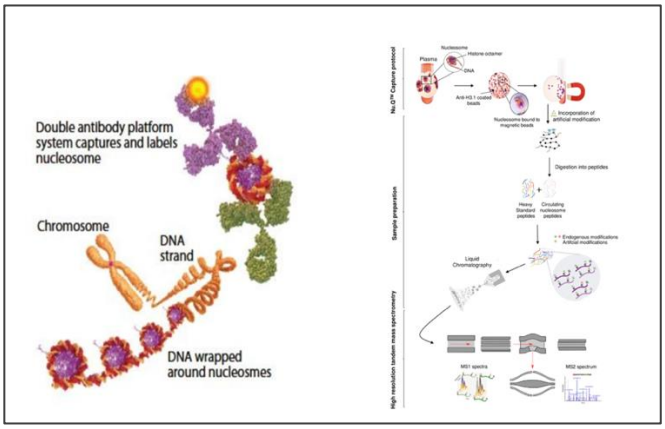

Figure 4: A) Plate based assay for detection of circulating nucleosomes using a double antibody platform [26]. (B) Process flow utilizing Nu.Q®, which uses antibodies bound to magnetic beads to immunoprecipitate circulating nucleosomes, followed by liquid chromatography and mass spectroscopy to detect PTM of histones in plasma [27].

Over the past several decades, the specific roles of more PTMs are becoming known. One study, focusing on colorectal cancer, found thirteen PTMs that were distinct to colorectal cancer patients. The upregulation of methylation of histone H3K9, of histone H3K27, and acetylation of histone H3 were found [27]. Figure 5A visually summarizes how an increase or decrease in methylation on a variety of lysines on the H3 and H4 histones impacts their biological role. Figure 5B lists a series of lysine demethylases (KDMs), the post-translational modifications that they effect, and their links to cancer [28]. The nucleosome studies presented in Chapter 4, focus on H3K4me2 nucleosomes. These are post-translationally modified histones that have 2 methyl groups

added to the fourth lysine on the H3 histone protein. Its links to cancer are highlighted by the blue boxes in Figure 5B.

A

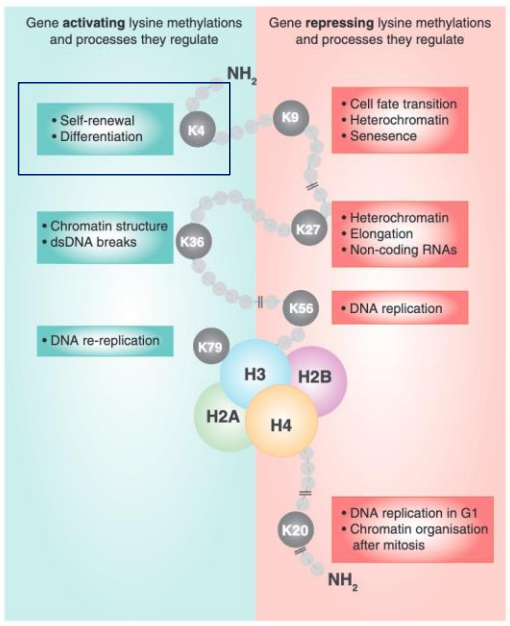

B

	Synonyms	Targets	Links to cancer
KDM1A	LDS1, AOF2, KIAA0601	H3K4me2/me1, H3K9me2/me1	Acute myeloid leukaemia—maintains clonogenicity and inhibits differentiation[36] Glioblastoma—inhibition degrades HIF1α and induces senescence[42] Overexpressed in prostate,[43] liver,[44] breast,[45] colorectal[46] and lung tumours[47]
KDM1B	LDS2, AOF1, C6orf193	H3K4me2/me1	Breast cancer—knockdown reduces colony formation[35] Glioblastoma—suppression maintains glioma-initiating cells in hypoxic environment[48]
KDM2A	CXXC8, FBL7, FBXL11, JHDM1A, KIAA1004	H3K36me2	Lung cancer—represses DUSP3 phosphatase, thereby activating ERK and JNK signalling, tumour growth and metastasis[65]
KDM2B	CXXC2, FBL10, FBLX10, JHDM1B, PCCX2	H3K4me3, H3K36me2	Glioblastoma—essential for proliferation of stem cells[61] Leukaemia—essential for self-renewal of stem cells[62]
KDM3A	JMJD1A, JHDM2A	H3K9me2/me1	Colorectal cancer—activates Wnt target genes, thereby enhancing self-renewal of stem cell[73] Prostate cancer—regulates proliferation, survival and drug resistance[76] Breast cancer—activates invasion, drug resistance and stemness[78] Lung cancer—drives tolerance to taxane-platin therapy[141]
KDM3B	JMJD1B, JHDM2B	H3K9me2/me1	Colorectal cancer—activates Wnt target genes, thereby enhancing self-renewal of stem cell[73] Prostate cancer—activates genes needed for metabolism and proliferation[77]
KDM3C	JMJD1C, JHDM2C	H3K9me2/me1	Leukaemia—critical for the growth of stem cells, independent of demethylase activity[80]
KDM4A	JMJD2A, JHDM3A	H3K9me3/me2, H3K36me3/me2, H3K23me3	Leukaemia—redundantly promotes proliferation[88] Breast cancer—knockout decreases tumour growth[91]
KDM4B	JMJD2B, JHDM3B	H3K9me3/me2, H3K36me3/me2, H3K23me3	Leukaemia—redundantly promotes proliferation[88] Gastric cancer—knockdown reduces IL-8, CXCL5 gene expression[92]
KDM4C	JMJD2C, JHDM3C	H3K9me3/me2, H3K36me3/me2	Leukaemia—redundantly promotes proliferation[88] Glioblastoma—activates Wnt target genes[93] Prostate cancer—knockdown reduces phosphorylation of proliferative kinases and increases expression of PTEN[89]
KDM4D	JMJD2D	H3K9me3/me2	Colorectal cancer—promotes tumour formation in mice[95]
KDM4E	JMJD2E	H3K9me3/me2	No function in cancer identified to date.
KDM5A	JARID1A, RBBP2	H3K4me3/me2	Breast cancer—decreases expression of tumour suppressors p16 and p27[99] Lung cancer—promotes proliferation by repressing NOTCH1/2 tumour suppressor target genes[100] Lung cancer—promotes tolerance to EGFR inhibitors[138,139] Glioblastoma—cantrols resistance to standard-of-care temozolomide[149]
KDM5B	JARID1B	H3K4me3/me2	Leukaemia—downregulates *Hox*/*Meis* genes required for acute myeloid leukaemia pathogenesis[102] Melanoma—tumour suppressive role[103] Melanoma—maintains slow-cycling stem cell population resistant to therapy[140,142] Myeloma—inhibition attenuates proliferation[101]

Figure 5: A) Summary of the biological roles of different lysines on the histone 3 and histone 4 proteins of the nucleosome. B) List of demethylase enzymes, their targets, and their links to cancer [28]. PTMs of H3K4 are studied in this work and are highlighted by the blue boxes.

The epigenome is implicated in everything from embryonic development and metabolism to cancer and autoimmune disorders. Yet it has not been identified in its entirety nor are many of the epigenome's basic functions, such as how it replicates and how its role changes as an organism develops known [3], [12], [29]–[31]. The ability to answer these questions is in part limited by the tools available to study the epigenome. The next section describes the most widely used tool to study epigenetics, chromatin immunoprecipitation.

1.2 Studying Epigenetics: Chromatin Immunoprecipitation

One of the main tenets of epigenetics is the relationship between DNA and its supporting and surrounding proteins. The most common method to study protein-DNA interactions, chromatin immunoprecipitation (ChIP), is the pull-down of chromatin using antibodies bound to a solid phase [32].

The ChIP protocol (shown in Figure 6) generally begins with a large culture of cells that are broken down to release their native or crosslinked chromatin [32]. Usually, samples are treated with formaldehyde, i.e. crosslinked, to ensure that the target protein travels with its DNA [4], [33], [34]. Crosslinking is especially important in weakly bonded or transient DNA-associated proteins. However, in some instances, such as when total genome sequencing or frequency is desired, native (or untreated) chromatin is preferred [35]–[37]. Crosslinking is also particularly useful when screening for antibody specificity against similar, yet distinct, epitopes that might cause nonspecific binding [38]–[40]. Next, after clearing away cellular debris, the sample is sonicated into 200-600 base pair fragments [32]. Then, the DNA-protein complex is immunoprecipitated using an antibody usually targeted to the protein and bound to either agarose or, more recently, magnetic beads. Magnetic beads are increasingly the preferred substrate because they are easier to prepare, require fewer washing steps, can be functionalized with different coatings, and require only a strong magnet to precipitate the beads as opposed to a centrifuge [1], [41], [42]. Once the supernatant is cleared and the beads are washed, all that should be attached is the DNA-protein complex of interest. This complex is then eluted off the beads and the protein is dissociated from the DNA using a chloroform-phenol extraction [33]. Following DNA purification, there are a plethora of

different ways to analyze or further prepare the sample: next generation sequencing, gel electrophoresis, tagmentation, library generation, barcoded arrays, mass spectroscopy, qPCR, western blot, and re-ChIP, to name a few [43]–[46].

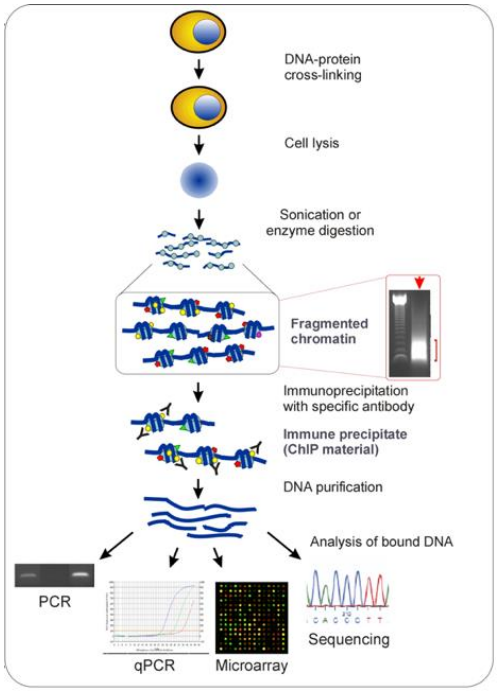

Figure 6: Schematic of general ChIP protocol [32].

ChIP, however, is not without its limitations. Prior to any post-ChIP analysis, it is critical that the analyte is specifically and adequately collected. Unfortunately, current methods rely on the downstream results to identify whether the analyte has been captured, and even at that point, a lack of signal does not necessarily identify which part of the procedure to troubleshoot. The most commonly used detection method, ChIP-PCR, analyzes the DNA by first amplifying the signal using PCR, i.e., making more copies of the isolated DNA for sequencing, and then detecting the proteins or DNA fragments using gel electrophoresis. The results form gel electrophoresis are

difficult to interpret and only provide a qualitative and relative representation of a given modification. If the signal-to-noise ratio is inadequate, assigning any biological significance can be inaccurate [1]. Second, ChIP is only as good as the antibodies used. Analysis can only be done using a previously known target against which an antibody exists. Furthermore, ChIP antibodies are well-documented to be non-specific, to vary by batch, and to have low sensitivity [38], [47]–[49]. Therefore, determining and optimizing a ChIP protocol requires screening of several antibodies, which can be expensive and time consuming. Third, even though the detection limit of most ChIP protocols is comparable to the amount of chromatin in a cell, current benchtop protocols have very low yield and therefore demand a high volume of starting cell culture (~10^6-10^8 cells) [50]. This exempts rare tissue types and makes detailed probing of cell-to-cell variability difficult using traditional ChIP. Fourth, because ChIP works on bulk cell cultures, the granularity necessary to detect variations between cells in a seemingly homogenous tissue are lost. Therefore, the variability that is present in the epigenome of cells within an otherwise homogenous tissue are masked [7]. Finally, processing ChIP samples is very time and labor intensive, often taking several days to over a week for just a few samples [1], [17], [40], [42], [43], [51], [52]. The next section looks at alternative methods to traditional benchtop ChIP as well as the translation of ChIP onto a digital microfluidic biochip.

1.3 Advancing Epigenetics

To make significant contributions in epigenetics, there is a need for an improved ChIP method. The new platform or method would need to include three major modifications to the current technology: (1) require a small quantity of starting material, (2) allow for target analytes and antibody performance to be analyzed prior to downstream analyses, (3) achieve greater granularity and resolution to detect single cell variation, and (4) streamline isolation and purification to decrease turnaround time, decrease labor costs per sample, decrease sample loss, and increase yield.

The development of microfluidic-based devices has allowed biological benchtop procedures to be adapted to small scales and highly automated devices. Microfluidic biochips can address the major drawbacks of benchtop ChIP by reducing sample usage and providing an easily integrated, automated, and high throughput platform [41], [53]–[55]. The next section highlights studies that have implemented ChIP onto flow-through microfluidic platforms.

Table 1 summarizes the studies discussed in this section and assesses their contributions to translating ChIP onto a microfluidic device.

1.3.1 ChIP Implementation on Flow-Through Microfluidic Platforms

Wu et. al., used a PDMS-based flowthrough microfluidic platform that utilized pumps to push liquids through the channels [56]. They implemented all stages of ChIP except for chromatin extraction and downstream analysis. They were able to perform multi-target, multi-sample immunoprecipitation on extracted chromatin by running 6 samples and 1 control from 2 biological sources using ~10,000 cells [56]. Although this device improved throughput, automation,

multiplexing and sample size issues, it still required a large initial cell culture, assessed bulk chromatin samples, and had a complex design of valves, channels, and pumps for liquid handling procedures.

Geng, et. al., isolated nucleosomes using a much simpler PDMS-based flowthrough device that only required ~50 cells [57]. Although the run-time was rather long (~8.5 hours), unlike Wu, et. al., they also performed chromatin extraction from whole cells on the device [57]. This device improved sample size issues and included chromatin extraction; however, it still assessed bulk chromatin samples, did not increase throughput, and did not multiplex.

Dirks, et. al., addressed multiplexing of ChIP on a PDMS-based flowthrough device [51]. The protocol started with extracted chromatin fragments that were loaded onto a device with 24 reaction columns packed with large beads to prevent the smaller Protein A/G beads from passing through. Chromatin that was antibody-bound to the Protein A/G beads was trapped in these columns. Then the columns were washed, the DNA was eluded off the Protein A/G beads and collected for qPCR off-chip. This study achieved a runtime of 4.5 hours, with only 30 minutes of hands-on time (not including chromatin extraction) using ~3,000 cells [51]. These devices were capable of ChIP multiplexing, had increased throughput, and demonstrated a high degree of automation, and a decrease in the starting cell culture. However, the samples were still derived from bulk cultures and the device had a complex design with many pumps, actuators, channels, and inputs.

The following studies although still flow-through, separated their samples into droplets, thereby introducing finer detailed analyses of the samples. Both used a T-junction and timed valves that crossed the flows of the aqueous samples and a stream of oil to generate droplets [5], [42].

Teste, et. al., drew samples, reagents, and beads from different wells in a 96 well plate sitting on an automated translational stand, and suspended these liquids in droplets. Magnetic tweezers were used to capture beads and perform immunoprecipitation, washing, elution and purification of DNA. By reducing the reaction volume, the run time was decreased to 7 hours, the amount of reagents needed was decreased, and the number of cells required was decreased by ~100 fold [42]. However, the run time was still substantial, and the device input sample was previously extracted chromatin from a bulk tissue sample.

Grosselin, et.al., presented a high throughput single-cell analysis method [5]. Cultured cells were suspended at a very low concentration so that, by the Poisson distribution, 95% of droplets containing cells had only one cell per droplet. These cell-containing droplets were co-flowed with lysis buffer and micrococcal nucleases to break open the cells and break down the chromatin into nucleosome fragments. The nucleosome droplets were electrocoalesced with droplets containing barcoded hydrogel beads. These barcodes uniquely identified each nucleosome droplet by associating it with a single cell of origin. The hydrogel beads, now carrying the barcoded nucleosomes, were collected, the beads digested, and the nucleosomes immunoprecipitated using antibody bound beads off-chip. The microfluidics portion of this study presented a unique method of generating a large number of barcoded nucleosomes for downstream single-cell analysis [5]. This study truly allowed for the high level of granularity that is critical in identifying potentially cancerous or pre-cancerous aberrant cells in tissue biopsies, which would have otherwise been lost in bulk tissue analyses. However, this study did not actually perform immunoprecipitation or DNA extraction on a chip, nor did it decrease the hands-on time to perform ChIP (this remained a several day protocol), nor provide a high degree of automation.

Despite the contributions that each study provided, none have yet addressed all five major drawbacks of ChIP. The next subsection looks at how using Digital Microfluidic Biochips (DMFBs) that utilize electrowetting-on-a-dielectric (EWD) for droplet generation and transport can provide a novel ChIP platform.

1.3.2 ChIP Implementation on Digital Microfluidic Platforms

Digital microfluidic biochips (DMFBs) can control micro- and nanoliter droplets via electrowetting-on-dielectric (EWD) actuation to perform all the actions necessary in a bioassay (dispensing, transport, mixing, and splitting) [41], [53]–[55]. With targeted reactions in small volumes and less sample handling, DMFBs need less starting material and shorter incubations, thus decreasing turnaround time and increasing yield. Furthermore, integrating on-chip magnetic control of superparamagnetic beads allows for bead washing steps, analyte capture, and analyte separation or elution form the beads [55]. Additionally, without the need for pumps and actuators, but simply electrical inputs, DMFBs have the freedom unavailable to the architecturally limited PDMS based, flow-through microfluidic devices. Studies showing integration of downstream analyses onto DMFBs present the opportunity to adapt ChIP from cell extraction to PCR and DNA sequencing, thus automating the entire protocol [58].

Although, an entire ChIP-on-chip device has not been developed on a DMFB, many of the steps necessary to perform ChIP have been demonstrated. DMFBs have been used to culture single cells [59], to lyse cells [60], to capture, wash, and transport functionalized magnetic beads [55], to immunoprecipitate analytes [61], to perform PCR [58], and to perform next-generation sequencing of DNA [62]. Furthermore, fluorescent detection using a CCD camera, an LED of the excitation

wavelength, and the necessary filters for detection has been demonstrated with a DMFB [63]. This provides a method for on-chip detection of analytes without specialized fluoroscopy instrumentation. Developing an immunoprecipitation assay that can detect chromatin on-chip would allow for rapid analyte identification, antibody screening, and reduce the need for costly and time intensive downstream analyses.

Table 1: Summary of the studies presented in section 1.3 Advancing Epigenetics. The table highlights the abilities of each device and their contributions to translating ChIP onto to a microfluidic device.

Type of Microfluidic Device	Author	Device Image	ChIP Protocol								Device Features									
			Cell Capture	Cell Lysis	Chromatin Digestion	Chromatin Extraction	ChIP	DNA Purification	PCR	DNA sequencing	Reduced Reaction Volumes	Reduced Cell Input	Single-Cell Analysis	Reduced Assay time	High Throughput	Multiplexed	Automated	On-Chip Detection	On chip Magnet	Simple Instrumentation
Flow through	Wu, et. al., 2012						✓				✓	✓		✓	✓	✓	✓			
	Geng, et. al., 2011			✓	✓	✓	✓				✓	✓		✓			✓			
	Dirks, et. al., 2021	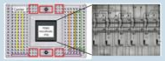					✓	✓			✓	✓		✓	✓	✓	✓			
	Teste, et. al., 2017	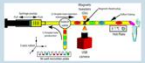					✓	✓			✓	✓		✓			✓			
	Grosselin, et. al., 2019	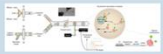	✓	✓	✓	✓					✓		✓		✓			✓		
Digital EWD	Zhai, et. al., 2020		✓								✓		✓			✓	✓	✓		✓
	Madison, et. al., 2015			✓							✓						✓	✓		✓
	Chen, et. al., 2016	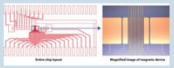									✓					✓	✓	✓	✓	✓
	Ng, et. al., 2012			✓							✓			✓			✓	✓		
	Chang, et. al., 2006								✓		✓						✓			✓
	Illumina, Inc.									✓	✓			✓	✓	✓	✓			
	Kalsi, et. al., 2017	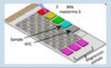									✓			✓			✓	✓		✓
	Bigdeli, et. al., 2022	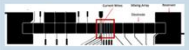					✓				✓	✓		✓			✓	✓	✓	✓

1.4 Motivation and Contributions

Epigenetics, the study of inheritable mechanisms that regulate gene expression, has clinical ramifications from cancer to autoimmune disorders to psychiatric pathologies. The main tool to study epigenetics is chromatin immunoprecipitation (ChIP), which probes the relationship between DNA and its structural nucleosome-forming histone proteins. Standard benchtop ChIP has five major drawbacks: (1) it requires a large input volume of cells, (2) it is very time consuming, work intensive, and low throughput, (3) it suffers from poor chromatin yield and sensitivity, (4) ChIP antibodies can be non-specific, vary by batch, and have low sensitivity, (5) ChIP performs bulk tissue analysis which loses the granularity necessary to detect cell-to-cell variations.

Digital microfluidic biochips (DMFBs) have proven to be successful at utilizing small volumes of reagents and samples to perform high throughput bioanalyses of macromolecules using various assaying techniques. Their ease of configurability, automation, and high sensitivity make them an ideal platform for ChIP adaptation. Droplet manipulation using electrowetting-on-dielectric (EWD) has been demonstrated extensively for moving, merging, splitting, and mixing of droplets. These capabilities, in conjunction with magnetic bead control using magnetic field gradients generated by a current running through a wire on a device, provide all the necessary functionality to successfully run ChIP more efficiently on a DMFB [41], [53]–[55].

Translation of the benchtop ChIP protocol onto a DMFB will address the five issues facing epigenetic study and workflow. Smaller volumes will reduce reaction time and reagent and sample use, while providing greater granularity and higher resolution when probing a sample. Automation will decrease turnaround and hands-on time for users. Parallel operations and multiplexing will increase throughput. Finally, streamlining ChIP onto one device greatly reduces sample loss, thereby expanding the types of possible studies to include low-yield and rare tissue types.

Although a lot of work has been done to translate ChIP onto flow-through microfluidic devices, there is a relatively small body of work to achieve the same goals on digital microfluidic biochips. As stated in the previous section, though not intended for ChIP applications, many of the steps of the protocol and post immunoprecipitation analyses have already been adapted to DMF platforms. These devices have demonstrated success in achieving results with low volumes, fast reaction times, on easily fabricated devices, and using minimal external instrumentation to drive experiments. However, the capture and detection of chromatin on a DMFB has not yet been reported.

Furthermore, there do not exist protocols nor devices for the detection of chromatin prior to downstream analyses (gel electrophoresis, PCR, etc.). The ability to detect chromatin before performing more complex and costly procedures, would decrease reagent and labor costs and decrease turnaround time by providing a rapid confirmatory platform. For quicker assay development, a front-end detection tool can also be applied when developing ChIP protocols for antibody specificity screening and assay parameter optimization. Additionally, traditional benchtop ChIP relies on PCR and DNA sequencing to indirectly determine relative abundance of post-translationally modified nucleosomes of chromatin. Therefore, in addition to detecting the chromatin, there also has not been work done to quantify isolated chromatin directly.

Finally, on-chip isolation of magnetic beads (a key reagent in ChIP) has been shown empirically and through COMSOL simulations [64] to perform poorly. A major challenge while running immunoprecipitation assays was the limitation of the device's ability to capture all the beads in a droplet and isolate them to a single area for analysis. Therefore, there was a need to improve a DMFB's on-chip magnetic capture mechanism for magnetic beads suspended in a droplet.

The work encapsulated in this dissertation, demonstrated some of the first steps towards implementation of the entire ChIP protocol onto a DMFB, developed new tools for chromatin analysis, and introduced a new DMFB design for magnetic bead capture. The contributions of this work are listed below:

1) Developed new fluorescent confirmatory chromatin and nucleosome immunoprecipitation assays.

2) Demonstrated that the immunoprecipitation assays are detectible on-chip without any complex downstream analyses nor specialized fluoroscopy instrumentation.

3) Demonstrated that the immunoprecipitation assays perform at higher sensitivity than traditional benchtop ChIP.

4) Developed a single-channel pixel intensity measurement system for semi-quantitative analysis of chromatin and post-translationally modified nucleosomes directly on-chip.

5) Designed a new DMFB for improved capture of magnetic beads with twice the measured signal intensity using a new pull-through droplet scan method with on-chip embedded magnetic controls.

1.5 Conclusion

This chapter outlined the importance of epigenetic research and its impact on human health and medicine. Current standards of epigenetic research tools were described, namely chromatin immunoprecipitation, and its shortcomings. This chapter went on to explore the current work done to adapt ChIP onto flow-through and digital microfluidic platforms. Finally, the main motivation and contributions of this work were presented.

The following chapters detail the background theory, fabrication techniques, and experimental setup for the proposed DMFB. In addition, a novel fluorescent sandwich assay protocol for chromatin detection, the steps necessary to adapt this protocol to a DMFB, and the expected challenges are discussed.

2. Background Theory

Advances in microfluidic devices have led to an era of the 'lab-on-a-chip', where benchtop bioassay protocols are translated to easily manufactured, small, automated, high-throughput devices. The digital microfluidic family of devices control movement of microliter scale droplets via electrowetting-on-dielectric (EWD) actuation and can combine multiple functionalities onto a single chip. Magnetic beads, which are manipulated using current wires that generate magnetic fields, provide the added ability to capture, isolate, and purify analytes [53], [55]. By combining these with a fluorescence detection system that can image droplets while they remain on-chip, it is possible to adapt a chromatin detection and precipitation immunoassay to a digital microfluidic biochip. The background theory behind EWD, on-chip magnetic control, and immunoassays, is discussed in this chapter.

2.1 Electrowetting-on-Dielectric (EWD)

For the devices and assays described herein, droplet handling was achieved via electrowetting. Conductive droplets sat atop a hydrophobic surface and were manipulated by applying a voltage across a metal electrode that was coated with a dielectric, insulative layer. A top plate that also touched the droplet, created the ground electrode. The voltage created an electric field across the dielectric layer that changed the contact angle between the droplet and the surface by lowering the interfacial tension, thus increasing the droplets wettability on the dielectric surface [65]. This phenomenon follows the Young-Lippman equation shown below.

Equation 1: Young-Lippman Equation [66]

$$\cos\theta(V) = \cos\theta(0) + \frac{\varepsilon_r \varepsilon_0 V^2}{2t\gamma_{lg}}$$

$\boldsymbol{\varepsilon}_r$ = 8.85x10^{-12} F/m Permittivity of vacuum
$\boldsymbol{\varepsilon}_0$ Dielectric constant of insulator
T Thickness of insulator
V Applied voltage
$\boldsymbol{\theta}(0)$ Contact angle when V = 0V
$\boldsymbol{\theta}(V)$ Contact angle when V≠ 0V

If a droplet is just large enough that it is touching the adjacent electrode, as shown in Figure 7A, it can be moved to that electrode simply by turning the destination electrode on and simultaneously turning the electrode beneath it off (Figure 7B, bottom row) [55], [67]. A droplet can be split by turning on two electrodes on either side of the droplet, and conversely two droplets can be combined by turning on a shared electrode. Mixing can be achieved by shuttling a droplet about an electrode array, as shown in Figure 7C [58]. Transport, splitting, combining, and mixing are the four droplet handling functions necessary for the ChIP protocol.

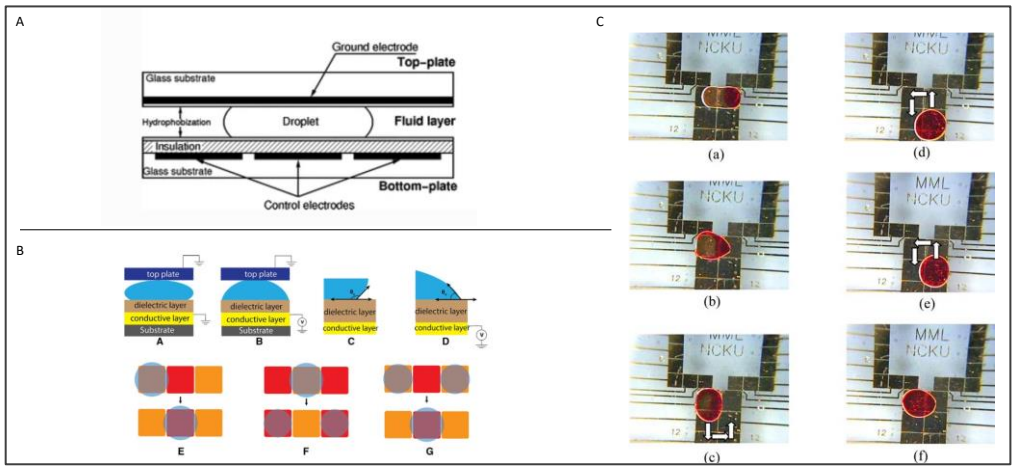

Figure 7: A) Side view of a digital microfluidic device [67]. B) Schematic showing how the application of a voltage affects the contact angle of a droplet and the different fluid handling functions capable on a DMF [55]. C) A series of images of two droplets being mixed by shuttling them around an array of electrodes [58].

2.2 Magnetic Bead Control

Intra-droplet control of functionalized superparamagnetic beads dispersed in a droplet was integral to capturing and separating the targets of ChIP. To achieve this, a movable magnetic field was created by fabricating embedded current conducting wires on the device [55]. A current, passing through a wire, results in a magnetic field around that wire. The magnetic field strength decreases with increasing distance from the wire, resulting in a gradient. Magnetic beads within this gradient will experience a force drawing them to the peak of the field at the center of the wire. Figure 8 shows a schematic of a bead at point P, r distance away from the red current wire with current I [55]. Using the Biot-Savert law, one can calculate the magnitude of the magnetic field, B, at a distance, r, perpendicular to the current wire carrying a current, I (Eq. 2) [55]. This result can subsequently be used to derive the magnetic force, F, as a function of distance away from the current wire (Eq. 3) [55].

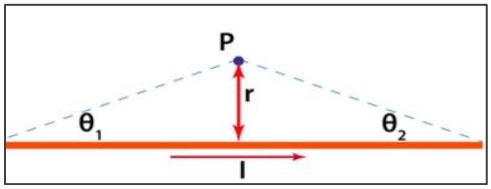

Figure 8: The magnetic field at point P, at a distance r away from the center of the wire with current, I [55].

Equation 2: Magnitude of the magnetic field B at point p [55].

$$B(p) = \frac{\mu_0 I}{4 * \pi * r}(\cos\theta_1 + \cos\theta_2)$$

Equation 3: Magnetic force as a function of distance away from current wire [55].

$$F = \mu * \frac{-\mu_0 I}{4 * \pi * r^2}(\cos\theta_1 + \cos\theta_2)$$

This phenomenon was used to control the beads within a droplet by turning on adjacent current wires one at a time, ‘sweeping’ through the droplet to collect all the magnetic beads within some distance of the wire. The beads can subsequently be held stationary above the wire as the liquid droplet is moved and another reagent is added in a serial manner diluting out the previous

reagent [55]. Reagent changing via serial dilution translates the removal of the supernatant, elution, and washing steps of the ChIP protocol. The effect of the current wires on magnetic beads on a DMF is shown in Figure 9. The red arrow indicates a current wire that had been turned on. The beads, a dark brown color, have accumulated on that wire.

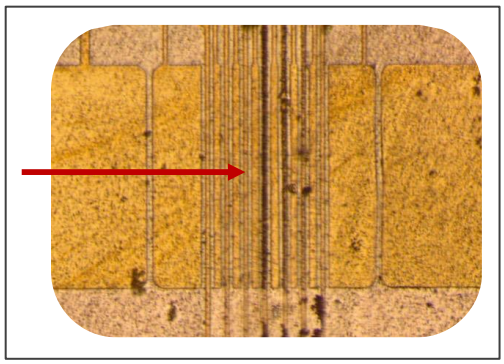

Figure 9: A bright field image of a DMFB with a single current wire turned on. The red arrow indicates the activated current wire, and the darkened color is the accumulation of magnetic beads onto that wire.

2.3 Immunoassay Development

This section focuses on the selection process for the immunoassay platform presented in this dissertation and gives an overview of the type of considerations necessary when developing an immunoassay. Immunoassays that were used in previous ChIP laboratory protocols were unsuitable for use in these studies because the immunoprecipitation was not detectable on-chip. Thus, new assay work was driven by the need to improve the current ChIP protocol and bypass downstream analyses (such as PCR-sequencing) to develop platform-specific immunoassays that were usable on a DMFB.

2.3.1 Assay Selection Process

Figure 10 is a generalized guideline for how to approach a new assay and what criteria need to be used as design inputs [68]. In this instance, the goal was to improve a current assay and add further functionality. Therefore, the original assay's output must be preserved, sensitivity and specificity must be at least the same, and it must fit within the capabilities of the platform on which the new assay was going to be used.

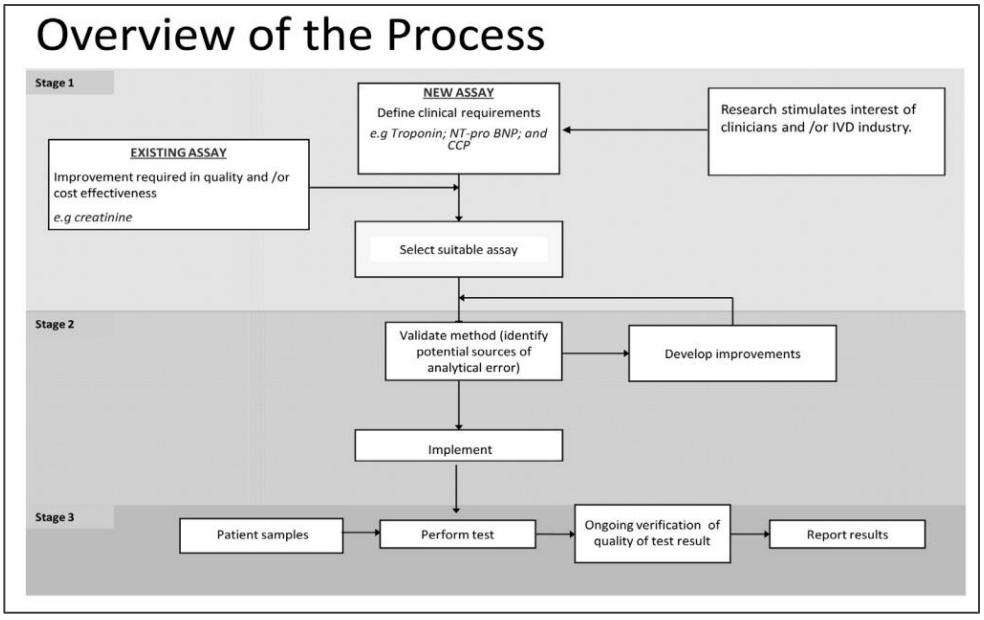

Figure 10: An overview of the general guidelines, stages, approaches, and considerations for developing a new assay [68].

Adopting these guidelines and applying them to this ChIP project, Figure 11 shows the inputs and considerations for the new assay developed herein. This new assay needed to capture chromatin, precipitate it out of solution for downstream analysis, be easily modifiable for different chromatin targets, and maintain a low level of added complexity to minimize error while still improving on the standard benchtop procedure. Furthermore, the assay selected needed to be compatible with a DMFB. As mentioned in Chapter 1, DMFBs were selected as the target platform for this application due to their use of small volumes of reagents and samples to perform high throughput bioanalyses of macromolecules, their ease of configurability, automation, and their high

sensitivity [41], [67]. Therefore, all reagents needed to have the ability to be actuated using EWD, while not damaging or fouling the device. In addition, based on the drawbacks of standard benchtop ChIP, this assay needed to have greater sensitivity to decrease sample size, and to detect and quantify chromatin on-chip to decrease reagent and labor costs associated with ChIP assay parameter determination.

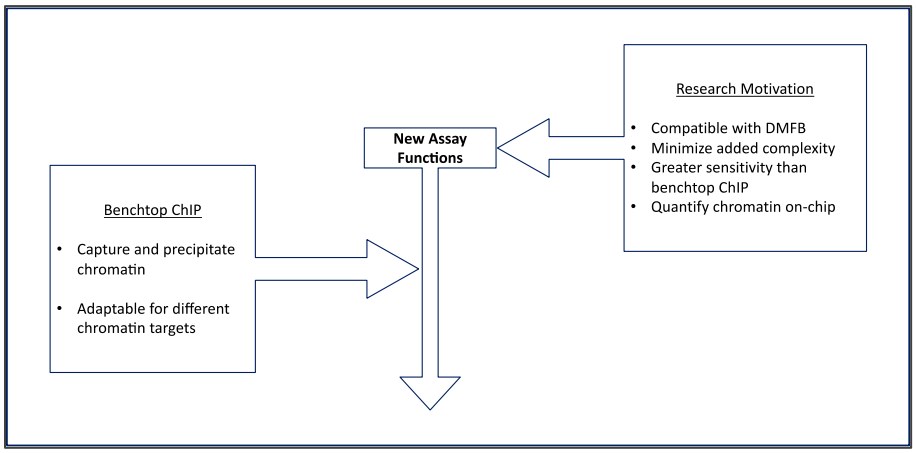

Figure 11: Adapted schematic summarizing design inputs guiding the development of the new assay.

Now that the general function and user needs have been established, the next section explains the different components inherited by the final assay whose protocol and results are shown in Chapter 4 Section 5.

2.3.2 Benchtop Chromatin Immunoprecipitation (ChIP)

Chromatin immunoprecipitation is an epigenomics tool to study the relationship between DNA and its structural proteins. The general protocol starts with a cell culture of approximately 10^6-10^8 cells. These cells are harvested, and the DNA and their structural proteins (histones organized into nucleosomes) are cross-linked. This ensures that for the entirety of the procedure the DNA-protein complex travels together. Then the cells are lysed to release their nuclear contents. Once the chromatin has been released from the nuclei, the samples are either sonicated or digested by nucleases to break the chromatin into smaller fragments. Using bead-bound antibodies against

specific post-translational modifications of the histones in nucleosomes, the chromatin region of interest is immunoprecipitated out of solution. Afterwards, the protein-DNA complex is eluted off the beads, the cross-links are reversed, and the DNA is extracted. The DNA is usually further analyzed using gel electrophoresis, PCR, and genome sequencing. Figure 12 summarizes the general protocol [69].

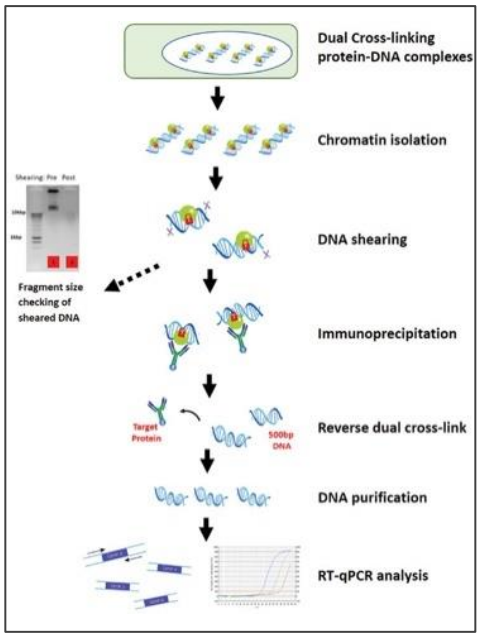

Figure 12: Summary of ChIP protocol [69].

Immunoassays, such as ChIP, are the current gold standard for analysis of biological analytes due to their inherent high sensitivity, specificity, and adaptability for high-throughput systems. An immunoassay depends on three main components: the analyte (in this case chromatin, nucleosomes, and primary antibodies), the antibody, and a detectable label. Antibodies lend immunoassays their specificity and the labels give immunoassays their generally high sensitivity and low limits of detection [70].

Antibodies are a class of immunoglobulin proteins used by the body to identify foreign objects (e.g., pathogens such as bacteria and viruses). The overall structure of a general antibody is shown in Figure 13. An antigen's epitope, which in the case of ChIP is the PTM of the histone,

binds the antibodies paratope. The paratope is part of the Fab region of the antibody and is modified for different antigens thus providing the specificity of the antibody. Antibodies and antigens bind in a lock and key format (spatial complementarity) via hydrogen bonds, electrostatic forces, hydrophobic interactions and van der Waals forces. Therefore, binding can be reversed and is dependent on the affinity between the antibody and antigen [71]. Consequently, when selecting an antibody, it is important that it has high affinity for the specific antigen to decrease cross-reactivity and increase binding efficiency. One of the challenges facing ChIP is finding the correct antibody. There is a high degree of batch-to-batch variability in manufactured antibodies and across manufacturers, despite being labelled 'ChIP grade' [38]. Addressing this issue would minimize sample waste and labor costs associated with ChIP assay development.

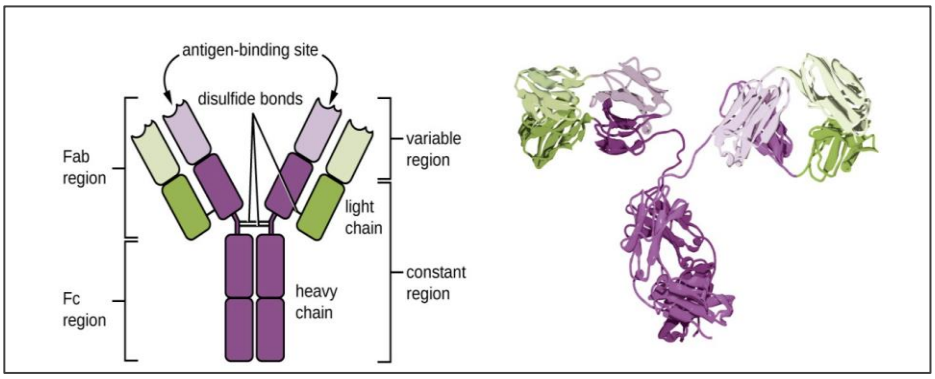

Figure 13: Labelled schematic and ribbon model rendering of an antibody [71].

The Fc region defines the antibody's immunoglobulin class, such as IgG, IgM, etc. These classes and their specie of origin are important when selecting a type of bead for ChIP. Previously, agarose beads with Protein A, Protein G, or a combination were used, and samples were centrifuged to gather the beads. However, the introduction of magnetic protein-coated beads, which are easier to precipitate by using a strong magnet, are increasingly becoming standard procedure. The coating on the beads is dependent on the class and specie of antibody used. Both Protein A and G beads have an affinity for IgG immunoglobulins, however Protein A has greater affinity for rabbit and

pig, while Protein G has a great affinity for mouse and human. Therefore, the specie the antibody was raised in will dictate which bead is selected for an immunoassay [72].

This subsection highlighted design inputs that the new assay and DMF platform need to inherit from benchtop ChIP to maintain the integrity of the analysis' aims and improve upon the current performance metrics. First, the assay must be an immunoassay as it is the gold standard for highly specific and sensitive capture of biological analytes such as the protein-DNA complex in ChIP. Second, the DMFB platform and assay must provide the functionality to rapidly screen for antibody quality to address the antigen-antibody affinity issues facing ChIP. Finally, magnetic beads will be used as the solid phase for chromatin IP for their ease of use and adaptability to a DMF platform. The coating of the magnetic beads will be determined by which antibodies are used.

In summary, the new immunoassay would have to detect chromatin using antibodies specific to the PTM of its histones and precipitate chromatin using magnetic beads. Furthermore, it would need to have greater sensitivity than benchtop ChIP, and the ability to detect and quantify chromatin on-chip to decrease reagent use, labor costs, and the number of cells necessary. The next section discusses the selection of the detection assay components.

2.3.3 Development Strategy of a Chromatin Detection and Immunoprecipitation Assay for a DMFB

The gold standard for protein quantification is the ELISA (enzyme-linked immunosorbent assay) [73]. This method is relatively low-cost, highly specific, and when the assay parameters are tuned, can be highly sensitive as well. Depending on whether the analyte of interest is an antigen or antibody, the counterpart is first immobilized on a surface (usually a 96-well plate), then the sample is added, excess reagents washed away, and then the analyte is detected. For sandwich ELISAs detection can be done either directly or indirectly. Direct ELISAs usually require a primary antibody that already has the tag, such as a horseradish peroxidase (HRP), directly attached to it.

Purchasing or developing HRP-tagged primary antibodies is expensive and difficult, therefore indirect detection is preferred [74].

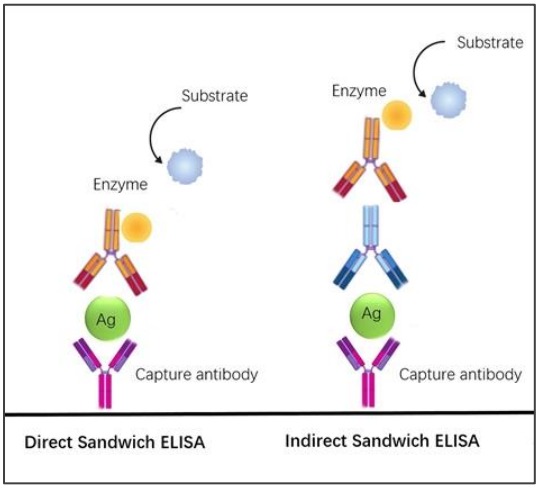

Figure 14: Schematic demonstrating the difference between a direct and an indirect sandwich ELISA [75].

When using indirect detection, the primary antibody is untagged and attaches to the antigen. Then a tagged secondary antibody is used for detection. This amplifies the signal; therefore, less primary antibody is used. Furthermore, only a single secondary antibody is needed to detect a myriad of primary antibodies, since they attach to the IgG constant region of the primary antibody [71]–[74]. Therefore, choosing the right species is critical when selecting assay antibodies. The antibodies used in the studies herein have human antigen-binding sites and rabbit IgG (Abcam). Thus, the secondary antibodies used are Goat anti-Rabbit (Thermo Fisher Scientific), meaning that they have goat IgG, but their antigen-binding site is intended for Rabbit IgG.

Enzyme based assays such as ELISA, although very powerful, add complexity to the assay design because they also require a developing substrate such as TMB to illicit a reaction from the enzyme that is either colorimetric or chemiluminescent [74], [75]. One way to simplify this procedure is to use a secondary antibody whose tag is detectable without any other reagents. A commonly used option is fluorescently tagged secondary antibodies. These are readily available in

a wide variety of excitation and emission wavelengths and grown in many different types of animals [76].

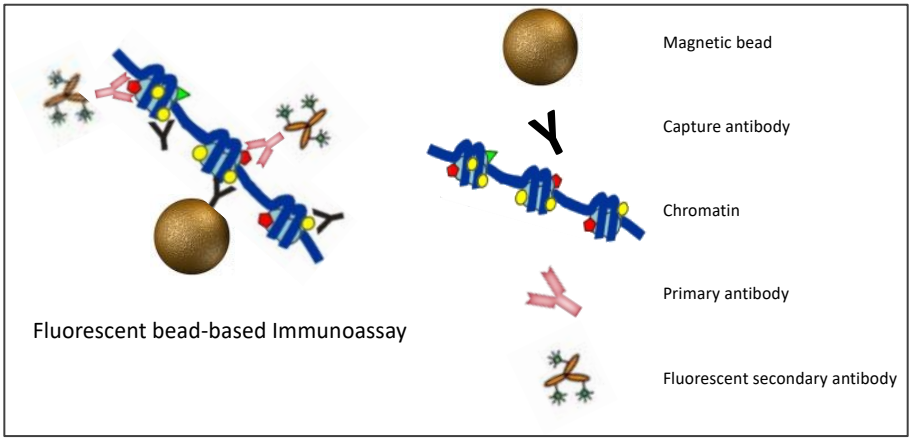

Figure 15: Schematic of a generalized fluorescent bead-based sandwich immunoassay.

Using the principles at the foundation of indirect sandwich ELISAs and the requirements of ChIP, adapting a fluorescent bead-based immunoassay onto a DMFB would be the suitable platform for a semi-quantitative chromatin detection assay. Through extensive experimentation the general assay depicted in Figure 15 was adapted to detect specific post-translational modifications of histones of nucleosomes and chromatin. Chapter 4 details the protocol and results of the assay development process. The next chapter discusses the fabrication methods for DMFBs and the supporting instrumentation necessary to run experiments.

3. Device Fabrication and Experimental Instrumentation

After identifying the major challenges facing current benchtop ChIP protocols and recognizing the benefit of translating ChIP onto a DMFB, the next step was to realize the devices for assay implementation. This chapter focuses on the fabrication of DMFBs and the instrumentation necessary to perform EWD and generate a magnetic field on the device. The latter sections of the chapter discuss the fluorescent detection setup, image acquisition, and the quantitative analysis method used during immunoassay experiments. While this chapter focuses on the fabrication and implementation of the devices, Chapter 4: Experimental Results discusses the development of the immunoassays.

3.1 DMFB Fabrication

This section outlines the fabrication methods used for experimental digital microfluidic biochips (DMFBs). All fabrication work was performed in part at the Duke University Shared Materials Instrumentation Facility (SMIF), a member of the North Carolina Research Triangle Nanotechnology Network (RTNN), which is supported by the National Science Foundation (award number ECCS-2025064) as part of the National Nanotechnology Coordinated Infrastructure (NNCI). The DMFBs described here consisted of three separately fabricated components: a silicon-based bottom plate, a double-sided adhesive gasket layer, and an optically clear acrylic top plate.

3.1.1 Bottom Plate

There were three different bottom plate designs that were used for immunoassay testing. The first, designed by former Fair Microfluidics Lab student, Dr. Liji Chen is shown in Figure 16 below [55]. As shown in the CAD rendering of the chip's layout, this design consisted of two reservoirs at either end of the device with a linear array of electrodes connecting them.

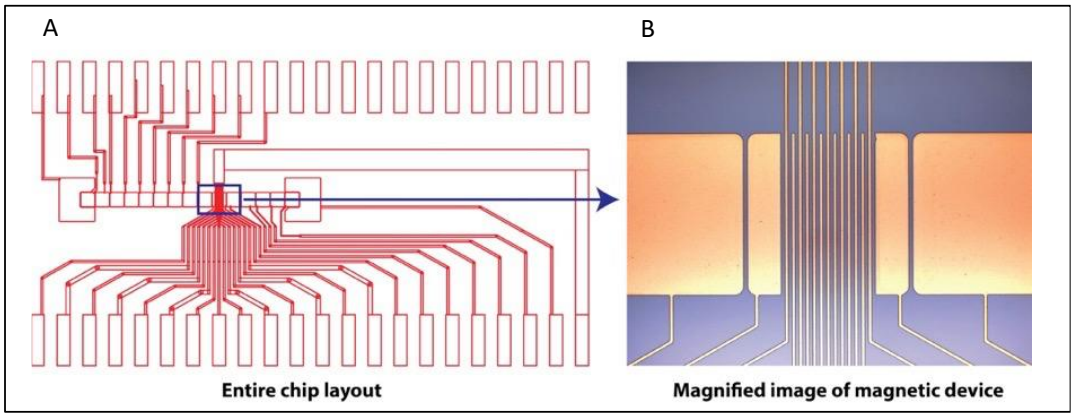

Figure 16: A) CAD schematic of the current wire DMFB B) Magnified image of magnetic region of device showing interspersed small electrodes and wires [55].

The central region of the device had an alternating electrode/current wire pattern, highlighted in Figure 16B, that was used to generate a magnetic field to capture the magnetic beads used in the immunoassays. The electrodes, reservoirs, and current wires were connected to an outer linear array of connector pads on either side of the device. The pads were the points of connection between the device and the electronic control system (see section 2.2). This device design was used primarily in detection and quantitative analysis experiments. The other two designs, shown in Figure 17, followed the same fabrication technique presented in this section and were used for experiments described in Chapter 5: Bead Capture Efficiency.

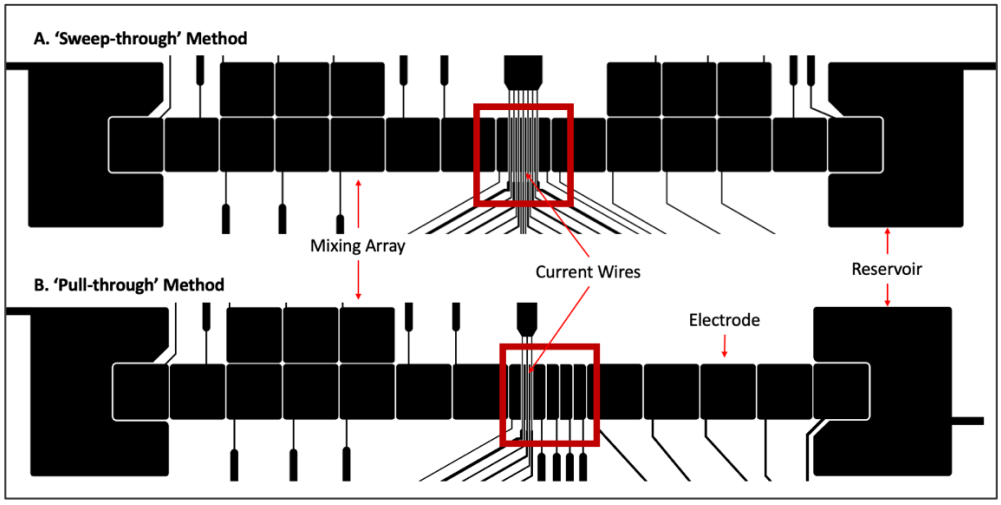

Figure 17: Photomask of DMFB with labelled components. A) 'Sweep-through' device and B) 'Pull-through' device. The red box indicates the major region of design differences between the two devices.

The 'sweep'-through device (Figure 17A) had current wires laid out in parallel over a single electrode region, similar to the traditional current wire device design described in the previous paragraph. However, the device layout included two 2 electrode by 3 electrode mixing arrays on either side of the current-wire electrode to be used in future studies requiring additional droplet mixing. The 'pull-through' device (Figure 17B) had only one mixing array adjacent to the current wire electrode. In addition, the wire region consisted of only three current wires that were next to a series of miniature electrodes intended to pull the droplet past the current wires in a stepwise fashion. A closer view of the regions of interest is shown in Figure 18 below.

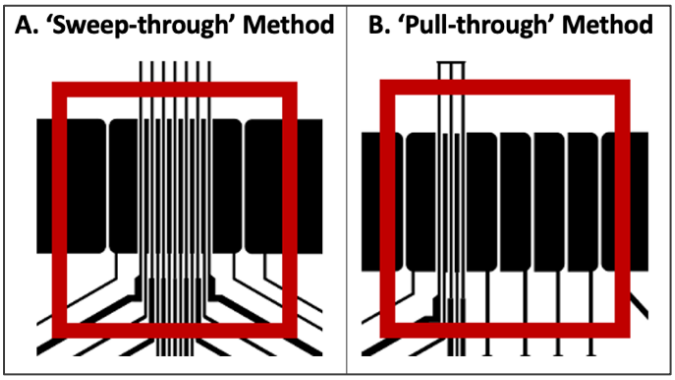

Figure 18: Enlarged image of the two devices. Note that in A) the beads were captured by sequentially turning on the current wires, whereas in B) the droplet was pulled past a single current wire that was turned on.

All elements of the three bottom plates shared the same dimensions but differed in the number present. Table 2 summarizes the similarities and differences between the three devices with respect to the number and type of electrodes, wires, and mixing arrays that are present.

Table 2 : Summary of the number of features on the three device designs.

Devices	Current wire	Sweep-through	Pull-through
Electrodes			
Regular	14	19	15
Interspersed	6	6	2
Miniature	2	2	5
Current Wires	7	7	3
Reservoirs	2	2	2
Mixing Arrays	0	2	1

Each device measured approximately 30 x 15 mm. The regular electrodes measured 700 µm x 700 µm and were primarily used for mixing or shuttling of droplets. The interspersed electrodes were in-between the current wires and measured 45µm x 700µm and were used to help move the droplet over the current wires until it became appropriately positioned. The miniature electrodes measured 92.5µm x 700µm and were used to hold the droplet in place for the current wire and sweep-through designs. These miniature electrodes were used to move the droplet stepwise on the pull-through devices. Droplets on all devices were actuated in a channel that had a gap height of 120 µm, i.e., the thickness of the gasket, meaning that each droplet had a volume of approximately 50 nl ($V = \pi(\frac{L}{2})^2 H$). Prior to the introduction of aqueous droplets, the channel was filled with approximately 20 µl of 0.65 cSt silicone oil (Gelest, Inc.). There were two reservoirs measuring 1.5 mm x 1.5 mm on each device, which were used for dispensing droplets. These reservoirs held approximately 210 nl of liquid. The current wires, which were used to generate magnetic fields, were 15 µm wide, 1 µm thick, and spaced 65 µm apart. The spacing between every

electrode was 10 µm. These measurements, shared by all devices, are represented in Figure 19 below.

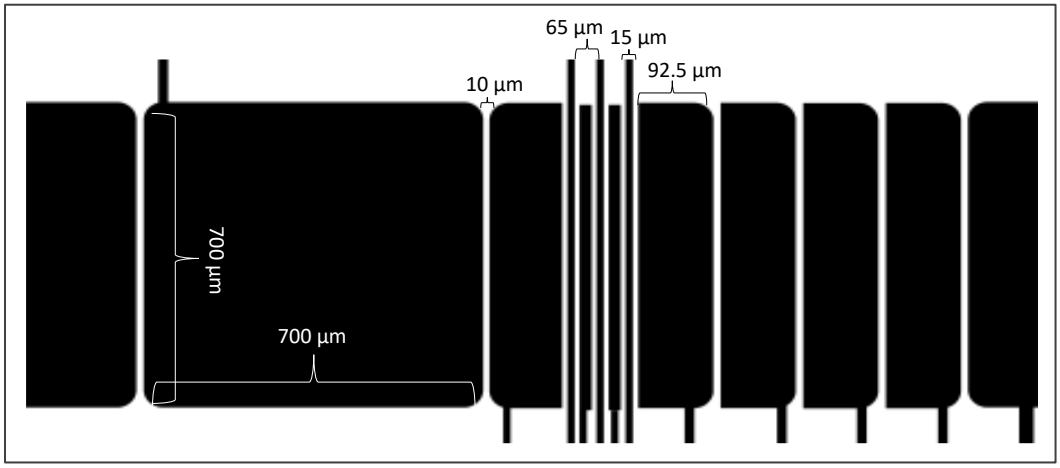

Figure 19: Dimensions shown on a representative photomask of the pull-through device.

Each batch of eight devices was fabricated on a 450 µm thick Si wafer with a 1 µm thick layer of thermally grown oxide (University Wafer, Inc.). First, layers of titanium and copper were sputtered on to the wafer using a Kurt Lesker DC sputter system. Titanium acted as an adhesive layer between the copper and the oxide layer. The copper was the conductive and active component of the bottom plate. After placing the wafers into the sputter system, the chamber was pumped down to 10^{-7} Torr. Prior to depositing the metals, the turbo pump was set to 50%. Then, Ti was sputtered on at 200 W at a deposition rate of approximately 0.6 Å/second. Next, the Cu was sputtered on at 500 W at approximately 5 Å/second.

After deposition, an adhesion primer (MicroPrime ™ P-20) was spun onto the wafer at 3000 rpm for 30 seconds, follow by a positive resist (Shipley Microposit S1813) which was also spun at 3000 rpm for 30 seconds for a thickness of approximately 1.7 µm. The wafers were baked on a hot plate for 1 minute at 115°C prior to exposure. A clear transparency mask (FineLine Imaging) with the device design, was placed on top of the wafer, which was then exposed to 365

nm light at 120 mJ/cm^2 intensity for 11 seconds (Karl Süss MicroTec). Then, the wafers were developed for 60 seconds in Microposit MF-319 developer.

Following patterning, the copper and titanium were etched using copper etchant 49-1 (Transene Company, Inc.) and buffered oxide etchant (BOE), respectively. Copper etchant ideally works by etching at a rate of 40 Å/second and BOE at a rate of 300 nm/minute with agitation. After etching, the photoresist was removed using acetone and IPA and a protective coat of photoresist (NFR 016D2 JSR Micro, Inc.) was spun onto the wafer at 3000 rpm for 30 seconds. The devices were individually cut with a DAD3220 dicing saw (Disco, Inc.).

After removing the protective resist using IPA and acetone, the connector pads of the devices were covered with Kapton tape to protect them during the next step of fabrication. The devices and 2 g of Parylene C were loaded into the Parylene coater (Cookson Electronics LABCOTER), and after the bell chamber was pumped down, 2 µm of Parylene C were deposited onto each device.

Finally, for hydrophobicity, a CYTOP™ layer was spun on at 1000 rpm for 10 seconds, ramping up at 100 rpm/s, then ramped up at 300 rpm/s to 3500 rpm for 45 seconds to achieve an 80 nm thin film. The Kapton tape was removed from the devices, and they were baked at 100°C for 10 minutes followed by a longer bake at 190°C for 20 minutes.

3.1.2 Gasket and Top Plate

1 mm Clarex Clear cast acrylic (Astra Products, Inc.) top plates and 0.12 mm SecureSeal™ (Grace Bio-labs) gaskets were designed with 2D AutoCad drafting software (Autodesk, Inc.) and cut using a laser system (TroTec) at the Pratt Student Shop at Duke University as shown in Figure 20. The gaskets followed the contour of the electrodes and reservoirs so that they created a channel in which liquid handling occurred. The top plates were cut to be slightly larger than the devices and designed with holes that aligned with the reservoirs on the bottom plate. Once the plastic coating

from the acrylic top plates was removed, they were placed into the RF Dielectric Sputter System's (Kurt J. Lesker Co.) vacuum chamber which was pumped down to 10^{-7} Torr. 100 nm of Indium tin oxide (ITO) was sputtered onto the top plates using 110 W for 1.5 hours. Finally, according to the recipe described in the previous paragraph, CYTOP™ was spun onto the top plates and they were allowed to air dry overnight.

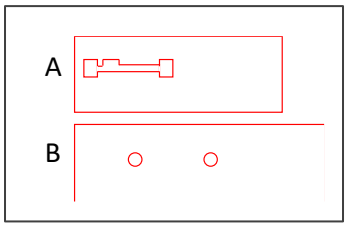

Figure 20: AutoCad outlines of A) the gasket layer and B) the top plate drawn by Zak Tini.

Once the top plates were ready, devices were assembled by removing the backing from the gaskets and joining the bottom and top plates together. First, one side of the gasket layer adhesive cover was removed, and the edge of the gasket layer was aligned with the edge of the bottom plate. The gasket was pressed down using the flat end of a tweezer to ensure that there were no gaps. Next the upper adhesive cover was removed and after aligning the holes of the tope plate with the location of the reservoirs and aligning the edges of the top and bottom plates, the top plate was pressed down onto the adhesive ensuring there were no gaps. A side-view of the completed devices with respective thicknesses of each layer and component is show in Figure 21 below.

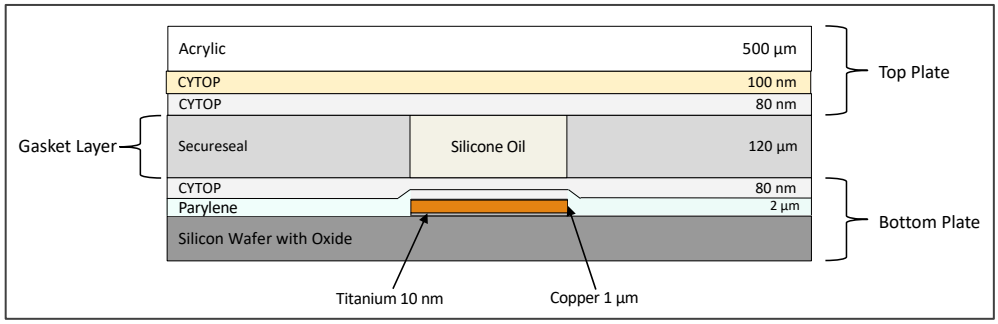

Figure 21: A side-view of a fully assembled device that shows each component and layer along with their respective thicknesses.

Once the devices had been fabricated and assembled, they were connected to their power sources by a PCB relay board and controlled by an Arduino. The following section describes the external systems that support and conduct the devices.

3.2 Experimental Instrumentation

This section details the ancillary electrical systems that control the EWD and magnetic field generation on the devices, the fluorescence excitation and detection instrumentation, and finally, the image acquisition and analysis used to evaluate obtained results.

3.2.1 DMFB Instrumentation

As shown in Figure 23, a waveform generator (Model 33250A, Agilent) coupled with an amplifier (Model F10A, FLC Electronics) for EWD control and an AC power supply for the current wires were connected to a PCB relay board designed by Dr. Zhanwei Zhong, formerly of Prof. Kirshnendu Chakrabarty's Lab at Duke University. Approximately 40-60 V at 1 kHz were necessary to provide adequate voltage to the electrodes to induce EWD of a droplet and 200 mA were applied to the current wires to generate a magnetic field strong enough to capture the magnetic beads used in the immunoassays. These electrical sources were individually connected to the PCB, shown in Figure 22, as inputs and were directed to the device via a AWQ212 Photo-MOS Relay that corresponded to each of the 22 connector pads on the device. This allowed for precise control of which electrode or wire was turned on from either a voltage or a current input, respectively.

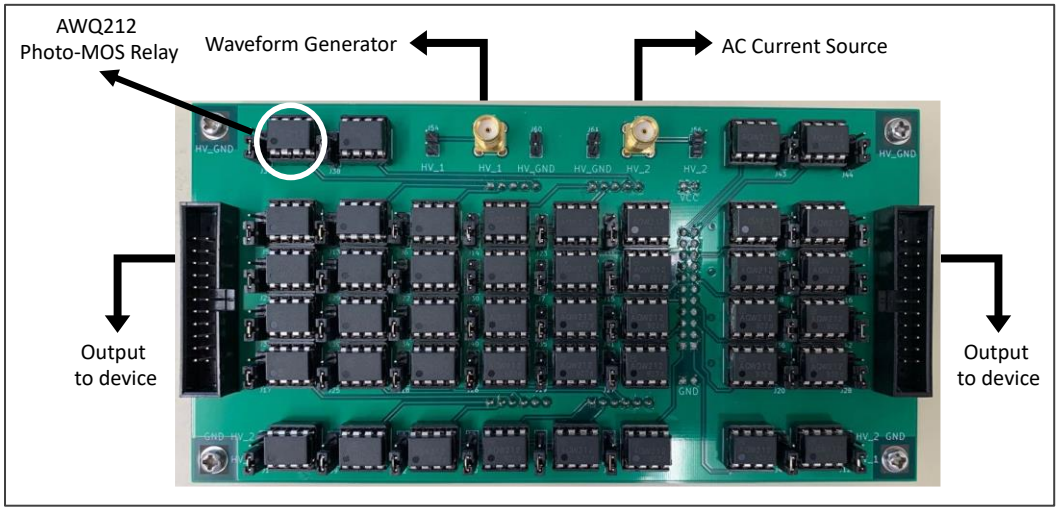

Figure 22: Relay board on PCB with arrows indicating voltage and current sources as well as the ribbon cable connectors that output to the device.

The board communicated with the device through ribbon cables that attached to a spring-loaded clip on a metal stage. The aluminum stage acted as a connector for the translational stage and as a heat sink for the device. The PCB was controlled by an Arduino Mega 2560 (Arduino), which received instructions from an in-house designed GUI written in Python (See Appendix A for Python code). Figure 24C shows a screenshot of the GUI, which allowed the user to selectively turn on and off each electrode or wire. This GUI as well as the optical relay were easily adapted to any device design. Figure 24A shows the relay board and Arduino next to one another and Figure 24B shows a side view of how they were assembled.

Above the translational stage, atop which the device sat, there was a telephoto lens (Optem Zoom 125, Qioptik) attached to a 1280 px x1024 px CMOS sensor camera (Model: acA1300-200uc, Basler) and an LED rechargeable flashlight (Nicchia 219C, RoyVon). The optically clear top plates coupled with the lens, camera, and light source allowed for bright field imaging and monitoring of the devices during experimentation. This same camera and scope were used as part of the fluorescence sensing instrumentation.

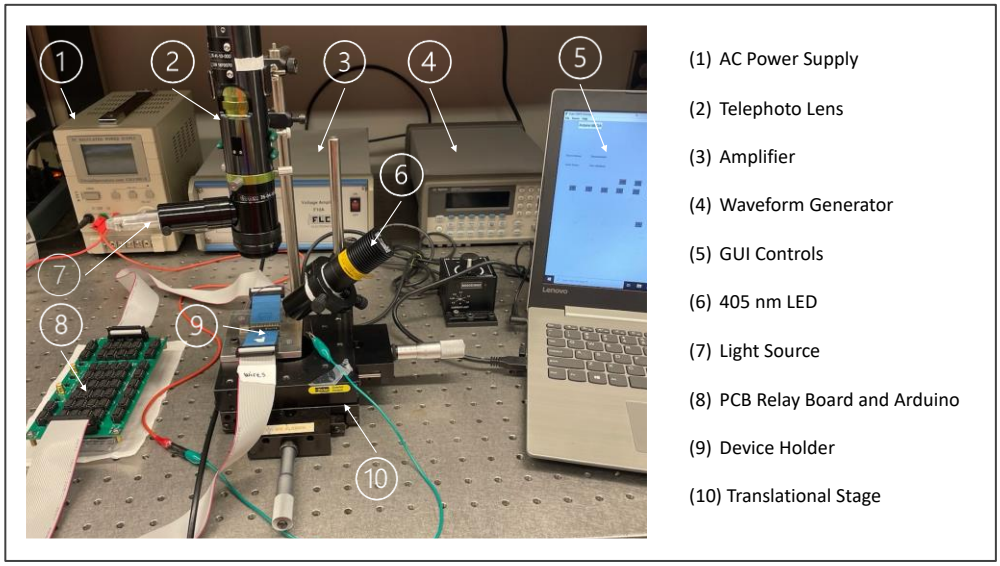

Figure 23: Electrical and optical instrumentation with labelled components.

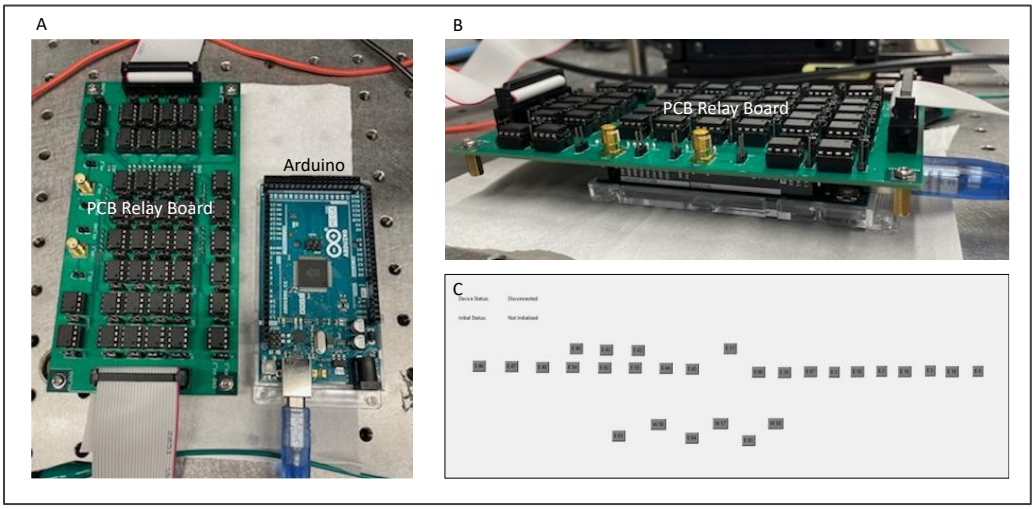

Figure 24: A) PCB relay board and Arduino shown. Each relay received a signal from a digital output pin of the Arduino to switch on signal to a device pin. B) Side view of how the PCB relay board and Arduino were assembled. C) Screenshot of GUI designed in Python used to precisely control which electrode or wire was turned on.

3.2.2 Fluorescence Detection Instrumentation

As discussed in the background section on immunoassays (see section 2.3), an antibody coupled with a fluorophore was used to detect a variety of analytes, namely primary antibodies, nucleosomes, and chromatin. The secondary (i.e., detection) antibody used in all experiments was

Goat anti-Rabbit IgG Alexa Fluor 405 (AF405) (Thermo Fisher Scientific, catalog # A-31556,). Since AF 405 has an excitation wavelength of 400 nm and an emission wavelength of 421 nm, the appropriate filters were chosen to maximize emitted signal. The transmittance of these filters is shown in Figure 25A in red. The schematic in Figure 26B, shows a 405 nm, 1000 mW mounted LED (M405L4, Thorlabs Inc.) coupled with a 395 nm band pass filter (Chroma) to narrow the wavelengths emitted by the wider spectra of the LED. The telephoto lens was fitted with a 420 nm long pass filter (Omega Optical) to capture as much signal emitted from the fluorophore as possible. The spectra for the excitation and emission filters are shown in Figure 25 B and C, respectively.

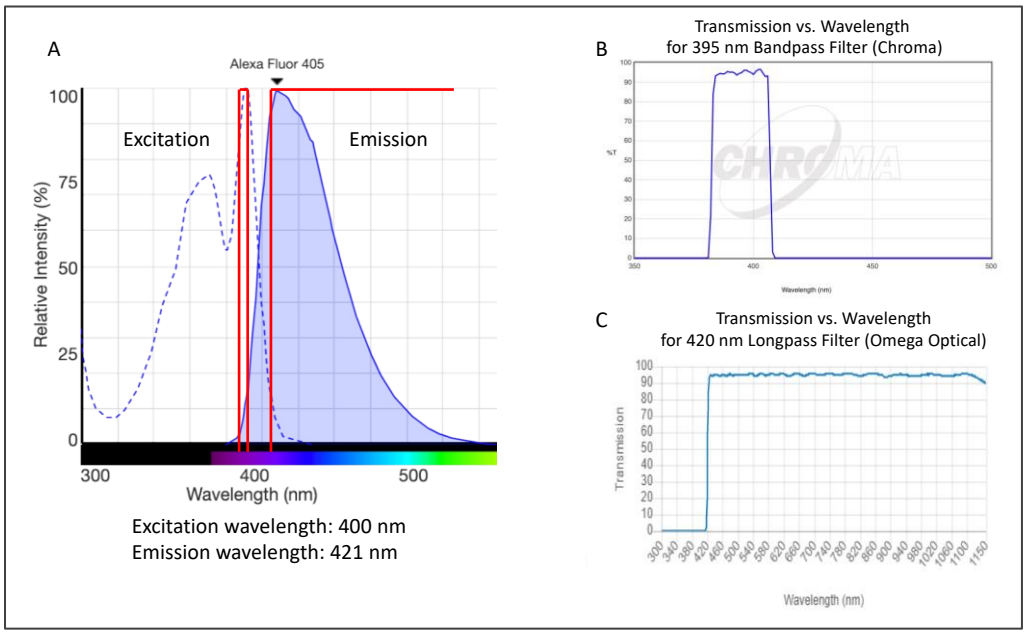

Figure 25: A) Excitation and Emission Spectra for Alexa Fluor 405 [77]. The red lines depict the wavelength ranges for the band pass and the long pass filters. B) Transmission vs. Wavelength for 395 nm Band pass Filter [78]. C) Transmission vs. Wavelength for 420 nm Long pass Filter [79].

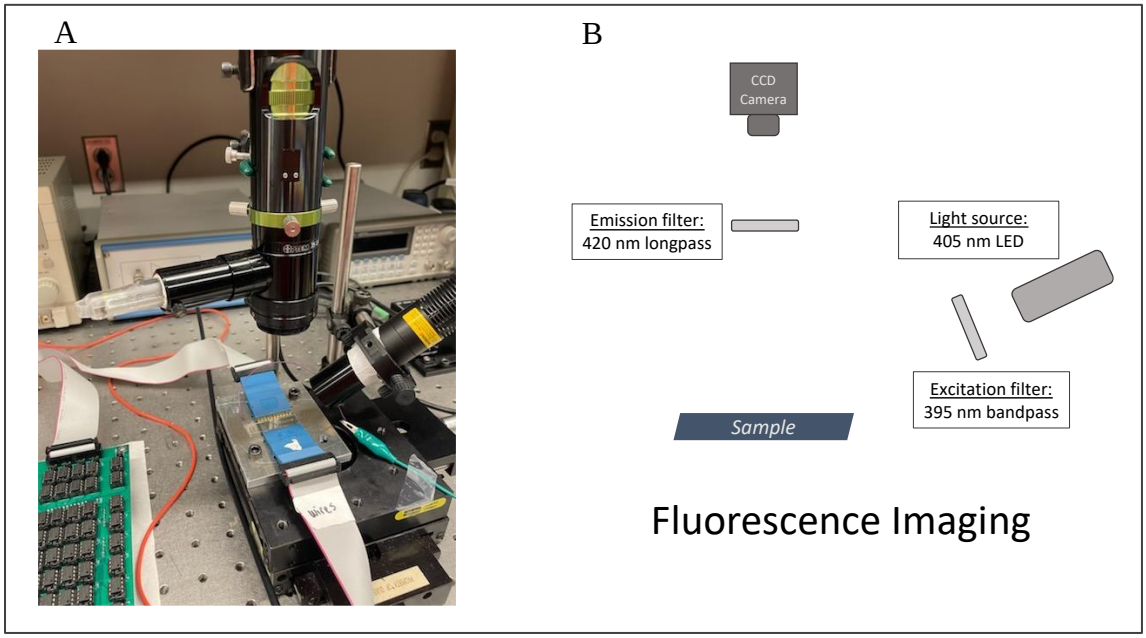

Figure 26: A) An image of the fluorescence imaging instrumentation setup. B) A schematic of the filters, excitation LED and the CCD Camera used to capture images.

Florescence sensing was easily accomplished with a few additions to the setup described in the previous section. As shown in Figure 26A, the 405 nm LED coupled with a focusing lens and band pass filter was mounted on the optical table with a ring at an empirically determined angle, and although not visible in this image, the long pass filter was placed within the telephoto lens. The relative low cost of the LED and the use of a long pass filter, allows for experimental flexibility with other fluorophore conjugated antibodies without greatly changing the setup.

Once the immunoassays were developed and this fluorescence imaging system detected analyte presence qualitatively, the next step was to measure the signals generated to create a semi-quantitative method of detection.

3.3 Image Acquisition and Analysis

This section discusses the analysis method for images taken during experimentation. After a droplet was either actuated or placed on the electrode of interest, the translational stage was used to move the device such that the droplet was in the correct position for exposure to the 405 nm LED. Although the angle of incidence of the LED was critical and empirically determined, the fluorescence emission from the device happened in all directions and therefore was easily captured by the telephoto lens and CCD camera. The 420 nm long pass filter fitted onto the telephoto lens ensured that as much signal as possible emitted from the sample was collected by the CCD camera. After an image was captured, it was stored as a TIFF file and imported into ImageJ Software (NIH). Since the emission wavelength of 420 nm corresponds to the blue visible region, the image was split into its red, green, and blue channels using ImageJ. The ensuing grayscale photo of the blue channel image was used for measurements. ImageJ allows users to select a region of interest (ROI) and measure the average pixel intensity across that region.

As shown in Figure 27 Step 1, droplets of diluted Alexa Fluor 405 were placed onto the device, imaged, and the blue channel was isolated. Step 2 of Figure 27 shows a representative image of magnetic bead-containing droplets that were placed on a device. A current wire was turned on that generated a magnetic field, which captured some of the beads in the droplet. After imaging and isolating the blue channel, the selection tool in ImageJ was used to delineate a rectangular region encompassing the wire of interest and the average pixel intensity within that rectangle was measured. As discussed in the quantitative analysis sections in Chapter 4: Experimental Results, average pixel intensities versus serial dilutions of analytes were measured and graphed in Excel, shown in Step 3 of Figure 27, as a preliminary step towards creating a standard curve for sample quantification.

This described method of image acquisition and analysis was used to compare samples against negative controls, to determine the lower limit of detection of assays and device, and to compare different device designs by calculating bead capture efficiency within a droplet (Chapter 5).

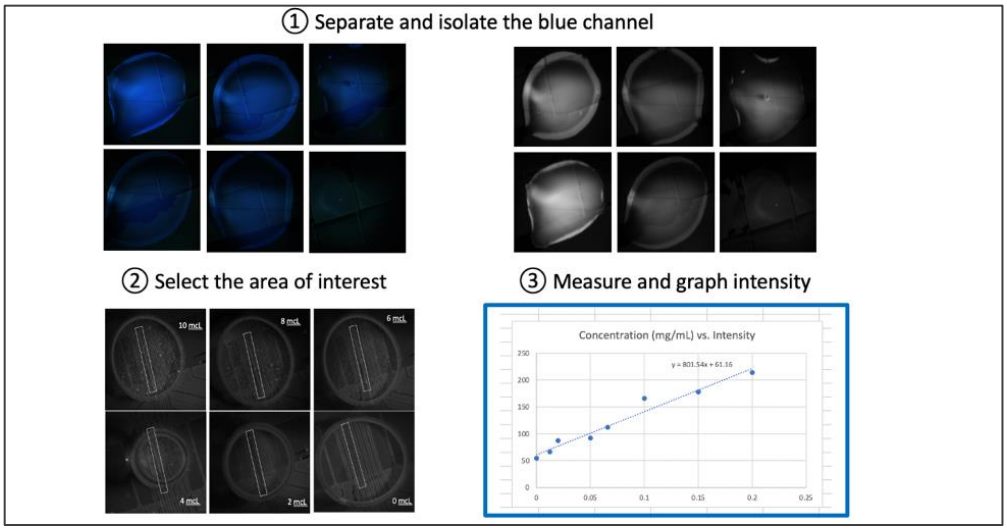

Figure 27: Overall method for image analysis using ImageJ software and Excel. Step 1 shows the raw image acquired by the CCD camera on the right-hand and the isolated blue channel image on the left hand. Step 2 shows a representative serial dilution of magnetic bead containing droplets, wherein the magnetic beads were captured on a single current wire and using ImageJ a ROI was selected for measurement. Step 3 shows a representative graph in Excel of the average pixel intensities measured by ImageJ versus the amount of analyte in a solution.

3.4 Conclusion

The first section of this chapter described the steps required to fabricate DMFBs onto which assay development and immunoprecipitation assays were translated. The relatively simple microfabrication techniques drew from standard industry methods and allowed for batch production of devices. This technique was used for all the devices discussed herein, with only alterations to the transparency photomasks for different device designs.

Similarly, the same instrumentation required to use the devices was consistent for all designs. Section 3.1 of this chapter discussed the external electrical components of the experimental setup. A waveform generator coupled with an amplifier and a DC power supply were connected to

a PCB relay array to provide a voltage source for EWD on the electrodes and a current source through the wire to generate a magnetic field, respectively. This PCB was controlled by an Arduino receiving instructions from an in-house designed GUI written in Python. By simply changing the switch cap on the relays and the device design in the GUI, this setup was easily adapted to the multiple device designs used in the experimental section.

Since fluorescent immunoassays were the platform used for analyte capture and detection, it was necessary to develop a fluorescence measurement system as described in Section 3.2. The system presented herein, was chosen because it was easily integrated with the existing electrical instrumentation. Furthermore, the system is adaptable to different fluorophores by simply switching out the LED and filters used to match the excitation and emission spectra of any new secondary antibody. For the fluorophore used in the ensuing chapter, a 405 nm LED fitted with a 395 nm band pass excitation filter and focusing lens was used to excite the detection antibody. The Alexa Fluor 405 conjugated antibody had an emission wavelength of 421 nm. This signal was collected using a telephoto lens fitted with a 420 nm long pass filter and coupled with a CCD camera.

Finally, section 3.3 discussed the acquisition and analysis of images used to compare samples qualitatively and quantitatively against their controls, determine assay and instrumentation specifications such as sensitivity and specificity, and compare device designs. This method used the images acquired by the CCD camera and imported them into an image analysis software, ImageJ. The blue channel of the images was isolated, a region of interest was selected, and the average pixel intensity over that region was measured. These measurements were then graphed to visualize and quantify the results.

In summary, this chapter detailed the device fabrication, external instrumentation, and analysis techniques that were used to successfully perform and assess the immunoassays developed and discussed in Chapter 4.

4. Assay Protocols and Experimental Results

The previous three chapters have laid out the primary motivation, fundamental theories, fabrication techniques, and experimental methods that enable the studies and results discussed in this chapter. The research presented herein was driven by the need to improve standard benchtop chromatin immunoprecipitation (ChIP) protocols for use on-chip. The solution proposed was to adapt ChIP to a digital microfluidic biochip (DMFB). The results from each section built on one another and inform the ensuing study.

In this chapter, the details of assay protocols are described followed by experimental results obtained by performing the assays on-chip. The first assay developed was a validation assay to determine the parameters of the fluorescence detections system and to determine whether a bead-based assay was possible on-chip. With the external control and detection systems parameterized, the next step was to develop an assay to detect nucleosomes on-chip. Following successful detection and quantification of nucleosomes, the studies shifted towards the detection and then immunoprecipitation of chromatin.

4.1 System Validation Assay

As discussed in detail in section 1.1, the building blocks of chromatin are nucleosomes. In turn, nucleosomes are comprised of two pairs each of four core histone proteins: H2A, H2B, H3, and H4. Therefore, in benchtop ChIP protocols, an antibody against one of the histones to isolate the chromatin is commonly used. However, prior to testing with more complicated and expensive chromatin samples, a system validation assay was developed to simply detect the presence of the antibody against the H4 histone, namely Anti-H4. A fluorophore conjugated secondary antibody was used for detection. The next section details a detection study to determine the parameters of the fluorescence detection instrumentation.

4.1.1 Materials

This section details the reagents and the protocol that were used and in the Anti-H4 assay. Table 3 lists the reagent used, their function in the assay, and the manufacturer.

Table 3: List of reagents used in the Anti-H4 benchtop assay.

Reagent	Function	Manufacturer	Catalog No.
Rabbit anti-Human Histone H4 antibody (Anti-H4)	Analyte	Abcam	Ab10158
Goat anti-Rabbit IgG Alexa Fluor 405 antibody (AF405)	Detection Antibody	Thermo Fisher Scientific	A-31556
Protein G magnetic beads	Capture platform	Dynabeads ™	10003D
20x PBS-Tween Buffer (PBST)	Buffer Solution	Pierce™	28352

4.1.2 Methods

First, 2.5 ml of the PBST buffer solution were diluted in 47.5 ml of deionized water to create the 1X PBST liquid phase that all the experimentation was carried out in. Next, a positive Anti-H4 containing sample was prepared in a micro-PCR tube. The positive sample, containing 10 µl of Ant-H4 and 10 µl of AF405 in 80 µl of 1x PBST, was incubated at room temperature for 30 minutes on rotation. A negative sample containing 10 µl of AF405 in 90 µl of 1x PBST was also incubated at room temperature for 30 minutes. Due to the light sensitive nature of AF405, this protocol was carried out in near darkness and the samples were either covered in aluminum foil or kept out of direct light.

Prior to the next step, the Protein G magnetic beads were washed using the following procedure. The stock solution was gently swirled to resuspend all the beads without the generation of bubbles. Next, 40 µl of beads were removed and placed into a micro-PCR tube and held against a magnet. After all the beads had migrated towards the magnet (approximately 15-20 seconds), the supernatant was removed using a pipette placed gently on the side opposing the mass of beads. Then, the beads were resuspended in 200 µl of PBST after which they were placed against a magnet

and the supernatant was discarded. This procedure was repeated a total of 3 times. The beads were resuspended to a final volume of 40 µl and separated into two 20µl partitions in separate micro-PCR tubes. The supernatant was removed from both tubes, prior to the next step.

After the initial incubation, the sample, and the control, totaling 100 µl each, were added to the pre-washed Protein G beads and incubated for 30 minutes at room temperature on rotation. After this final incubation, the beads were washed three more times to ensure that any excess reagents were removed. Both the sample and control were resuspended in a final volume of 200 µl of PBST. The general procedure is shown in Figure 28 below. The figure depicts Rabbit Anti-Human Histone H4 antibody (pink) incubated first with the Goat Anti-Rabbit AF 405 conjugated secondary antibody (orange). The constant region of the Anti-H4 is Rabbit and therefore binds to the active region of the AF405 antibody. The Anti-H4 constant region also binds to the magnetic bead. In the negative control, however, due to the lack of Anti-H4 and the AF405's preferential binding to Anti-H4, nothing binds to the magnetic bead, and all excess AF450 is washed away.

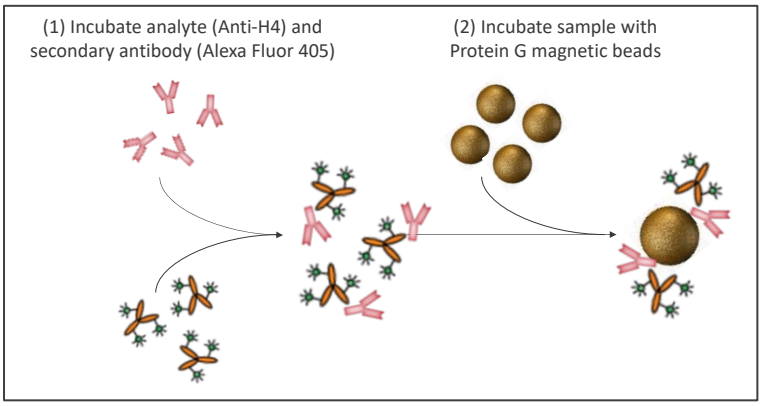

Figure 28: General procedure for Anti-H4 Assay.

The following sections discuss the implementation of this assay as a verification of the parameters of the fluorescence measurement system.

4.1.3 Detection Study

The objective of the detection study was to determine whether the fluorescence measurement setup would detect the presence or absence of an analyte using an Alexa Fluor 405 conjugated antibody as the detection probe. To briefly recapitulate the setup described in 3.2.2, Figure 29A shown below shows the spectral data for the AF405 and the transmittance regions for the filters in red. Figure 29B is a schematic of the fluorescence measurement system setup. The current wire device introduced in 3.1.1 was used. The benchtop assay protocol was the same as described in section 4.1.2.

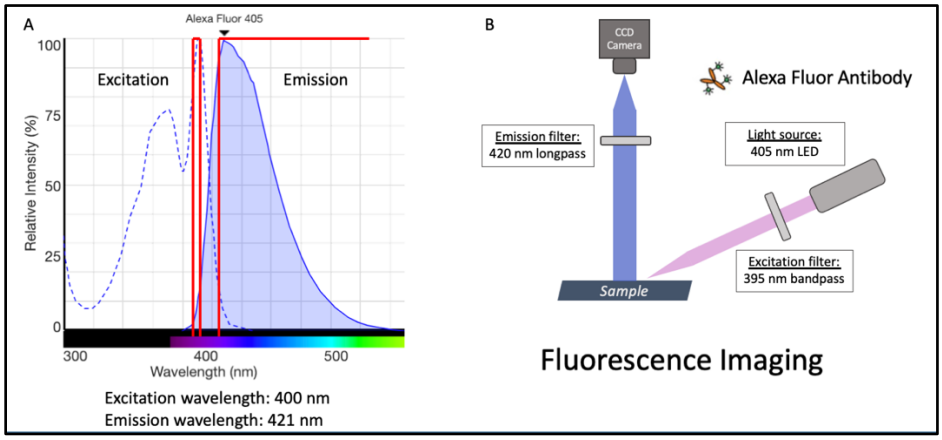

Figure 29: A) Excitation and Emission Spectra for Alexa Fluor 405 [77]. The red lines depict the transmittance for the band pass and the long pass filters. B) Fluorescence Imaging setup.

This section details the on-chip portion of the protocol and the results obtained from these preliminary experiments.

4.1.3.1 Experimental Protocol

After performing the protocol described in section 4.1.2, an approximately 50 nl droplet of either the control or the positive sample was placed onto a bottom plate of a current wire device. Next, the 405 nm LED (Thor Labs) was turned on and the translational stage was moved until the droplet was visible under the camera. The LED had to be positioned and angled in such a way that it would hit the droplet at the same location that it was under the camera. Following these studies, the position of the LED was finalized with respect to the device and the camera. Therefore, droplet placement, light exposure, and imaging would be consistent between samples for subsequent studies.

4.1.3.2 Experimental Results

Figure 30 below shows the results from the Anti-H4 detection assay. Figure 30A is a positive sample droplet placed onto the device and imaged as described above. The sample was fluorescing, and the beads were dispersed throughout the droplet. In Figure 30B an external magnet was held above the sample. The beads migrated towards the magnet and the supernatant remained clear, showing that it was in fact what was bound to the beads that was fluorescing and not the supernatant. Figure 30C is a bright field image of the negative control to show that there were beads present in the droplet despite that in Figure 30D the droplet did not fluoresce, as expected since no Anti-H4 was present. The extremely bright artifacts in Image 30A and B were dust particles.

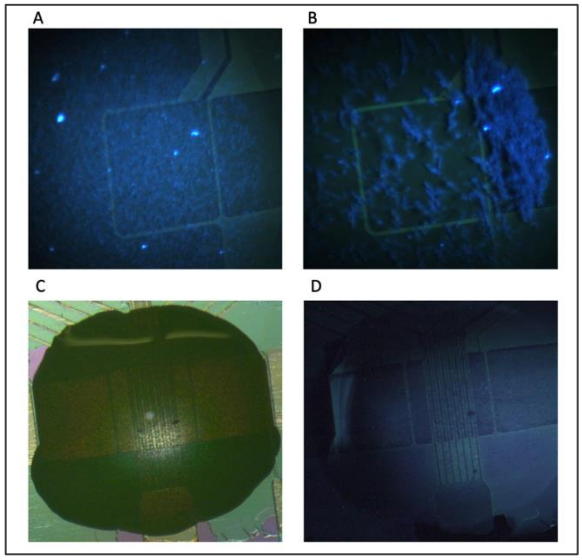

Figure 30: Anti-H4 Assay Detection Study Results. A) Positive sample droplet placed on a current wire bottom plate. B) The same droplet imaged again with an external magnet held above. C) Bright field image of the negative control to show density of beads. D) Negative control droplet placed on same current wire bottom plate; no signal was detected.

4.1.4 Conclusion

The results from the Anti-H4 detection study showed that the fluorescence sensing system can detect Alexa Fluor 405 bound antibodies on a magnetic bead scaffold in a droplet on a DMFB. The next study focused on developing a quantitative image analysis method simply using Goat Anti-Rabbit Alexa Fluor 405 antibody.

4.2 Image Analysis Methodology Development

This study focused on the development of an image analysis methodology that would preclude the necessity for visual verification of results by the user. This method was used in subsequent studies to compare samples against their controls, for semi-quantitative measurement of analytes, and to compare bead capture efficiency of different devices.

4.2.1 Materials

In this study, Goat Anti-Rabbit IgG Alexa Fluor 405 antibody (AF405) (Thermo Fisher Scientific, Cat. # A-31556) was both the analyte and the source of fluorescence. First, 1X PBS-

Tween (PBST) was prepared using 2.5 ml of the 20X PBST buffer solution (Pierce™, Cat. #28352) were diluted in 47.5 ml of deionized water. Next, a serial dilution of AF405, 0-0.2 mg/ml, was made in the 1X PBST solution. Table 4 shows how the serial dilution was made.

Table 4: Volumes for experimental dilution.

Volume of AF405 (µl)	Volume of PBS (µl)	Final Concentration (mg/ml)
0	50	0
3.1	46.9	0.01
6.2	43.8	0.02
12.5	37.5	0.05
25	25	0.1
50	0	0.2

4.2.2 Experimental Protocol and Results

Since AF405 is light sensitive, the following procedure was carried out in darkness and the samples were either under foil or out of direct light except during imaging when they were exposed to a 405 nm LED (Thor Labs) for excitation. An approximately 50 nl droplet from each solution was placed onto the bottom plate of a current wire device. Then, using the stage, the droplet was moved under the camera and in direct line of the LED. Once all the droplets had been imaged, the images were saved as TIFF files and were imported into ImageJ software (NIH) as shown in Figure 31 below.

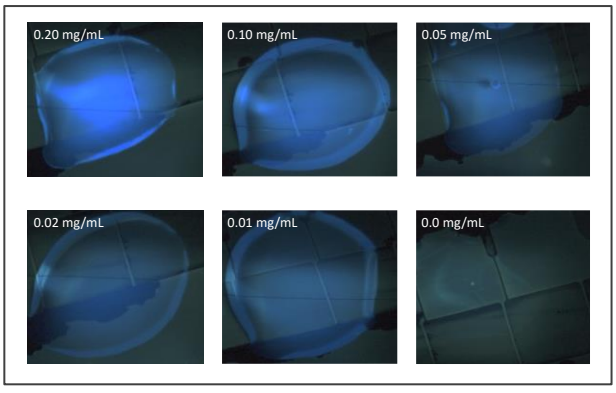

Figure 31: Fluorescence images of AF405 serial dilution droplets on a DMFB.

Since the emission wavelength of AF405 is 420 nm, which corresponds to the blue visible region, the image was split into its red, green, and blue channels. The ensuing grayscale photo of the blue channel image, Figure 32, was used for measurements.

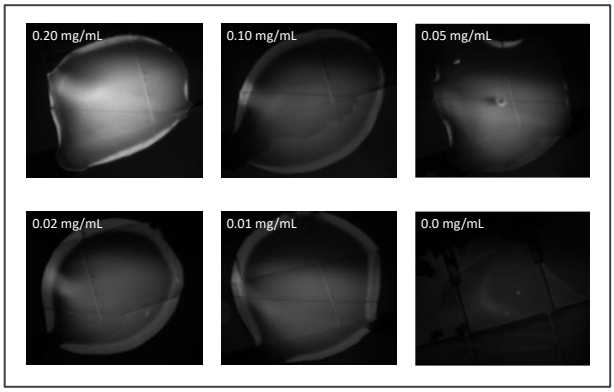

Figure 32: Isolated blue channel images of AF405 serial dilution droplets on a DMFB.

ImageJ allows users to select a region of interest (ROI) and measure the average, minimum, and maximum pixel intensity across that region. In this study, as shown in Figure 33A, the entirety of the droplet was selected and measured using ImageJ. The resulting area, mean, minimum, and maximum values are shown in Figure 33B. The maximum pixel intensity was graphed against the concentrations of the droplets, shown in Figure 34.

A

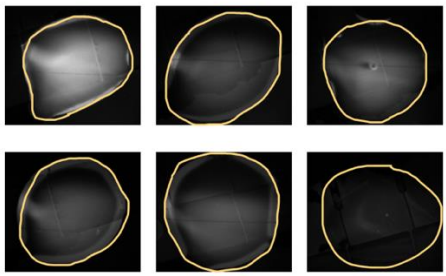

B

Concentration (mg/mL)	Area	Mean	Min	Max
0.2	113118	78.908	0	214
0.1	116720	50.394	2	166
0.05	104748	37.985	1	92
0.02	114658	19.635	1	87
0.0125	87550	19.377	1	66
0	147989	8.226	0	54

Figure 33: Image analysis results. A) A region of interest consisting of the entire droplet was selected by hand on the blue channel image in ImageJ. B) The resulting area, mean, minimum, and maximum pixel intensities were measured.

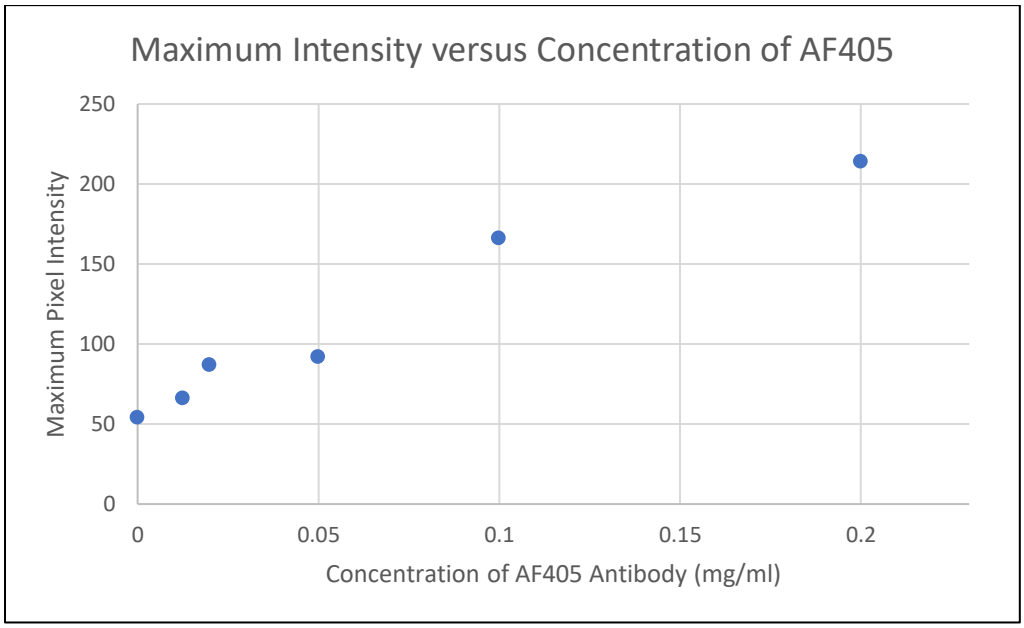

Figure 34: Maximum pixel intensity versus Concentration of AF405 Antibody (mg/ml).

As seen in the Figure 33, the area selected by hand varied between droplets and the presence of light reflections in the droplets added a high degree of variation between droplet measurements. To counteract these issues in subsequent studies, the magnetic beads were isolated onto a single current wire on the device and the fluorescence was measured on that wire alone. Furthermore, a set of commands were programed for ImageJ to follow so that it would treat each image equally. The droplets were actuated onto a particular electrode, were held in place, and the beads were isolated onto a single current wire, so ImageJ was able to select the same area on each device, for each droplet, for each study. Furthermore, the integrated density of pixel intensity was used for semi-quantitative analyses. These modifications standardized the protocol and ensured greater uniformity and reproducibility.

4.2.3 Conclusions

Having established a working fluorescence measurement system and an image acquisition and analysis protocol, the next step added complexity to the assay and detected the building blocks of chromatin, nucleosomes. Section 4.3 discusses the procedure and results from two nucleosome immunoprecipitation assay studies. The first study focused on detecting a specific nucleosome modification and the second study generated data for semi-quantitative analysis.

4.3 Nucleosome Immunoprecipitation Assay

Fundamentally, the study of epigenetics is linked with DNA structure, how it is packaged, stored, and utilized in the cell nucleus. Every 147 base pairs the DNA helix wraps around a nucleosome, an octameric structure consisting of four pairs of protein monomers, namely the histones H2A, H2B, H3, and H4. These nucleosomes are the building blocks of chromatin [1]. Post-translational modification sites of nucleosomes are markers that signal nuclear events which modify chromatin structure. Thus, studying the 'nucleosome code' is inherently critical to understanding epigenetic controls at their most fundamental levels as well as the functionality of chromatin [19].

Herein, a Nucleosome Immunoprecipitation (NuIP) assay is introduced that targeted post-translationally modified nucleosomes with fluorescent antibodies using magnetic beads. This assay was developed for use on a digital microfluidic biochip (DMFB) to address the throughput, sample size, and antibody variability drawbacks inherent to other methods of detection.

The NuIP assay can be used to detect a particular nucleosome modification but can also be used as an assay development platform for other techniques. The following sections discuss the workflow and implementation of the NuIP assay on a DMFB through (1) results of a verification study to determine if the assay developed was viable, (2) results of a semi-quantitative analysis study that established the protocols for standard curve derivation and quantitative comparisons, and

(3) the results of a complex sample study that assessed the specificity of the antibodies used and the ability of the NuIP assay to perform as an antibody screening tool.

4.3.1 Materials and Methods

The table below shows the reagents used in the NuIP assay, their role in the assay, their manufacturers, and their catalog numbers.

Table 5: List of reagents used in NuIP assay.

Reagent	Function	Manufacturer	Catalog No.
Human H3K4me2 Biotinylated Nucleosome (H3K4me2)	Analyte	Epicypher	16-0334
Rabbit anti-Human Histone H3K4me2 Antibody (Anti-H3K4me2)	Primary Antibody	Epicypher	13-0027
Goat anti-Rabbit IgG Alexa Fluor 405 Antibody (AF405)	Detection Antibody	Thermo Fisher Scientific	A-31556
M280 Streptavidin-coupled magnetic beads	Capture platform	Dynabeads ™	11205D
20x PBS-Tween Buffer (PBST)	Buffer Solution	Pierce™	28352

The general procedure for the NuIP is shown in Figure 35 below. The figure depicts the biotinylated human H3K4me2 nucleosome (blue) incubated first with the M280 streptavidin coated beads. The biotinylated ends of the nucleosomes bind to the streptavidin on the surface of the beads. Simultaneously, Goat Anti-Rabbit AF 405 conjugated secondary antibody (orange) was incubated with the Rabbit Anti-H3K4me2 primary antibody (pink). The constant region of the Anti-H3K4me2 was Rabbit and therefore would bind to the active region of the Goat Anti-Rabbit AF405 antibody, forming a detection complex. This detection complex was then incubated with the sample. The active region of the Anti-H3K4me2 binds to the nucleosomes, which are bound to the beads. In the negative control, however, due to the lack of H3K4me2 nucleosomes, the detection complex had nothing that allowed binding to the magnetic beads, and all excess detection complex was washed away.

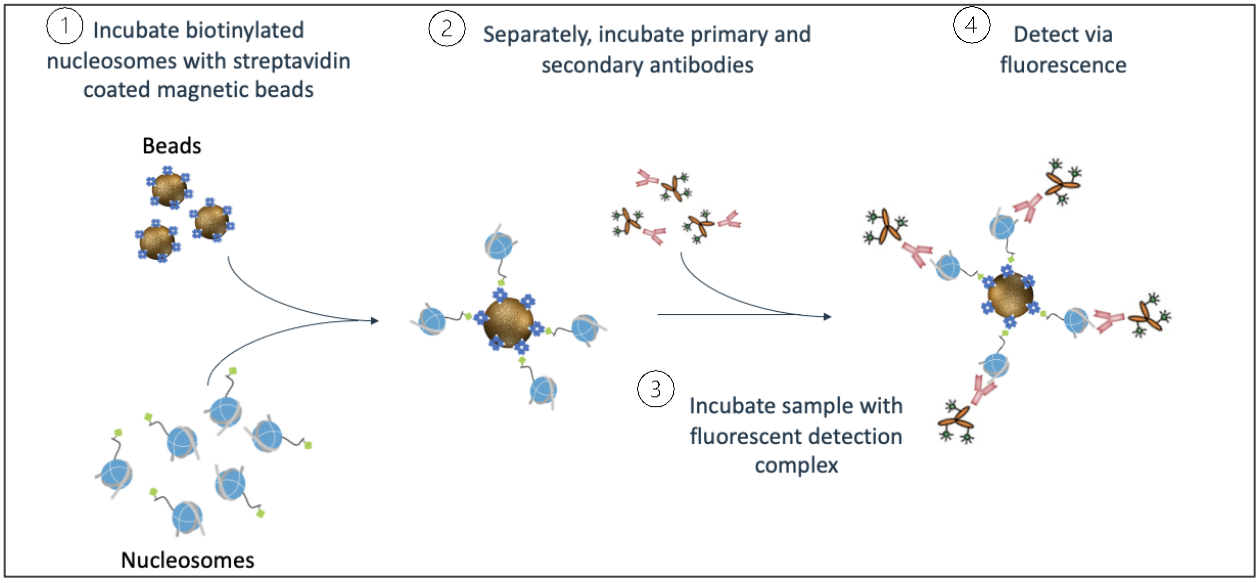

Figure 35: Nucleosome Immunoprecipitation assay schematic [80].

The following paragraphs detail the assay shown above. First, 2.5 ml of the PBST buffer solution were diluted in 47.5 ml of deionized water to create the 1X PBST liquid phase which was used in all the experimentation. Next, the M280 magnetic beads were washed. The stock solution was gently swirled to resuspend all the beads without the generation of bubbles. Then two 60 µl aliquots of the suspended beads were removed and placed into micro-PCR tubes and held against a magnet. After all the beads had migrated towards the magnet (approximately 15-20 seconds), the supernatant was removed using a pipette placed gently on the side opposing the mass of beads. Then, the beads were resuspended in 200 µl of PBST after which they were placed against a magnet and the supernatant was discarded. This procedure was repeated a total of 3 times. The beads were resuspended to a final volume of 180 µl for the sample and 200 µl for the negative control.

20 µl of H3K4me2 nucleosomes was added to the sample tube. Then, both the sample and the control were incubated at room temperature for 30 minutes on rotation. Meanwhile, in two separate micro-PCR tubes, the detection complex consisting of 20 µl of Anti-H3k4Me2, 20 µl of AF405, and 160 µl of PBST, were incubated at room temperature for 30 minutes on rotation. Due

to the light sensitive nature of AF405, this protocol was carried out in near darkness and the samples were either covered in aluminum foil or kept out of direct light.

After the initial incubation, the sample and control were held against a magnet, the supernatant was removed, and the beads were washed as described above. This step removed any unbound nucleosomes from the beads. Then the 200 µl detection complex solutions were added to both the sample and the control and incubated for 30 minutes at room temperature on rotation. After this final incubation, the beads were washed three more times to ensure that any excess reagents were removed. Both the sample and control were resuspended in 200 µl of PBST.

4.3.2 Experimental Protocol and Results

4.3.2.1 Detection Study

After performing the protocol described in section 4.3.1, an approximately 0.1 µl droplet of either the control or the positive sample was placed onto a bottom plate of a current wire device. Before imaging, a top plate was placed atop the device, which already had the gasket attached to the bottom plate. Next, the 405 nm LED (Thor Labs) was turned on and the translational stage was moved until the droplet was visible under the camera.

The results from the detection study are summarized in the images shown in Figure 36 below. The negative control droplet that did not contain any nucleosomes is shown in Figure 36A and the nucleosome-containing sample droplet is shown in Figure 36B. An external magnet was used to show that the beads, not the supernatant, were fluorescing, as shown in Figure 36C. The same control and sample were then deposited into the reservoir of a DMFB. Figures 36D and 36E show that the sample was manipulated and transported on a DMFB using EWD and on-chip current mediated magnetic control.

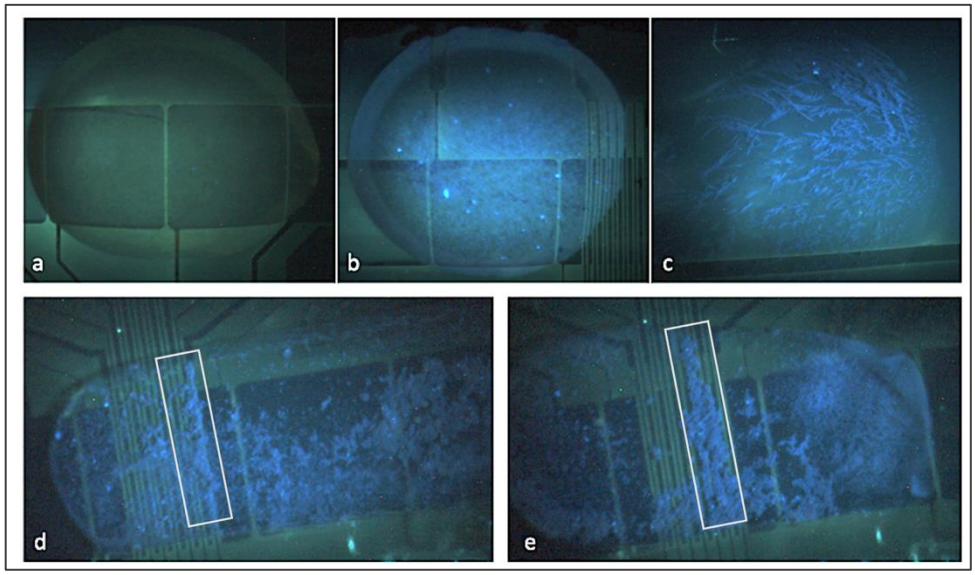

Figure 36: NuIP assay results. A) Negative control B) Nucleosome containing sample C) Sample in presence of external magnet. D, E) Actuated sample droplet and current wire magnetic activation. The white rectangles indicate magnetic accumulation of beads on a current wire [80].

Having successfully demonstrated that the benchtop NuIP protocol could be detected on the device and that the product could be actuated on-chip, the next step was to run a semi-quantitative analysis on the NuIP assay using the image analysis method described in Chapter 3 Section 3.

4.3.2.2 Semi-Quantitative Analysis Study

Next, a series of samples ranging from 0 µl - 20 µl of stock H3K4me2 biotinylated nucleosomes were immunoprecipitated using the same protocol outlined in 4.3.1 to develop a semi-quantitative method of analysis. The concentrations were prepared individually as per the table below.

Table 6: Volumes of H3K4me2 and diluent PBS used to prepare samples for NuIP semi-quantitative analysis study.

Volume of H3K4me2 (µl)	Volume of PBS (µl)	Final Concentration (µg/ml)
0	20	0
5	15	0.025
10	10	0.05
15	5	0.075
20	0	0.1

For each concentration a droplet was introduced into the DMFB reservoir of a current wire device. This droplet was actuated to the current wire electrode, where the beads were concentrated onto a single wire. Next, using the ImageJ algorithm discussed in 3.3, an image was taken and split into its separate red, blue, and green color channels. For each concentration, using the blue channel image, equal rectangular areas in the same location were used to analyze the pixel intensity average over that area. Four droplets of each concentration were measured. The averaged droplet values, normalized by subtracting the intensity of the control droplet, are shown in the graph below.

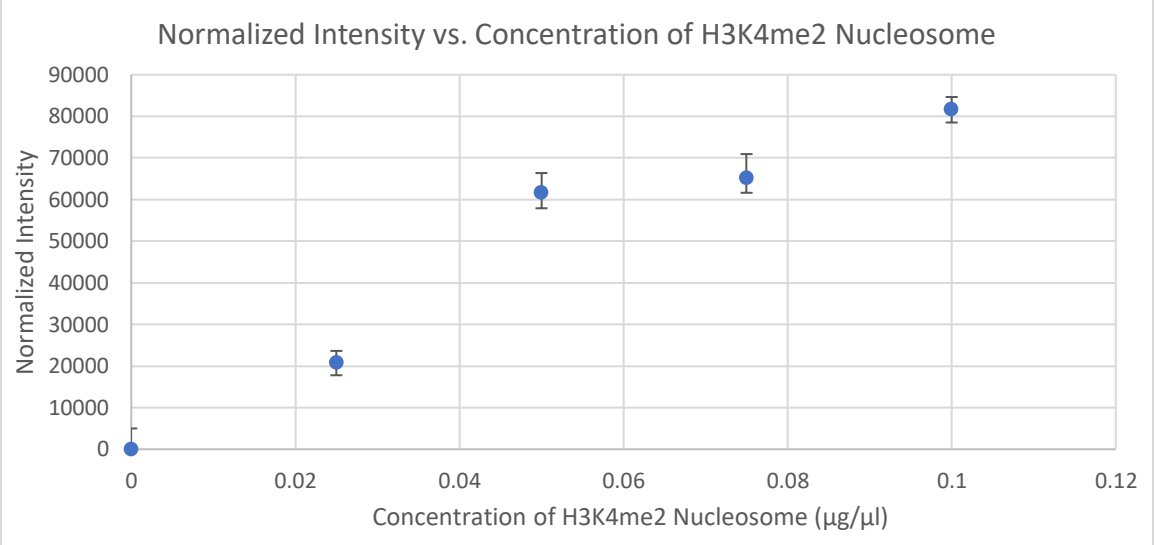

Figure 37: Normalized Intensity vs Concentration of H3K4me2 Nucleosomes [80]. The error bars show the spread in the values.

Having developed a method of quantitative analysis, we can ascertain the limit of detection of an assay as well as develop a standard curve to calculate unknown sample concentrations. Furthermore, this same methodology can be used to compare signal intensity of a set of samples

under different experimental conditions. The next study utilized this feature to determine whether antibodies from different manufacturers against the same histone modification were equally detectable.

4.3.2.3 Antibody Specificity Study

A complex sample consisting of 20 µl of histone H3K4me2 (the target analyte, EpiCypher, 16-0334), 5 µl of histone H3K9me3 (EpiCypher, 16-0315), and 5 µl of human chromatin (Active Motif, 53015) was incubated with a one of three antibody cocktails. Each cocktail had 20 µl of one of the three anti-H3K4me2 antibodies from different manufacturers (Epicypher, Abcam, and BPS), 10 µl of anti-H3K9me2 (Epicypher), 10 µl anti-H4 (Abcam), and 10 µl of anti-H3 (Abcam). This experiment was designed to test the specificity of the antibodies and to showcase the difficulty and variability that is a part of antibody selection. The sample and antibody cocktail were prepared as in the NuIP assay described in section 4.3.1. After performing the immunoprecipitation, one droplet of the control and one of each sample was actuated onto the current wire device. The beads were concentrated onto a single wire and the average pixel intensity of the blue channel image was measured using ImageJ software. The results are summarized in the bar graph and table below.

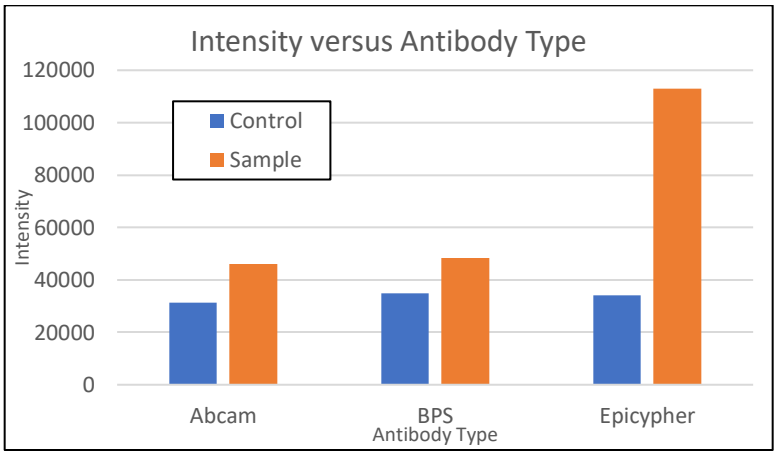

Figure 38: The bar graph shows the intensity of signal versus the type of antibody used to detect the antigen H3K4me2. The blue columns represent the negative controls for each experiment.

Table 7: Summary of antibody specificity study showing that only Epicypher was able to detect the analyte.

Antibody- Anti H3K4me2	Antigen Detected?
Epicypher	YES
Abcam	NO
BPS Bioscience	NO

This bar graph compares the control droplet and the sample experiment as well as the different samples. The chart simply summarizes the results, which show that even though the antibody from all three manufacturers was listed as compatible with the antigen H3K4me2 histone, they all were not able to detect with the same intensity. In fact, the signals from the Abcam and BPS Bioscience antibodies were not significantly distinguishable from the negative controls.

4.3.3 Conclusion

The NuIP assay provides a novel, yet simple, method for confirmatory experiments when developing benchtop protocols and fine-tuning diagnostic methods prior to performing expensive and time-intensive downstream analyses such as mass spectroscopy, liquid chromatography, and next-generation sequencing. This assay can be used to determine the specificity and sensitivity of each antibody option and between manufacturer's batches of antibodies to ensure reproducibility of assay conditions and reliability of results. Furthermore, the NuIP studies laid the foundation on which the chromatin assays in the next sections were built.

4.4 Chromatin Detection Assay

Although the traditional, primary tool to study epigenetics is Chromatin Immunoprecipitation, the method suffers from key drawbacks. Transitioning from ChIP performed on a benchtop to a DMFB platform will help to address these issues. First, utilizing smaller volumes reduces reaction times and reagent and sample use, while providing greater granularity and higher resolution when probing a sample. Automation will decrease turnaround and hands-on time for users. Parallel operations and multiplexing will increase throughput. Finally, streamlining ChIP onto one device greatly reduces sample loss, thereby expanding the types of possible studies to include low-yield and rare tissue types.

The detection assay herein, presents the foundational work towards translating ChIP from the benchtop onto a DMFB.

4.4.1 Materials and Methods

This section details the materials used in the chromatin detection assay and the assay protocol itself. The chart below lists the reagents, their roles in the assay, the manufacturer, and the catalog number.

Table 8: List of reagents used in the chromatin detection assay.

Reagent	Function	Manufacturer	Catalog No.
HeLa Chromatin	Analyte	Active Motif	53015
Rabbit anti-Human Histone H3 Antibody (Anti-H3)	Primary Antibody	Active Motif	91299
Goat anti-Rabbit IgG Alexa Fluor 405 Antibody (AF405)	Detection Antibody	Thermo Fisher Scientific	A-31556
Protein G magnetic beads	Capture platform	Dynabeads ™	10003D
20x PBS-Tween Buffer (PBST)	Buffer Solution	Pierce™	28352

The general procedure for the chromatin detection assay is shown in Figure 39 below. First, purified human chromatin (blue) was incubated with Anti-H3 primary antibody (pink) and AF405 secondary antibody (orange). The active region of the primary antibody would bind to the histone H3 on the chromatin and the AF405 would bind to the constant region of the primary antibody as shown. Then, the samples were incubated with protein G coated magnetic beads. The steric hindrance from binding to the chromatin, did not allow the Anti-H3 primary antibody to bind to the surface of the magnetic bead. Therefore, after washing the beads to remove any unbound materials, the chromatin containing sample did not fluoresce, while the negative control did.

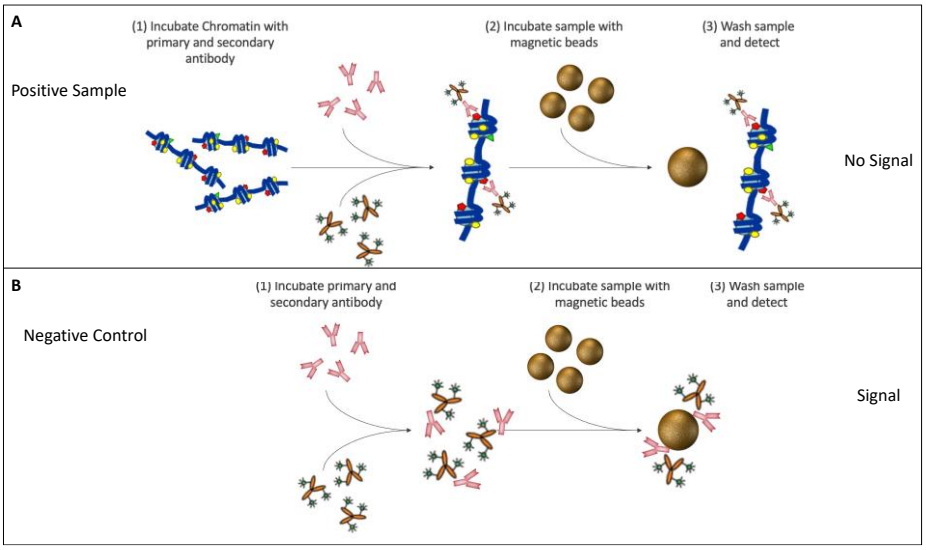

Figure 39: Chromatin detection protocol. A) The protocol and expected outcome of a positive chromatin containing sample are shown. This sample did not fluoresce. B) A negative control protocol and expected outcome are shown. This sample did fluoresce.

The following paragraph details the assay shown above. First, 2.5 ml of the PBST buffer solution were diluted in 47.5 ml of deionized water to create the 1X PBST buffer that all the experimentation was carried out in. Next, the sample (containing 50 µl of Chromatin, 5 µl of Anti-H3, 10 µl of AF405 in 35 µl of PBST) and the control (containing 5 µl of Anti-H3, 10 µl of AF405 in 85 µl of PBST) were incubated at room temperature for 1 hour on rotation. Near the end of that

incubation, the protein G beads were prepared. First, the stock bottle of protein G beads was gently rotated to resuspend all the beads without generating any air bubbles. Then two aliquots of 20 µls each of the beads were placed in separate micro-PCR tubes and placed against a magnet. After all the beads had migrated towards the magnet (approximately 15-20 seconds), the supernatant was removed using a pipette placed gently on the side opposing the mass of beads. Then, the beads were resuspended in 200 µl of PBST after which they were placed against a magnet and the supernatant was discarded. This was repeated a total of 3 times. After the initial incubation, the sample and negative control were added to the protein G beads and incubated for 1 hour at room temperature on rotation. After the final incubation, the supernatant was discarded, and the beads were washed with PBST three times using the method described above to remove any unbound reagents. The beads were resuspended in 200 µl of PBST.

4.4.2 Experimental Protocol and Results

4.4.2.1 Detection Assay

Approximately 0.1 µl of each the sample and the negative control were placed onto the bottom plate of a current wire device fitted with a gasket. Before imaging, the top plate was placed onto the device. Then the 405 nm LED was turned on and the droplet was moved under the camera.

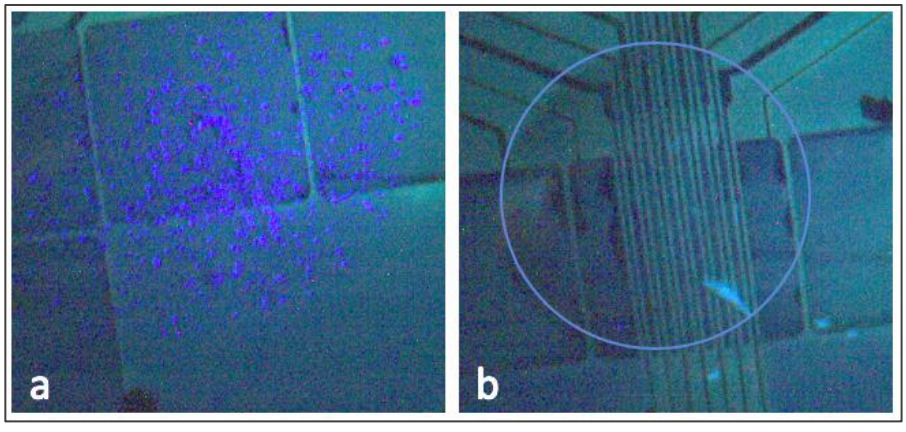

Figure 40: Chromatin detection assay results. A) Negative control B) Sample containing chromatin. Circle is drawn to indicate droplet.

Figure 40 shows the preliminary results from the nucleosome detection assay. Figure 40A is the negative control which did fluoresce due to the direct binding of the primary and secondary antibodies to the magnetic bead. Figure 40B shows the positive sample that did not fluoresce, most likely due to steric hinderance caused by the binding between the chromatin and the primary antibody. It is also possible, that the binding of the primary antibody to the chromatin also prevented the secondary antibody from binding to the primary antibody. Therefore, even if the chromatin was attached to the bead, it could not be detected. The chromatin immunoprecipitation assay discussed in section 4.5 explores this possibility.

4.4.2.2 Semi-Quantitative Chromatin Assay

Chromatin samples prepared using the procedure in 4.4.1 were serially diluted, as shown in Table 9, then introduced sequentially on to a current wire device. This droplet was actuated onto the current wires, where the beads were concentrated onto a single wire.

Table 9: Volumes of chromatin and diluent PBS used to prepare samples for chromatin semi-quantitative analysis study.

Sample	Dilution	Volume of Chromatin (µl)	Volume of PBS (µl)
A (Positive Control)	None	100	0
B	1:2	50 of A	50
C	1:4	50 of B	50
D	1:8	50 of C	50
E	1:16	25 of D	25
Negative Control	None	0	50

Next, using the ImageJ algorithm previously discussed in section 3.3, an image was taken and split into its separate red, blue, and green color channels. For each concentration, using the blue channel image, equal rectangular areas in the same location were used to analyze the pixel intensity average over that area. Three droplets were measured for each dilution. The average values are shown in the bar graph below.

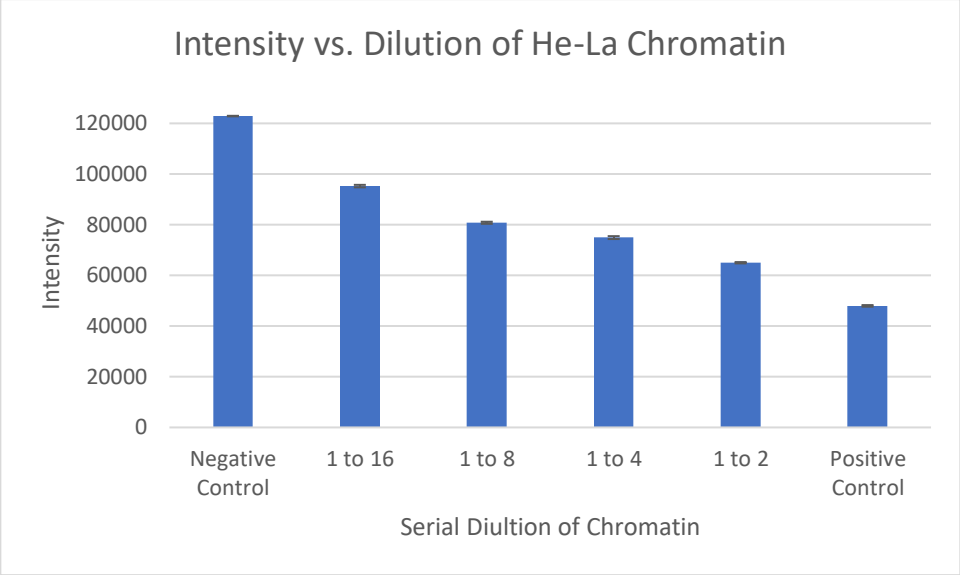

Figure 41: Intensity vs. Dilution of He-La Chromatin.

It is important to note that the negative control, which does not contain the chromatin analyte, had the highest signal. Conversely, the positive control, which is undiluted chromatin had the lowest signal. The limit of detection for this assay is approximately at 3.125 µl of stock solution.

4.4.3 Conclusion

Typically, $4x10^6$ cells or approximately 25 mg of a tissue sample are necessary per single sample immunoprecipitation [81] This is equivalent to approximately 20 µg of chromatin per immunoprecipitation, which is enough to perform downstream PCR and gel electrophoresis to confirm that the target has been isolated. However, it is important to note that 20 µg of chromatin is not sufficient for replicates nor accounts for assay development. During the development process of only a single target, several runs are necessary to determine the correct chromatin isolation protocol, dilution factor, antibody compatibility, and antibody dilution factor. This also does not include the potential need to vary the protocol when using different batches or manufacturers of antibodies. The fluorescent chromatin immunoassay method discussed in this section can be used to detect amounts of chromatin much lower than the standard benchtop protocol. Using gel

electrophoresis, Active Motif, the manufacturer of the He-La chromatin used in this protocol, confirmed that 50 µl of the stock solution were necessary to run a ChIP protocol that was detectable [82]. The fluorescent immunoassay described above, can detect as low as 3.125 µl of stock solution, or the equivalent of approximately 0.47 µg of chromatin, which is about 40x less than the amount currently required for benchtop protocols [81].

The chromatin detection fluorescent immunoassay introduced herein, provides a rapid method to screen for antibody specificity and sensitivity, as well as a confirmatory check point to ensure that the correct analyte is targeted prior to moving forward with more downstream analyses. The next section focuses on an immunoprecipitation assay that not only detects chromatin but captures it as well.

4.5 Chromatin Immunoprecipitation Assay

Although the last section described an assay that can detect the presence or absence of chromatin and can relatively quantify it within a sample, the detection assay either does not capture or is unable to confirm if chromatin is captured on the magnetic beads. In section 2.3, a bead-based fluorescent sandwich immunoassay was described as the selected assay format to develop for ChIP that was detectable on-chip. However, the sandwich method of using a capture primary antibody to adhere the chromatin to the bead and a second detection primary antibody proved unsuccessful (see Appendix B for a full list of experiments). Therefore, pivoting from the original design, this section describes an assay that utilized the strength of the biotin-streptavidin bond to capture chromatin, while reserving the region that binds with the primary antibody for detection [83]. In contrast with the chromatin assay presented in the previous section, this assay both detected the presence of chromatin and precipitated it out of solution, a critical step towards ChIP integration and automation on a digital microfluidic platform.

4.5.1 Materials and Methods

This section details the materials used in the chromatin immunoprecipitation assay and the assay protocol itself. The table below lists the reagents used, their roles in the assay, the manufacturer, and the catalog number.

Table 10: List of reagents used in the chromatin immunoprecipitation assay.

Reagent	Function	Manufacturer	Catalog No.
HeLa Chromatin	Analyte	Active Motif	53015
Rabbit anti-Human Histone H3 Antibody (Anti-H3)	Primary Antibody	Active Motif	91299
Goat anti-Rabbit IgG Alexa Fluor 405 Antibody (AF405)	Detection Antibody	Thermo Fisher Scientific	A-31556
Coating Buffer	Buffer	Invitrogen	CB01100
Elution Buffer	Buffer	Pierce	21004
EZ-Link®Biotinylation Kit	Capture mechanism	Thermo Fisher Scientific	21935
M280 Streptavidin-coupled magnetic beads	Capture platform	Dynabeads ™	11205D
20x PBS-Tween Buffer (PBST)	Buffer Solution	Pierce™	28352

The general workflow for the biotinylation of chromatin is shown in Figure 42 below. First, an Eppendorf Tube was coated with the primary antibody used to capture the chromatin. Next, chromatin was added to the tube and incubated to allow binding. Then, using the protocol from a biotinylation kit, biotin was added to the chromatin. The chromatin was then disassociated from the antibody and ready to use in the immunoprecipitation assay. The antibody binding sites of the chromatin should be protected from biotinylation and remain viable.

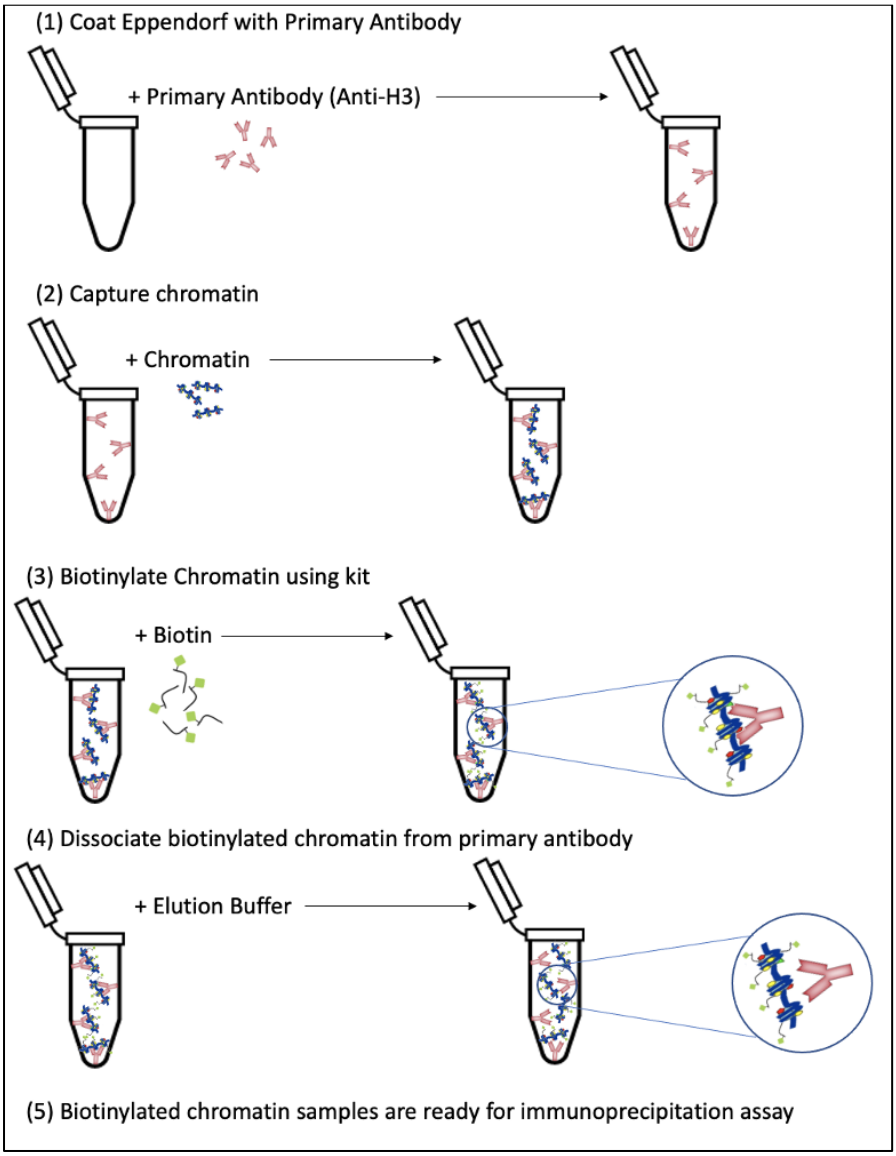

Figure 42: Chromatin biotinylation workflow.

Once the biotinylated chromatin was prepared, it was used in the immunoprecipitation assay shown in Figure 43. The biotinylated chromatin was first incubated with streptavidin coated beads. Meanwhile, the primary and secondary antibodies were incubated to create a detection complex. The detection complex was added to the beads and would bind to any chromatin that is present. Unlike the previous chromatin detection assay, when the beads were washed in the final

step, the chromatin remained bound to bead in the positive sample and thus fluoresced. By comparison. in the negative control the detection complex was washed away.

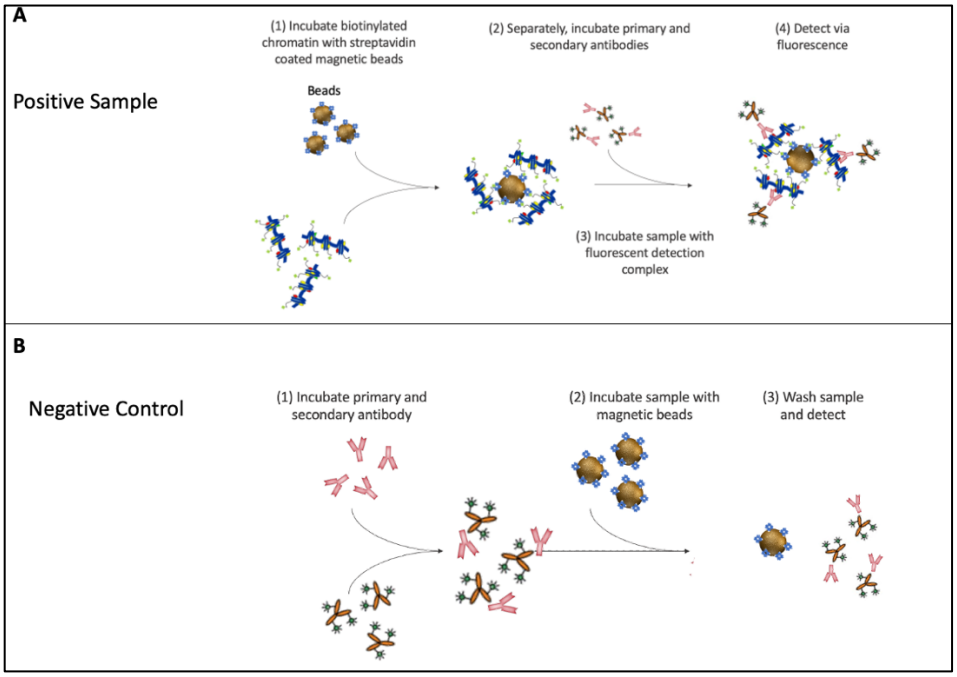

Figure 43: Schematic of Chromatin Immunoprecipitation assay.

4.5.1.1 Chromatin Biotinylation Protocol

This paragraph details the protocol for chromatin biotinylation. First, 2.5 ml of the PBST buffer solution were diluted in 47.5 ml of deionized water to create the 1X PBST buffer. Then 10 µl of Anti-H3 was diluted in 1.0 ml of Coating Buffer in a 2ml Eppendorf tube and incubated overnight at 4°C. After washing the Eppendorf three times with 1ml of PBST to remove unbound Anti-H3, 50 µg of Chromatin diluted in 500 µl was added to the Eppendorf tube and incubated at room temperature for 1 hour. The tube was washed again to remove any unbound chromatin. The chromatin that was bound to the Eppendorf tube was biotinylated using the manufacturer's protocol provided with the kit. Prior to removing excess biotin in a buffer exchange desalting column, the biotin solution was pipetted out of the Eppendorf and the chromatin was dissociated from the bound Anti-H3 antibody with 0.5 ml of elution buffer for 30 minutes at room temperature. After excess

biotin removal as per the manufacturer's directions, the biotinylated chromatin was ready for the immunoprecipitation protocol.

4.5.1.2 Chromatin Immunoprecipitation Protocol

First, the streptavidin coated beads were prepared. The stock bottle of streptavidin beads was gently rotated to resuspend all the beads without generating any air bubbles. Then two aliquots of 60 µl each of the beads were placed in separate micro-PCR tubes and placed against a magnet. After all the beads had migrated towards the magnet (approximately 15-20 seconds), the supernatant was removed using a pipette placed gently on the side opposing the mass of beads. Then, the beads were resuspended in 200 µl of PBST after which they were placed against a magnet and the supernatant was discarded. This was repeated a total of 3 times. For the sample, 50 µl of the biotinylated chromatin diluted in 150 µl of PBST, were added to the beads. For the negative control 200 µl of PBST was added to the beads. Both were incubated for 1 hour at room temperature on rotation. Meanwhile, separately, 10 µl of Anti-H3 and 20 µl of AF405 in 170 µl of PBST were also incubated at room temperature for 1 hour on rotation to form the detection complex. After this initial incubation, the supernatant was removed from the beads, and they were washed three times. Then 100 µl of the detection complex was added to both the sample and the negative control. These were incubated again for 1 hour at room temperature on rotation. After the final incubation, the supernatant was discarded, and the beads were washed with PBST three times to remove any unbound reagents. The beads were resuspended in 200 µl of PBST.

4.5.2 Experimental protocol and results

For the experimental protocol, in addition to the sample and the negative control, a second negative control was also prepared off-chip. This negative control went through the entire biotinylation and immunoprecipitation methods without any chromatin. This control was

established to show that any binding that occurred was a result of the presence of chromatin and not artifacts of biotinylated Anti-H3. For clarity, this will be referred to as the biotinylation negative control and the other will be referred to as the immunoprecipitation (IP) negative control

For this study, a droplet of approximately 0.1 µl was placed onto a current wire bottom plate fitted with a gasket. Before imaging, a top plate was affixed to the bottom plate. Each droplet was imaged, and the results are shown in Figure 44 below.

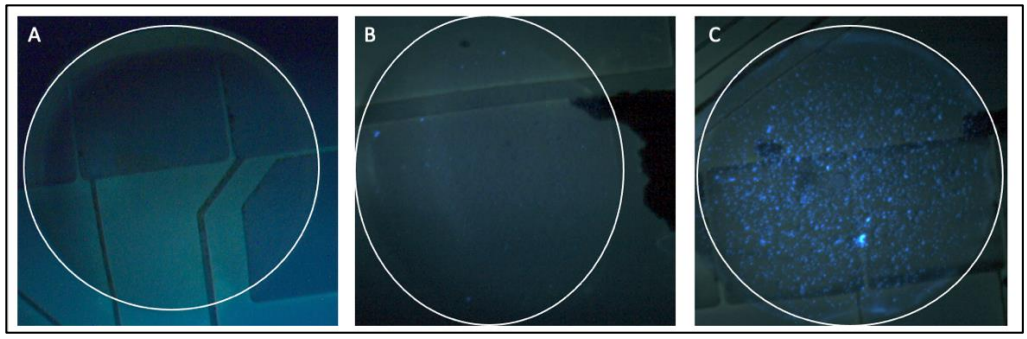

Figure 44: ChIP Experimental Results. All droplets are delineated with a white circle. A) IP negative control. B) Biotinylation negative control. C) Chromatin positive sample.

Figure 44A shows the IP negative control, which confirmed that no signal was detected when there was no chromatin present unlike the detection assay in the previous section. Figure 44B shows the biotinylation negative control, which had a weak signal suggesting that there was background noise and that the biotinylation protocol needed to be optimized for these assay parameters. However, when compared to Figure 44C, which had a very strong signal, it was apparent that it was the presence of the chromatin that was truly being detected in the assay.

4.5.3 Conclusion

The chromatin immunoprecipitation assay presented in this section used techniques taken from oriented ELISA protocols to protect the region of the chromatin to which the primary antibody binds, while increasing capturability by taking advantage of the extremely strong affinity between streptavidin and biotin. The directed biotinylation of the chromatin can be applied to other analytes

of interest and frees the user from the need to purchase expensive pre-biotinylated chromatin and presents a customizable capture mechanism. Furthermore, this assay not only detects but precipitates the chromatin. Therefore, the bead bound chromatin would be available for downstream analyses and further manipulation on-chip.

4.6 Conclusion

Each section of Chapter 4 builds on the results gathered and the protocols developed in the previous section. This chapter culminated in a collection of techniques and methodologies that address the main motivation of this dissertation; to improve the tools currently available to study epigenetics.

This chapter opened with two studies, which verified that the fluorescence measurement system and the image acquisition and analysis methods were functioning for the fluorophores used and standardized for all experiments. This laid the instrumentation foundation upon which the devices and experimental results relied.

Next, a novel fluorescent nucleosome immunoprecipitation study was introduced demonstrating the implementation of a benchtop protocol on a DMFB without the need for external magnets or specialized fluoroscopy equipment. Using current wires to generate an on-chip magnetic field, the specifically modified nucleosomes were collected while bound to magnetic beads. These samples were detected using fluorescently labelled secondary antibodies in an easily adaptable fluorescent detection system. Furthermore, the assay can be used to create a standard curve for quantitative analysis to detect the prevalence of nucleosomes in a sample.

The NuIP study laid the groundwork for the chromatin detection assay. This assay detected extremely low amounts of chromatin in a sample, approximately 40x less than benchtop protocols, thus addressing one of the biggest drawbacks of ChIP. In combination with a DMFB platform,

which will lessen sample handling and thus loss, this should decrease the number of cells necessary to run ChIP.

Although the chromatin detection assay did an excellent job of indicating whether chromatin is present in a sample, it did not precipitate the chromatin from solution. Therefore, the ChIP presented herein both detected and isolated the chromatin of interest. This assay utilized directed biotinylation of the chromatin to create a more easily capturable analyte while preserving the portion of the chromatin that binds to the primary antibody. Although the assay is in its preliminary stages, the methodology behind it can be adapted for a variety of analytes and formats. For example, instead of biotinylating the analyte, one could add biotin to the antibody instead and orient the capture mechanism of an analyte on a magnetic bead differently. This assay frees the user from traditional well-plate formats often used in ELISAs, and the multi-day isolation process of ChIP.

The next chapter presents a novel device design for on-chip magnetic bead capture to address some of the challenges observed empirically while running studies on the current wire devices.

5. Bead-Capture Efficiency Study and Experimental Results

A major challenge while running the assays discussed in the previous chapter was the limitation of the integrated current wire actuator's ability to capture all the beads in a droplet on a single wire. See section 2.2 for the background theory on current wire function and section 3.1 for their fabrication. During actuation, beads would either clump and remain on the first wire that was turned on, which was not necessarily the final wire destination, or they would reside too far away in the droplet to be actuated by the local magnetic field generated by a given wire.

This chapter introduces an alternative bottom plate design and compares a new, 'pull-through' method of bead capturing against the previous 'sweep-through' method. The experimental results herein were obtained by running the NuIP and chromatin detection assays discussed in Chapter 4 on the two different devices. The experiments determined the bead capture efficiency, which is the ratio of the fluorescent signal on a single current wire to the fluorescent signal of the overall droplet. Bead capture efficiency is the basis for comparing the different bead capture mechanisms. The objective of this study was to improve sample fluorescent signal detection of bead-based assays on a DMFB.

5.1 Device Designs

There were two designs compared in this study. The established 'sweep-through' device and the newly proposed 'pull-through' device. The fabrication technique for both bottom plate designs was the same, however the masks for each design were different than the current wire devices presented in the 3.1: DMFB fabrication. The photomasks of both devices are shown in Figure 45 below.

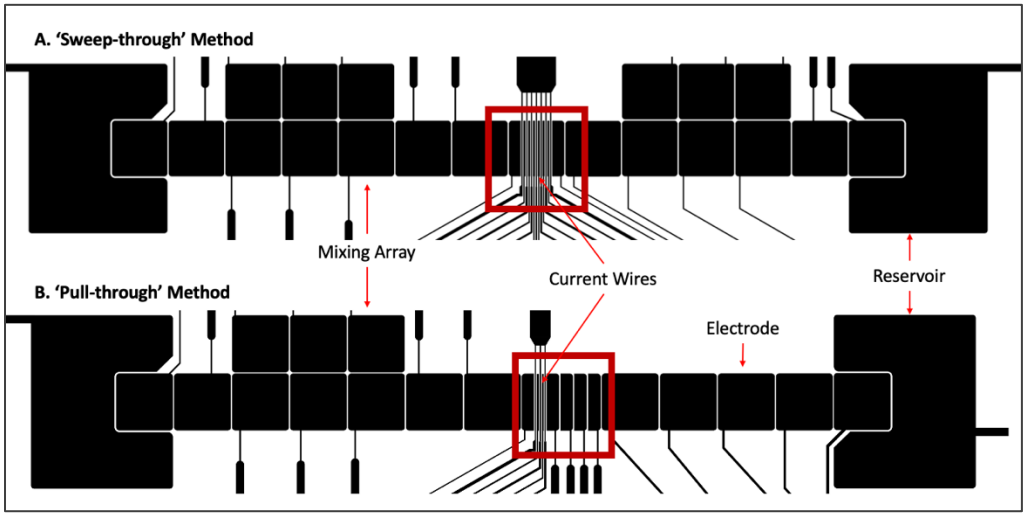

Figure 45: Photomask of DMFB with labelled components. A) 'Sweep-through' device and B) 'Pull-through' device. The red box indicates the major region of design differences between the two devices [84].

The 'sweep'-through device (Figure 45A) had current wires laid out in parallel over most of the area of a single electrode region, similar to the traditional current wire device design in section 3.1. However, the device layout included two 2x3 electrode mixing arrays on either side of the current-wire electrode. The 'pull-through' device (Figure 45B) had only one 2x3 mixing array adjacent to the current wire electrode. Although, these arrays are not used in this study, they were included in the device design to allow additional assay steps to be integrated onto the device. Combining two droplets and then shuttling the combined droplet quickly around the arrays is a common method of droplet mixing on a DMFB. In addition, the wire region of the pull-through device consisted of only three current wires that were next to a series of miniature electrodes intended to pull the droplet past the current wires in a stepwise fashion. A closer view of the regions of interest is shown in Figure 46 below.

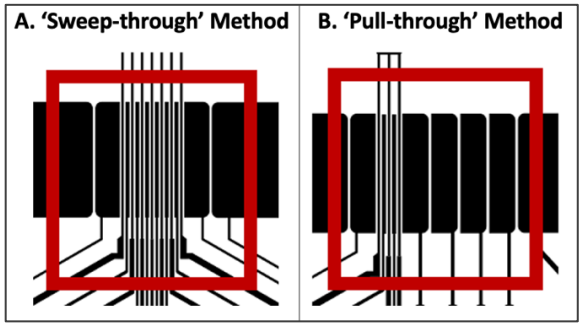

Figure 46: Enlarged image of the two devices. Note that in A) the beads were captured by sequentially turning on the current wires, whereas in B) the droplet was pulled past a single current wire that is turned on.

5.1.1 Sweep-through devices

The current wire devices described in Chapter 3 and used in all early experiments implemented a 'sweep-through' method of capturing the beads in a stationary droplet. This means that the droplet was held in place by the activated miniature electrodes on either side of the current wire region, while the current wires were turned on one after another to sweep the magnetic beads through the entirety of the droplet with the aim of capturing all the beads on the final outside wire. This method and design were developed by Dr. Liji Chen, a previous student in the Fair Microfluidics Lab [55]. The intended mechanism of Chen's design is depicted in the schematic below. The figure shows a droplet with magnetic beads atop the current wire region of the device. The droplet was held in place by the portions of the current wire electrode not covered by the current wires (i.e., the two miniature electrodes on either side of the current wires). Each wire was turned on sequentially from left to right with the intention of gathering all the beads during sequential wire activation (left to right in Figure 47) onto the final wire.

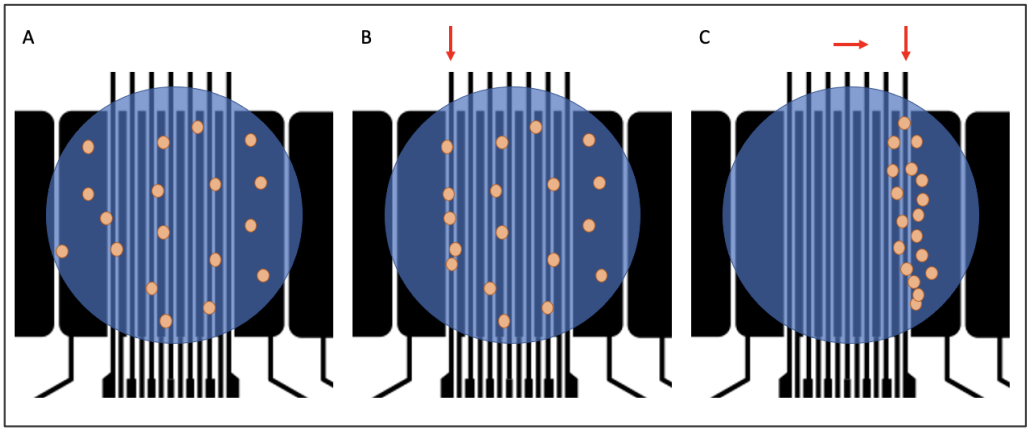

Figure 47: Sweep-through device mechanism. A) A magnetic bead containing droplet atop the current wire area. B) The red arrow indicates that the first current wire was turned on and the closest beads aggregated on that wire. C) The wires were turned on sequentially and gathered the beads along the entirety of the droplet, until they were all bound on the final wire.

The number of wires that the electrode can accommodate was based on electrode geometry. The design of the current wire electrode used here had the current wires extending over the entire width of the electrode to ensure that the magnetic beads experienced the same force regardless of their location inside the droplet. Thus, the current wires themselves were 15 µm wide, 1 µm thick, and had wire-to-wire spacing of 65 µm. Electrodes covered with an insulator were interspersed in the spaces between the wires to hold the droplet in place during sequential actuation of the current wires.

COMSOL simulations performed by fellow lab mate and Ph.D. candidate Shruti Preetam on similar current wire electrodes have shown that when 200 mA wire currents were used in the structure, the resulting magnetic field gradients around each wire did not extend more than 10 µm away from the wire. However, the effect on magnetic beads moving in a liquid under the influence of the field gradient around a wire, was observed by Chen to be over a distance of 40 µm [55].

In the experiment cited, Chen utilized devices with the same characteristics as the sweep-through devices described here. Each wire had a cross sectional area of 15 μm^2 and were 65 µm apart. The gasket layer was 120 µm thick, and the current electrode was also 700 µm wide. The

main difference was that Chen used 2 cSt silicone oil as opposed to 0.65 cSt silicone oil used in the experiments presented in this dissertation. His studies showed that it took 2.8 µm superparamagnetic beads (M-270, Invitrogen) approximately 16 s at 200 mA to cross a 65 µm wire-to wire spacing. Additionally, it took four passes of sweeping through the droplet to collect 96% of the beads onto a single wire [55].

Taking the 120 µm gasket height, the 700 µm current electrode width, the 15 µm current wire width, the 10 µm effective distance of the magnetic field gradient, and an assumption of equal bead dispersion in a droplet into account, approximately only 0.15% of the beads would experience the magnetic field generated by a current wire. The calculations are as follows:

Total volume of droplet
L_{drop} = electrode width
H_{drop} = gasket height
L_{drop} = 700 µm
H_{drop} = 120 µm
$V_{drop} = \pi (L_{drop}/2)^2 H_{drop} \approx 46$ nL

Volume affected by a single current wire
L_{eff} = width of current wire + 2(effective distance of gradient)
H_{eff} = thickness of wire + effective distance of gradient
L_{eff} = 35 µm
H_{eff} = 11 µm
$V_{eff} = \pi (L_{eff}/2)^2 H_{eff}$ 0.01 nL

Percent of beads affected by a single current wire
$(V_{eff}/V_{drop})*100 \approx 0.022\%$

Percent of beads affected by 7 current wires
$7*(V_{eff}/V_{drop})*100 \approx 0.15\%$

Therefore, the observed long-range effect was likely due to currents induced in the droplet by the moving beads, as observed by Preetam in simulations, since the flux of magnetic beads is likely to be strongest for those beads localized in the vicinity of a current wire.

5.1.2 Pull-through devices

As a proposed improvement to the bead gathering technique described in Chapter 3, the pull-through devices moved the droplet across a single current wire that was turned on to capture the beads. The mechanism is depicted in Figure 48 below. Thus, instead of using a stationary

droplet and sequencing current wire actuation, the droplet moved in increments relative to a single stationary, actuated wire.

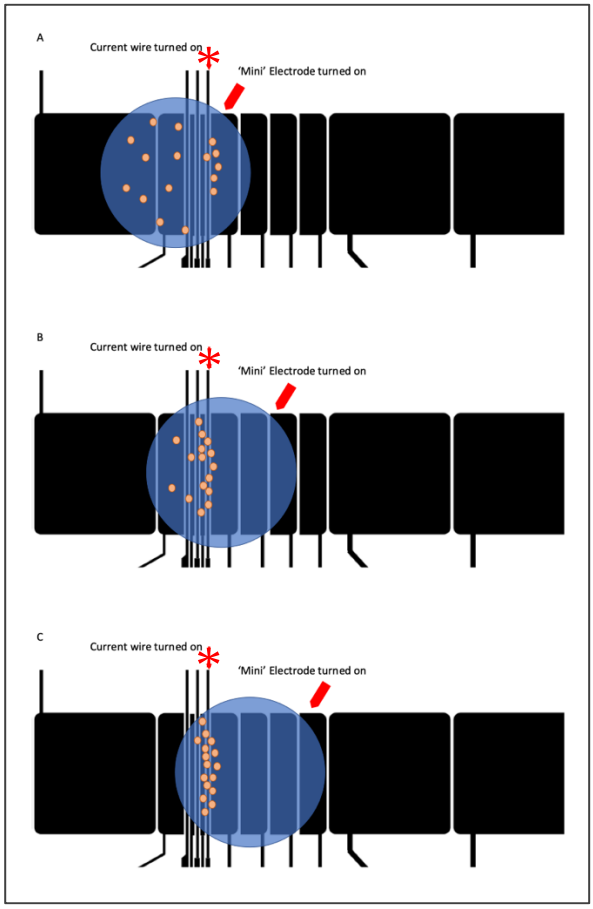

Figure 48: Pull-through device mechanism. A) A magnetic bead containing a droplet atop the current wire area being held in place by a miniature electrode, indicated by the red arrow, while only one current wire was turned on, indicated by the red Asterix B) The droplet was moved to the right via the next miniature electrode while the same wire was kept on. C) The entirety of the droplet was pulled past the current wire and the beads aggregated on the final wire.

The objective of the pull-through devices was to use the current wire as a sieve, past which the droplet moved while the beads were captured. Therefore, a bead-containing droplet was moved onto the current wire region using the miniature electrodes and only one current wire was turned on, indicated by the red Asterix in Figure 48. Next, the droplet was moved region by region using the miniature electrodes, indicated by the moving of the thick red arrow in Figure 48A-C. In summary, in the sweep-through method the droplet was held in place while the current wires were

sequentially turned on, whereas in the pull-through method the droplet was moved in steps over a single, stationary active wire.

Section 5.5 further discusses how the moving droplet induced internal flow patterns in the droplet, which mixed the beads inside under advective flow, allowing more beads to circulate and to come in proximity to the active current wire during each step. The following sections detail the experiments performed to compare the two device designs.

5.2 Device Fabrication and Operation

All DMFBs were fabricated as described in Chapter 3 section 1. The photomask was designed such that there were 4 sweep-through and 4 pull-through devices per wafer. The bottom plate dimensions were the same as the current wire devices. The table below summarizes the similarities and differences between the current wire, sweep-through, and pull-through devices.

Table 11: Summary of the number of features on the three device designs.

Devices	Current wire	Sweep-through	Pull-through
Electrodes			
Regular	14	19	15
Interspersed	6	6	2
Miniature	2	2	5
Current Wires	7	7	3
Reservoirs	2	2	2
Mixing Arrays	0	2	1

The regular electrodes measured 700 µm x 700 µm and were primarily used for mixing or shuttling of droplets. The interspersed electrodes were in-between the current wires and measured 45µm x 700µm and were used to help move the droplet over the current wire electrode until the droplet was fully actuated to the adjacent regular electrode. The miniature electrodes measured

92.5µm x 700µm and were used to hold the droplet in place for the current wire and sweep-through designs, whereas the miniature electrodes were used to move the droplet stepwise on the pull-through devices. Droplets on all devices were actuated in a channel that had a gap height of 120 µm, i.e., the thickness of the gasket, meaning that each droplet had a volume of approximately 46-50 nl ($V = \pi(\frac{L}{2})^2 H$). Prior to the introduction of aqueous droplets, the channel was filled with approximately 20 µl of 0.65 cSt silicone oil (Gelest, Inc.). There were two reservoirs measuring 1.5 mm x 1.5 mm on each device, which were used for dispensing droplets. These reservoirs held approximately 210 nl of liquid. The current wires, which were used to generate magnetic fields, were 15 µm wide, 1 µm thick, and spaced 65 µm apart. For the pull-through devices there were 3 current wires, even though only one was used. The multiple wires were simply for redundancy during experimentation, in the event of wire failure. The spacing between each electrode was 10 µm. These measurements, although shared by both devices, are represented in Figure 49 below.

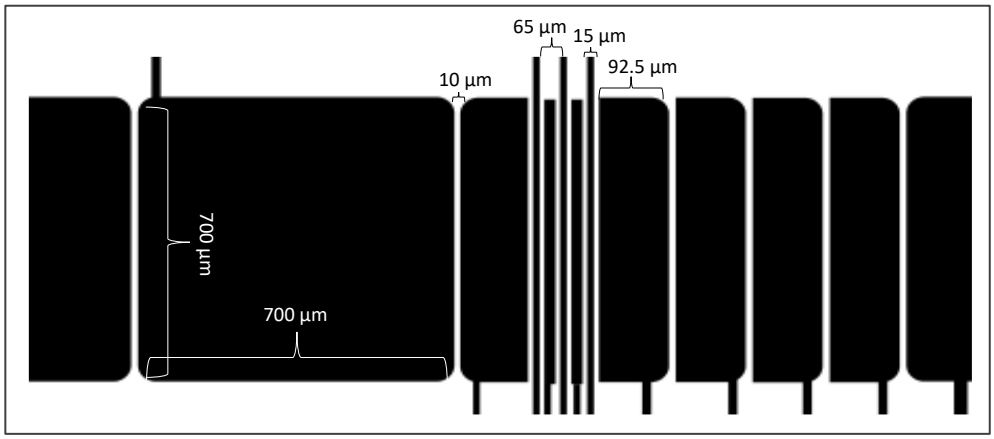

Figure 49: Dimensions shown on a representative photomask of the pull-through device.

The experimental DMFB instrumentation was the same as described in Chapter 3 section 2.1. A waveform generator (Model 33250A, Agilent) coupled with an amplifier (Model F10A, FLC Electronics) provided 40V at 1kHz to the electrodes for actuation of droplets. An alternating current (AC) source (Circuit Specialists, Inc.) provided 200 mA to the current wires to generate magnetic

fields strong enough to capture the magnetic beads. There were two types of beads used. For the NuIP experiments, M280 Streptavidin (Invitrogen) coated beads were used. For the chromatin detection experiments, Protein G (Invitrogen) coated beads were used. These are both superparamagnetic beads measuring 2.8 μm in diameter. During experimentation for the sweep-through devices, each current wire was turned on for approximately 10 seconds, allowing a total of 70 seconds to gather beads per droplet. Similarly, for the pull-through devices, each miniature electrode was turned on for 10 seconds following each droplet step actuation, allowing the single current wire the same amount of time to gather the beads per droplet. This amount of time was used because it allowed sufficient time for almost all bead movement that was observed to occur, without causing dielectric breakdown due to Joule heating by the current wires. The electrical current and voltage sources were individually connected to a PCB relay board as inputs and were directed to the device via an array of AWQ212 Photo-MOS Relays that corresponded to each of the 22 connector pads on the device. The PCB connected to an Arduino, which allowed for precise control of which electrode or wire would be activated from a 40 V AC voltage or a 200 mA AC current source, respectively.

For each experiment, samples (consisting of beads, the target analyte, and the detection antibody complexes) were prepared off chip and approximately 200 nl of the sample was dispensed into the left-hand side reservoir. Then a droplet of approximately 46 nl was dispensed and actuated onto the current wire region into the starting position, shown in Figure 50 below, for experimentation.

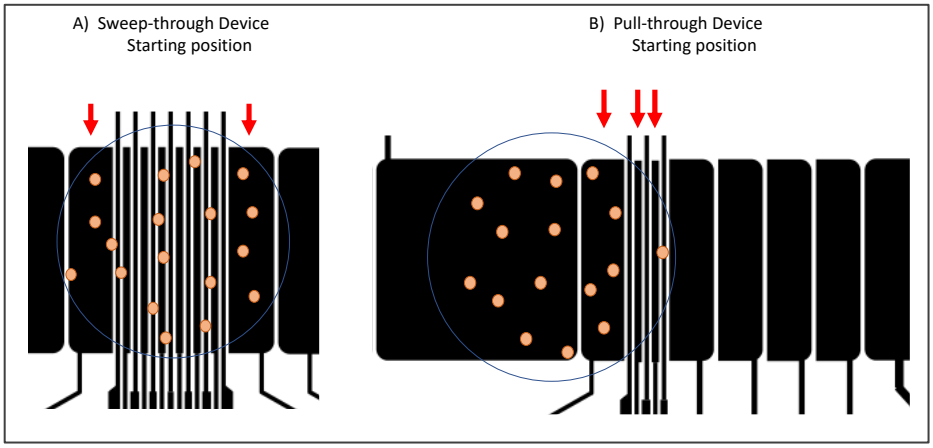

Figure 50: Starting positions for Device Comparison studies. Active electrodes are indicated by the red arrows. A) Sweep-through device. The droplet was held by the two miniature electrodes adjacent to the current wires. B) Pull-through device. The droplet was held in place by the left-most miniature electrode and the two interspersed electrodes.

For the sweep-through method the droplet was transported into its starting position by using the miniature electrodes and interspersed wire electrodes to actuate the droplet to a position over the electrodes/wires. Once the droplet was in place, it was held using the miniature electrodes on either side of the current wire region. Next, the left most wire was turned on 10 seconds. Immediately after it was turned off, the adjacent wire was turned on, also for 10 seconds. All seven of the wires were sequentially turned on/off in this manner from left to right. Once completed, an image was acquired and the fluorescent signal on the seventh, or last, wire and the fluorescent signal of the entire droplet were measured using the ImageJ protocol previously described in section 3.3.

For the pull-through method, the miniature and interspersed electrodes were also used to actuate the droplet to the starting position. Once the droplet was in its initial position, the current wire was turned on for 10 seconds, then the droplet was actuated to the first adjacent miniature electrode. The single wire remained active for the entire 70 seconds of the experiment. After 10 seconds, the next miniature electrode was turned on and the droplet actuated to cover that electrode. This second electrode was kept on for 10 seconds before the droplet was moved to the next

electrode. The droplet was moved in this stepwise fashion across all 4 miniature electrodes. Once completed, an image was acquired and the fluorescent signal on the wire and over the entire droplet were measured using the ImageJ protocol. Each sample droplet signal was normalized by subtracting the signal from the negative control droplet, which contained no analyte.

The following sections detail the comparison studies and their results.

5.3 NuIP Device Comparison Study

Using the NuIP assay developed in section 4.3, a study was done to compare the pull-through and sweep-through devices. The first experiment was a single wire signal comparison and the second, looked at bead capture efficiency. The protocols and results are reported below.

5.3.1 Experimental Protocol and Results

The first study compared the measured intensity of the fluorescent signal on a single wire after a sample had completed its respective bead-collection protocol. Samples and controls were prepared off-chip following the protocol in section 4.3.1. Then approximately 200 nl of the sample was dispensed into the left-hand side reservoir. A 50 nl droplet was actuated to its starting position on the current wire. As described in the previous section, after the beads were isolated onto the final wire, an image was taken, and the fluorescent signal measured. The fluorescent instrumentation is described in section 3.2.2 and the image acquisition and analysis methodology is described in section 3.3.

Figure 51A shows the intensity of the signal for both sample and control droplets in a bar graph to compare the devices. A total of four droplets were measured for each sample and control on each device. Figure 51B highlights the normalized signal difference between the methods. The signal was normalized by subtracting the background negative control signal from the sample signal. In this study, it was shown that using the pull-through method nearly tripled the signal for the same amount of analyte.

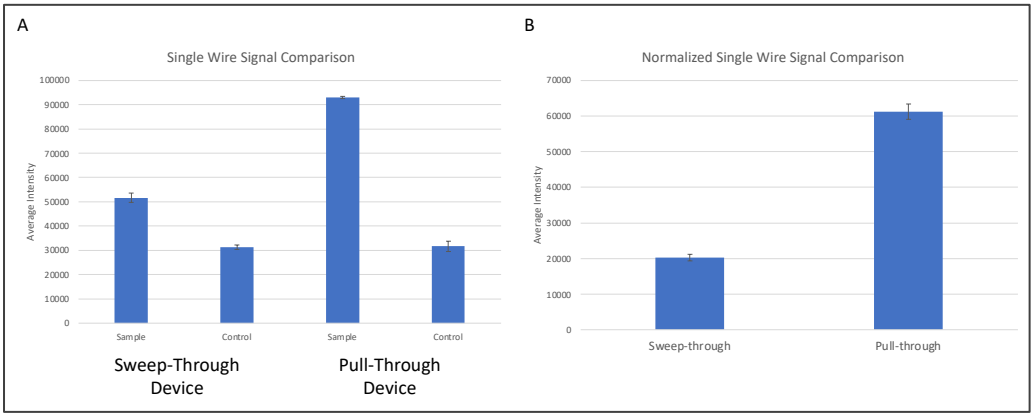

Figure 51: Device comparison results for NuIP. A) Single wire signal comparison. B) Normalized single wire signal comparison [84].

The next study looked at the bead capture efficiency of the devices. The bead capture efficiency is defined as the ratio of the signal on a single current wire to the signal over the entire droplet. This calculation probes at the relationship between the numbers of beads attached to a wire and the number of beads that remained suspended in a droplet. This study followed the same protocol as the single wire study. Briefly, a sample droplet was introduced onto the device, the beads were isolated, and both the fluorescent signal on a single wire and the fluorescent signal of the entire droplet were measured. A total of 4 droplets were used for each measurement and values were normalized by subtracting the background control signal from the sample signal. Table 12 summarizes the comparison of the bead capture efficiency between the sweep-through and the pull-through devices. This experiment showed that the bead capture efficiency of the pull-through devices was more than double that of the traditional sweep-through method. The modified pull-through device design introduced here improved bead capture efficiency.

Table 12: Results of NuIP bead capture efficiency experiment [84].

		Signal on a Single Wire	Signal over an Entire Droplet	**Bead Capture Efficiency** *
'Sweep-through' Method	Sample	52039	176932	29%
	Control	31363	80396	
	Normalized	**20676**	**96549**	**21%**
'Pull-through' Method	Sample	92891	120758	77%
	Control	30230	42322	
	Normalized	**62661**	**78436**	**80%**

*Bead Capture Efficiency $= \frac{signal\ on\ 1\ wire}{signal\ over\ entire\ droplet} \times 100$

5.4 Chromatin Detection Comparison Study

Using the chromatin detection assay developed in section 4.4, a study was done to compare the pull-through and sweep-through devices. This study consisted of two experiments. The first experiment compared the fluorescent signal on a single wire from a chromatin dilution series on the devices. The second experiment evaluated the bead capture efficiency for each of the dilutions.

5.4.1 Experimental Protocol and Results

The first study examined the fluorescent signal from a single wire for serial dilutions of chromatin to assess whether there was an improvement in the limits of detection by using the pull-through device. The samples were prepared off-chip according to the protocol in section 4.4.1. Table 13 lists the volumes used to prepare each sample in the serial dilution.

Table 13: Volumes of chromatin and diluent PBS used to prepare samples for chromatin semi-quantitative analysis study.

Sample	Dilution	Volume of Chromatin (µl)	Volume of PBS (µl)
A (Positive Control)	None	100	0
B	1:2	50 of A	50
C	1:4	50 of B	50
D	1:8	50 of C	50
E	1:16	25 of D	25
Negative Control	None	0	50

The left -hand reservoir of each device was filled with approximate 200 nl of sample, then an approximately 46 nl droplet was actuated onto the current wire regions of each device. After the beads were isolated onto a single wire, the fluorescent signal on the wire was imaged, and the signal was measured. Sample fluorescent signals were normalized by subtracting the background signal from the sample signal. This methodology was performed on three droplets per sample and per control for each device. The bar graph in Figure 52A shows that the normalized fluorescent signal from the pull-through device was significantly greater than the normalized fluorescent signal from the sweep-through device, especially at lower analyte concentrations. This result is significant, especially since the background signal was not significantly different between the two device measurements. As a result, the lower and upper limit of detection of the device improved, thereby increasing the quantification range of the assay.

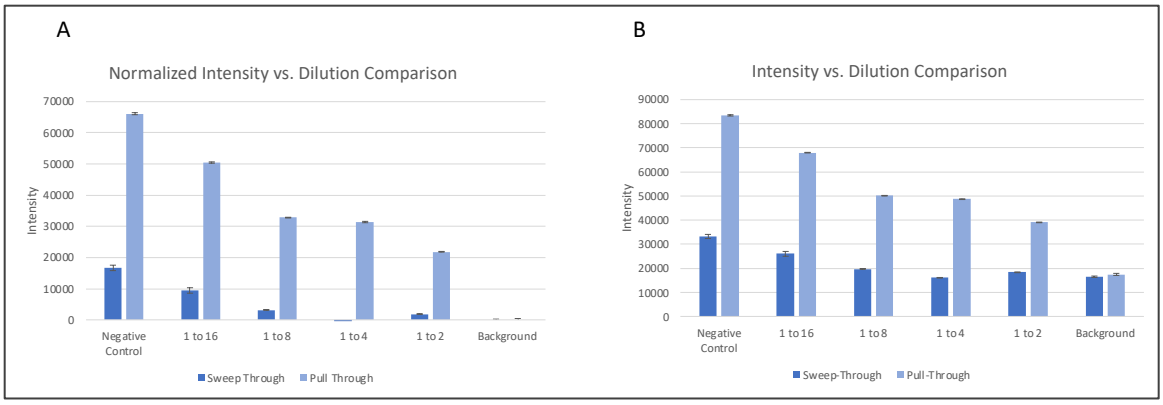

Figure 52: A) Normalized bar graph comparing the average intensity on a single wire for a serial chromatin dilution on sweep-through and pull-through devices. Normalized intensities have had the background fluorescent signal subtracted from the sample fluorescent signal. B) Non-normalized average intensities on a single wire for a serial chromatin dilution compared on sweep through and pull through devices.

The next study looked at the bead capture efficiency of a chromatin serial dilution. After a droplet was transported to the respective current wire region, the beads were isolated, and the sample imaged. Two measurements were taken. The first measurement was the intensity on a single

wire and the second measurement was the intensity over the entire droplet. The ratio of these two measurement values gave the bead capture efficiency. Table 14 summarizes the results.

Table 14: Summary of results from bead capture efficiency study of serial chromatin dilution.

Method Chromatin	Dilution	Single Wire Intensity	Entire Droplet Intensity	Bead Capture Efficiency*
Sweep Through	Negative Control	33228	112974	29%
	1 to 16	25500	94445	27%
	1 to 8	19758	70566	28%
	1 to 4	15754	67039	24%
	1 to 2	18337	61123	30%
	Positive Control	16889	48253	35%
Pull Through	Negative Control	83679	108674	**77%**
	1 to 16	67609	90145	**75%**
	1 to 8	50362	66266	**76%**
	1 to 4	48936	62739	**78%**
	1 to 2	39208	56823	**69%**
	Positive Control	31646	43953	**72%**

*Bead Capture Efficiency $= \frac{signal\ on\ 1\ wire}{signal\ over\ entire\ droplet} \times 100$

As shown in Table 14, the bead capture efficiency of the pull-through devices was more than double that of the sweep-through device design.

5.5 Analysis of Bead Capture Efficiency Results

For both the NuIP and the chromatin detection assays, the fluorescent signal on a single wire on a pull-through device increased by 2-3x the signal detected when collecting beads using the sweep-through devices. To ensure that this observation was not due to differences in the number of beads loaded or variations in droplets, the bead capture efficiency was measured. This measurement compares the fluorescent signal on a single wire against the fluorescent signal over the entire droplet. The bead capture efficiency studies showed a similar trend; bead capture efficiency nearly doubled for the pull-through device. Furthermore, for the chromatin detection assay dilution series, the detectable range increased. With the sweep-through device, only 0 µl – 6.5 µl of chromatin were distinguishable from the background level, whereas with the pull-through

device 0 µl - 25 µl were measurable above the background level. These results echoed those of section 4.4.2 that showed a significant improvement of the lower limit of detection as compared to the 50 µL of chromatin necessary, as suggested by the manufacturer, to run a single immunoprecipitation [82]. Furthermore, the upper limit of detection also increased. This is an important improvement because the intended use of this device is not only for low cell numbers or poor yield experiments but should be adaptable to any ChIP protocol. By having a large detectable range, chromatin extraction samples with a high concentration would not need to be diluted prior to being run on this DMFB to be detectable.

Another key takeaway from these experiments is that although the coefficient of variation (CV) of the fluorescent intensity between different droplets of the same sample on the same device is very low, below 10% for sweep-through devices and below 5% for pull-through devices, the measured fluorescent signal intensities vary greatly from device to device. Contributors to this signal variation can include positioning of the device with respect to the camera and the LED, movement that causes a change in the incidence angle of the LED source, and the motion of the beads within the droplet. Therefore, the selection of a background control is vital when running experiments on these DMFBs and should be included with every run. When normalizing these results, the background measurement was subtracted from the sample measurement because the control is known to have no fluorescence and therefore can be considered as noise. Once these assays and the devices are further developed, it will be critical to create and replicate a standard curve to use as a self-regulating comparison for each run.

The improvement in bead capture efficiency can be accounted for by intra-droplet flow that occurs as droplets are actuated and moved. On the sweep-through devices, when a droplet is stationary and the seven interdigitated wires are turned on sequentially, intra-droplet flow is observed to decrease over the 70 seconds that the experiment is carried out. Generally, magnetic

beads will settle when left stationary for a long time, hence the need to mix the regent bottle before pipetting the desired volume of beads and the need to perform benchtop experiments on rotation.

Furthermore, bead clumping was observed when a magnetic source was introduced and then removed, akin to the serial on/off sweep-through procedure [85]. As observed and explained by Tsaloglou when using a DMF device to perform a bead-based immunoassay. They observed that the superparamagnetic nature of the beads allowed them to magnetize and to demagnetize when in the presence or absence of a magnetic field, respectively. However, magnetization sometimes persisted and caused hysteresis, which promoted clumping of the beads. Bead clumping impacts the available surface area for binding, reducing sensitivity and reproducibility. Tsaloglou addressed bead settling by shuttling the droplet back and forth between two electrodes for 10 seconds to redisperse the magnetic beads. Both bead settling and clumping can also affect the bead dispersion throughout the droplet by decreasing the number of beads that are actively circulating by advective currents. This can impact the likelihood that a bead will come within the vicinity of an active current wire and feel the influence of the magnetic field gradient.

On the pull-through devices, a single current wire was turned on and the droplet was moved stepwise past that wire. A possible explanation for the improved bead capture efficiency on these devices was that each step forward induced flow and kept the beads circulating inside the droplet. Paik, et. al., studied mixing on DMF devices using fluorescence and linear arrays of electrodes [86]. They combined a droplet containing 1 mM fluorescein, 0.125 M KCl, and 0.125 M NaOH with a non-fluorescent droplet of just 0.125 M KCl and 0.125 M NaOH. Then they shuttled the combined droplet between linear arrays of 2, 3, and 4 electrodes. The fluorescein would allow them to image the flow patterns within the droplet [86]. Figure 53 shows their results when using a 3-electrode mixing scheme.

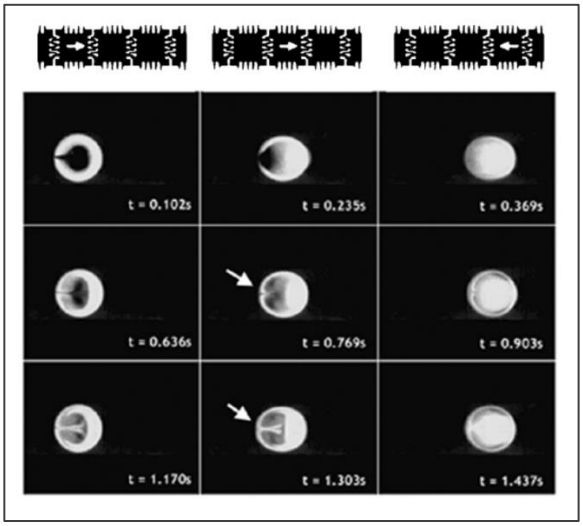

Figure 53: Time lapse images of combined fluorescent and non-fluorescent droplets mixing [86].

In Figure 53 the droplet was being moved at 8 Hz, which was the switch time between one electrode and its neighbor. In the first two columns the direction of the droplet was from left to right, and in the third column the droplet was moving back towards the left. This study showed that flow patterns on linear array mixers are not chaotic, but rather laminar and almost reversible. Furthermore, the fluorescein followed the currents within the droplet, which were particularly visible each time the droplet moved from left to right [86]. Considering this finding, it would follow that the beads behaved similarly and followed the current patterns within a droplet. Thereby, the improved bead capture efficiency can be credited to the advective bead circulation, which allowed beads to pass within the range of the localized magnetic field gradient around a current wire, thus increasing the likelihood that more beads would be captured.

These findings are significant because they improve NuIP and chromatin detection assay performance on a DMFB. Furthermore, utilizing the pull-through method of bead capture will increase sensitivity and expand the lower limit of detection for future bead-based immunoassays. This becomes particularly important with ChIP whose benchtop procedure suffers from poor yield.

Therefore, capturing as much of the analyte as possible becomes critical when dealing with rare tissue types and low cell number cultures.

5.6 Conclusion

The objective of the work presented in this chapter was to address an empirically observed phenomenon in which the previously established current wire method of capturing beads was not effective at gathering a significant percentage of magnetic beads in a droplet onto a current wire. This previous method involved the capture of magnetic beads by holding a droplet over seven interdigitated current wire electrodes and sequentially turning on each of the seven parallel current wires until some percentage of the magnetic beads in the droplet were collected on the last wire. However, it was both observed during experiments and simulated by Preetam, that the distance over which a current wire generates a magnetic field gradient was insufficient to capture a significant percentage of magnetic beads in the volume of the droplet [64]. There are two main consequences of poor bead capture: device functionality and analyte detection limits. First, poor collection affects device functionality by limiting the effectiveness of the magnetic bead-collection protocol. Poor bead collection also affects sample detection limits because the fluorescent signal detected on a single wire will be an underrepresentation of the actual amount of analyte in the droplet, and thus the sample. This limited collection impacts the limit of detection and sensitivity of an assay, which may increase false negatives since lower concentrations of analyte will fall closer to the background level. Furthermore, during wash steps in which fresh buffer is introduced to dilute out the old media in the droplet, there will be a higher amount of bead loss which will contribute further to loss of signal. Finally, these consequences also have implications for the amount of starting material necessary to achieve detectable results, which is counterproductive for an assay such as ChIP that is initially low yield.

This chapter presented a new device design for on-chip magnetic bead capture to address the drawbacks of the previous current wire design. Using the principles introduced by Chen on the sweep-through current wire devices, the design was modified to capture beads more efficiently on a single wire for fluorescence measurement and analysis [55]. The experiments performed using the NuIP and chromatin detection assays showed that bead capture efficiency approximately doubled across experiments using the pull-through device. Combined with the other benefits, such as small volumes, fast reaction times, automation, and multiplexing, the pull-through bead capture mechanism greatly enhances the successful translation of ChIP onto a DMFB.

6. Conclusion

This chapter summarizes the work presented in this dissertation as it relates to the motivation of the research, its contributions to the translation of ChIP onto a DMFB, and finally its discussion of future directions for further impact.

6.1 Summary

Epigenetics, the study of inheritable mechanisms that regulate gene expression, has clinical ramifications from cancer to autoimmune disorders to psychiatric pathologies [1], [5], [29], [87], [88]. The main tool to study epigenetics is chromatin immunoprecipitation (ChIP), which probes the relationship between DNA and its structural proteins [33], [87]. Standard benchtop ChIP has several major drawbacks, which can be addressed using digital microfluidic biochips [32]. The contributions from the studies described in this dissertation have provided the first steps towards ChIP implementation on a DMFB.

Chapter 4 first introduced a simple magnetic bead-based fluorescent immunoassay to detect the Anti-H4 antibody. This assay was used to verify that the electrical and fluorescent instrumentation (described in 3.1 and 3.2) were able to detect a signal on a DMFB. Once verified, the same assay was used to develop the image acquisition and analysis (see 3.3) that would be used for the semi-quantitative analysis of the necessary experiments conducted in this research. Adding to the complexity of the fluorescent immunoassay, a nucleosome immunoprecipitation assay was developed (see 4.3). This study showed that the assay reagents and samples could be actuated on the DMFB devices and that the magnetic beads used as reaction substrates could be controlled by local, on-chip magnetic field gradients. Next, a chromatin detection immunoassay was developed, showing that chromatin could not only be detected but also quantified on-chip (see 4.4). This assay could detect approximately 40x less chromatin than is used in standard benchtop protocols. Finally, after several unsuccessful iterations that attempted a sandwich bead assay, such as the one described

in section 2.3.3, a different approach was taken. After immobilizing Anti-H3, a primary antibody to bind with chromatin in a micro-PCR tube, the chromatin underwent a directed biotinylation modification so that the paratope would not be affected. Then, streptavidin beads were used to capture the chromatin and a detection complex of primary and secondary fluorescent antibody was used to detect the chromatin on-chip. This is the first successful chromatin immunoprecipitation assay reported on a digital microfluidic chip.

While running the experiments described in Chapter 4, it was observed that even after the current wires had been turned on to actuate magnetic beads so as to 'sweep-through' the droplet and to accumulate the beads on a single wire, many beads remained in solution within the droplet. Presented in Chapter 5, a new bottom plate was designed to improve the low bead capture efficiency observed with the older 'sweep-through' method. This new 'pull-through' design moved a droplet in a stepwise manner over smaller electrodes while a single current wire was turned on. Through a series of semi-quantitative experiments, it was shown that the bead capture efficiency approximately doubled using the 'pull-through' devices, likely due to internal flow patterns within the droplet.

6.2 Contributions

Though the standard ChIP protocol remains the most widely used method of studying epigenetics it has five major drawbacks. First, there is no way to verify that the analyte has been captured until post-ChIP analyses are performed. Second, ChIP antibodies are well-documented to be non-specific, to vary by batch, and to have low sensitivity [38], [40], [47]–[49]. Furthermore, the target must be known prior to ChIP and the antibody against it must exist. Therefore, several iterations of the assay must be run before finalizing the assay parameters. Third, due to the low yield of chromatin extraction and the poor sensitivity of the standard ChIP protocol, each experiment requires 10^6-10^8 cells [81]. Fourth, the standard ChIP protocol performs assays on bulk

cell cultures, which suffer from a loss in the granularity necessary to detect cell-to-cell variability within a tissue [5]. Finally, standard ChIP is time and labor intensive. The entire procedure can take several days to perform for only a few samples [1], [17], [40], [42], [43], [51], [52].

To address these challenges facing the current ChIP methodology, the following changes would be necessary: (1) require a smaller quantity of starting material, (2) allow for targets and antibody performance to be analyzed directly without downstream analyses, (3) achieve greater granularity and resolution to detect single cell variation, and (4) streamline sample isolation and purification. Implementing these improvements would decrease turnaround time, decreases labor costs per sample, decreases sample loss, and increases yield and throughput.

The development of microfluidic-based devices has allowed biological benchtop procedures to be adapted to small scales on highly automated devices [41]. Microfluidic biochips can address the major drawbacks of benchtop ChIP by reducing sample usage and providing an easily integrated, automated protocol on a high-throughput platform. Although a lot of work has been done to translate ChIP onto flow-through microfluidic devices, the capture and detection of chromatin on a DMFB has not yet been reported.

The first major contribution of this work is in developing both chromatin and nucleosome immunoprecipitation assays adapted for a DMFB. Second, unlike traditional ChIP that relies on gel electrophoresis or PCR-sequencing to detect whether the target region of chromatin has been captured, the chromatin detection and immunoprecipitation assays described herein are detectable on-chip. Therefore, the user can both detect and quantify the relative amount of a particular post-translationally modified nucleosome or chromatin on-chip. This addresses one of the drawbacks of standard ChIP that would necessitate additional time and labor-intensive protocols to determine whether immunoprecipitation was successful. Furthermore, this same DMFB platform can be used to validate antibodies during the assay development phase, when utilizing a new batch of antibodies

from the same manufacturer, or when using an antibody from a new manufacturer. Assay development can be a lengthy and cell-intensive process. Standard ChIP is inherently low throughput, taking several days to process only a few samples, each of which requires a large number of cells. The ability to quickly validate antibodies and targets while optimizing assay parameters on a DMFB will save time, labor, reagent, and sample usage.

These additional tools for ChIP are particularly helpful when coupled with the improved sensitivity achieved by the chromatin detection assay in this work. Traditional benchtop ChIP requires approximately 20 µg of sample to perform successfully [81]. By contrast, the DMFB chromatin detection protocol described in Chapter 4 can detect as little as 0.47 µg of chromatin. Approximately 40 assay runs could be accomplished with the same amount of chromatin to run a single benchtop immunoprecipitation. This eases the cellular burden during assay development and provides a method of detection for low-yield studies, rare tissue types, and single-cell analyses.

To detect the signal from fluorescent immunoassays, a very simple and adaptable fluorescent detection system was used. By only adding an LED coupled with a filter of the appropriate wavelengths and an emission filter within a telescopic lens attached to a CCD camera, it was possible to perform adequate fluorescence imaging. Furthermore, an image analysis methodology was introduced to quantify nucleosomes and chromatin. This approach allows for rapid and semi-quantitative analysis of the relative abundance and enrichment of post-translational modifications of histones. Finally, a new DMFB was designed to improve the capture of magnetic beads. By nearly doubling the captured signal, this new design increases the lower and upper limits of detection for chromatin assays. Better bead capture increases the amount of fluorescent signal detected from a sample and decreases the number of beads necessary to get the equivalent level of fluorescence.

In summary, these contributions have advanced the translation of ChIP onto a DMFB, addressed some of the major drawbacks facing benchtop ChIP, provided the study of epigenetics a set of alternative tools to detect and analyze the epigenome, and finally improved the performance of on-chip magnetic control on DMFB.

6.3 Future work

To move the work presented here further, the next steps would be to fabricate a more complex device that would have multiple reagent and waste reservoirs, several wire electrode regions, and several branches for multiplexing. This proposed device would also be capable of accomplishing DNA elution and purification protocols that prepare the captured DNA for PCR and sequencing. Once an integrated device is achieved that performs on-chip PCR and sequencing, the next challenge would be to develop a method of sample removal from the device.

Overall, the next stage for ChIP-on-chip development is the consolidation of all the components in the protocol onto a single device. As described in section 1.3.2, many of the steps involved in ChIP, such as cell capture, lysis, PCR, and DNA sequencing have already been shown successfully on DMF devices. Additionally, new tools and platforms have been developed that, if adapted for ChIP, can address its current challenges.

Lamanna et. al., developed a single cell isolation DMFB that performed proteome, transcriptome, RNA, and single nucleotide variation analyses using an imaging-based machine learning algorithm [89]. Their DISCO system allows researchers to study the morphology and phenotype of a cell using image analysis while also probing at the DNA, RNA, and proteins using targeted laser lysis of the cell within a droplet [89]. With the introduction of an antibody detection complex containing droplet and a droplet of magnetic beads, this platform could also do single-cell analysis of chromatin.

Millington, et. al. review SEEKER®, a high-throughput point-of-care diagnostic newborn screening DMF device [90]. This system can run enzymatic and targeted biomarker assays on the same platform to detect Pompe Disease, Fabry Disease, and Hurler Syndrome [90]. Adapting ChIP to a similar platform would allow researchers to run entire analyses from cell isolation and lysis to DNA sequencing on multiple samples simultaneously in a thoroughly automated and self-contained platform. This would decrease the number of instruments currently used for ChIP (approximately 5) to one device, one cartridge, pipettes, and reagents.

GenMark's ePlex ® system is a large-scale DMF instrument capable of multiplexed infectious disease panel diagnostics [91]. These machines have barcoded cartridges that are loaded with the patient's whole blood sample and tested for up to 25 diseases simultaneously. Their impedance based ferrocene-oligonucleotide probe detection system provides a means to detect multiple targets from one sample [91]. Multiplexing can accelerate ChIP assay development when probing with multiple antibodies to determine sensitivity and specificity. Furthermore, adapting ChIP to a multiplexed whole blood-to-result platform can advance cancer detection and diagnosis using nucleosomes that are circulating in the bloodstream that have been released from apoptotic cancer cells.

The work to streamline the entire process onto a single device can be separated into four parts: (1) cell capture and lysis, (2) chromatin digestion/fragmentation and extraction, (3) ChIP and DNA purification, and (4) PCR and DNA sequencing. Once these functionalities have been incorporated onto a single device, automating the entire process will allow for a hands-free, complete ChIP-on-chip platform. Additionally, advances in single-cell analysis, image-based machine learning, multiplexed pathogen detection, and high-throughput disease screening have provided new platforms and techniques that can further advance and commercialize ChIP development on a DMFB.

Appendix A: Software code

Raspberry Pi GUI

The python code in this appendix was designed in conjunction with Dr. Zhanwei Zhong. This code is written for use on a Raspberry Pi to create a GUI. The GUI allows the user to turn electrodes and current wires on and off by pressing a button on the screen, which communicates with an Arduino that controls the switch relay PCB, as shown in Figure 52 below.

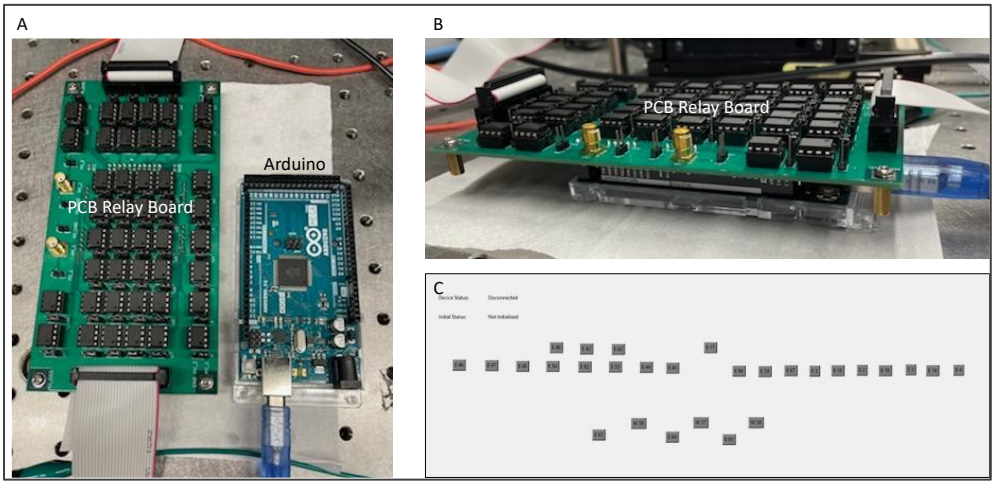

Figure A.1: A) PCB relay board and Arduino shown. B) Side view of the PCB relay board/Arduino assembly. C) Screenshot of GUI designed in Python.

```
#===============Import required libraries===============
from pyfirmata import ArduinoMega, OUTPUT, INPUT
import time
from tkinter import *
from tkinter import ttk
from tkinter import Canvas
from functools import partial
from time import sleep
from tkinter import filedialog, messagebox
from PIL import Image, ImageTk
import pickle
import os
import csv
import tkinter as tk

#=============== Handshake with Arduino ================
def connect_to_device():
    global a
    global connectivity

    try:
        a = ArduinoMega ('COM3')
        messagebox.showinfo('Info', 'Now connected to Arduino!!!')
        connectivity.set('Connected')
    except:
        messagebox.showinfo('Info', 'Cannot connect to Arduino!!!')
        exit()

#================= Set up window ========================
window = Tk()
window.geometry("800x600")
window.title("Duke DMFB Desinger")

#================ Global Variables ======================
connectivity = StringVar()
connectivity.set('Disconnected')
initialization = StringVar()
initialization.set('Not Initialized')
lst_info_button = [] # information of buttons
lst_inst_button = [] # instance of buttons


#======= Modify pin numbers here for the ones in use ===========
lst_idx_used = [46, 47, 48, 54, 62, 55, 49, 42, 43, 44, 45]
lst_idx_used.extend([17])
lst_idx_used.extend([66, 59, 67, 3, 18, 2, 19, 5, 16, 4])
lst_idx_used.extend([62,63, 56, 64, 57, 65, 58])
```

```
# ======= Index all the pins =========
lst_idx_all = [46, 47, 48, 49, 42, 43, 44, 45, 38, 39, 40]
lst_idx_all.extend([41, 34, 35, 36, 37, 30, 31, 32, 33, 28, 29])
lst_idx_all.extend([54, 62, 55, 63, 56, 64, 57, 65, 58, 66, 59])
lst_idx_all.extend([67, 3, 18, 2, 19, 5, 16, 4, 17, 1, 20])

# ===== Set the status of all the pins======
dict_idx_all = {}


# ====== Method: Toggle the output of wires and electrodes_____

def toggle(idx, widget):
    global dict_idx

    if connectivity.get() != 'Connected':
        messagebox.showinfo('Info', 'Arduino MEGA not yet connected.')
        return
    if idx <=53:
        if dict_idx_all[idx] == 1:
            a.digital[idx].write(0)
            dict_idx_all[idx] = 0   # update the database
            widget['bg'] = 'gray'
            widget['activebackground'] = 'gray'
            print('Pin {0} set to LOW'.format(idx))
        else:
            a.digital[idx].write(1)
            dict_idx_all[idx] = 1   # update the database
            widget['bg'] = 'green'
            widget['activebackground'] = 'green'
            print('Pin {0} set to HIGH'.format(idx))
    else:
        if dict_idx_all[idx] == 1:
            a.analog[idx-53].mode=OUTPUT
            a.analog[idx-53].write(0)
            dict_idx_all[idx] = 0   # update the database
            widget['bg'] = 'gray'
            widget['activebackground'] = 'gray'
            print('Pin {0} set to LOW'.format(idx))
        else:
            a.analog[idx-53].mode=OUTPUT
            a.analog[idx-53].write(1)
            dict_idx_all[idx] = 1   # update the database
            widget['bg'] = 'green'
            widget['activebackground'] = 'green'
            print('Pin {0} set to HIGH'.format(idx))
```

```
 # ======= Method: Initialize by Setting pins to 0 ========
def initialize():
    if connectivity.get() != 'Connected':
        messagebox.showinfo('Info', 'Arduino MEGA not yet connected.')
        return
    for idx in range(2,54):
        #inputstr = 'd:'+str(idx)+':o'
        #a.get_pin(inputstr).mode = OUTPUT
        a.digital[idx].write(0) # set it to low voltage
        #a.digital[idx].mode=OUTPUT
        dict_idx_all[idx] = 0        # update the database
    for idx in range(1,15):
        #inputstr = 'a:'+str(idx)+':o'
        #a.get_pin(inputstr).mode = OUTPUT
        a.analog[idx].mode=OUTPUT
        a.analog[idx].write(0) # set it to low voltage
        dict_idx_all[idx+53] = 0        # update the database
    messagebox.showinfo('Info', 'All 44 GPIOs are initialized to LOW!')
    initialization.set('Initialized')


# ===== Method: Set up File Menu, Design Chip Layout =======

def start_design():
    window.bind('<Button-1>', lambda event, name='E': _create_button(event, name))
    window.bind('<Button-3>', lambda event, name='W': _create_button(event, name))
    window.bind('<Return>', end_design)
    messagebox.showinfo('Info', 'Left mouse click for electrodes\nRight mouse click for
wires.\nHit enter when finish.')

def _create_button(event, name):
    global lst_info_button, lst_inst_button, lst_idx_used, dict_idx_all

    idx_pin = lst_idx_used[len(lst_info_button)] # need to check lookup table

    if dict_idx_all[idx_pin] == 0:
        button = Button(window, text='{0} {1}'.format(name, idx_pin), bg='gray',
activebackground='gray')
    else:
        button = Button(window, text='{0} {1}'.format(name, idx_pin), bg='green',
activebackground='green')

    button.place (x = event.x, y = event.y)
    button.config(command=lambda idx=idx_pin, widget=button:toggle(idx, widget))

    info_button = (name, idx_pin, event.x, event.y)
    lst_info_button.append(info_button)
    lst_inst_button.append(button)
```

```
# ===== Use buttons to create design =========
def end_design(event):
    window.unbind('<Button-1>')
    window.unbind('<Button-3>')
    window.unbind('<Return>')
    messagebox.showinfo('Info', 'Enter detected.\nDesign Complete!')

# ===== Load a design =======
def open_design():
    window.filename = filedialog.askopenfilename(initialdir="/Users/ybigd/Documents/old rasppi
files/", title="Select file", filetypes= (("jw files", ".jw"), ("all files", "*.*")))

    #global a

    if window.filename:
        # retrieve lst_info_button
        with open(window.filename, 'rb') as handle:
            _load_design(handle)

            for idx in range(2,54):
                #inputstr = 'd:'+str(idx)+':o'
                #a.get_pin(inputstr).mode = OUTPUT
                a.digital[idx].mode=OUTPUT
                a.digital[idx].write(0) # set it to low voltage
                dict_idx_all[idx] = 0       # update the database
            for idx in range(1,15):
                a.analog[idx].mode=OUTPUT



                inputstr = 'a:'+str(idx)+':o'
                a.get_pin(inputstr).mode = OUTPUT
                dict_idx_all[idx+53] = 0       # update the database

            messagebox.showinfo('Info', 'Design opened from {0}.'.format(window.filename))

# ======= Load and Clear Design =======
def _load_design(handle):
    global lst_info_button, lst_inst_button, dict_idx_all

    # clear design
    for button in lst_inst_button:
        button.destroy()
    lst_inst_button = []

    lst_info_button = pickle.load(handle)
    for info_button in lst_info_button:
```

```
        name, idx_pin, loc_x, loc_y = info_button
        button = Button(window, text='{0} {1}'.format(name, idx_pin), bg='gray',
activebackground='gray')

        button.place (x = loc_x, y = loc_y)
        button.config(command=lambda idx=idx_pin, widget=button:toggle(idx, widget))

        lst_inst_button.append(button)

def clear_design():
    global lst_info_button, lst_inst_button, dict_idx_all

    for button in lst_inst_button:
        button.destroy()
    lst_inst_button.clear()
    lst_info_button.clear()

    if dict_idx_all:
        for idx in dict_idx_all:
            a.digitalWrite((idx), a.LOW) # set the value
            dict_idx_all[idx] = 0    # update the database

    messagebox.showinfo('Info', 'Design completely clear!')

# ======== Save Design =================
def save_design():
    window.filename = filedialog.asksaveasfilename(initialdir="/Users/ybigd/Documents/old
rasppi files/", title="Select file", filetypes= (("jw files", ".jw"), ("all files", "*.*")))

    if window.filename:
        with open(window.filename, 'wb') as handle:
            pickle.dump(lst_info_button, handle)
            messagebox.showinfo('Info', 'Design saved to {0}'.format(window.filename))
# ======== Exit Design and set pins to 0 =========
def exit_window():
    global dict_idx_all

    for idx in dict_idx_all:
        a.digitalWrite((idx), a.LOW) # set the value

    window.destroy()

def donothing():
    pass

# ========= Set up Main GUI window design =============
if __name__ == '__main__':
    menubar = Menu(window)
```

```
file_menu = Menu(menubar, tearoff=0)
file_menu.add_command(label="New Design", command=start_design)
file_menu.add_command(label="Open Design", command=open_design)
file_menu.add_command(label="Save Design", command=save_design)
file_menu.add_command(label="Clear Design", command=clear_design)
file_menu.add_command(label="Exit", command=exit_window)
menubar.add_cascade(label="File", menu=file_menu)

# ======= Menu Bar Device ================
device_menu = Menu(menubar, tearoff=0)
device_menu.add_command(label="Connect to Device", command=connect_to_device)
device_menu.add_command(label="Device Pins", command=donothing)
device_menu.add_command(label="Initizalize Pins", command=initialize)
menubar.add_cascade(label="Device", menu=device_menu)

# ========= Menu Bar Help ==================
help_menu = Menu(menubar, tearoff=0)
help_menu.add_command(label="Help Index", command=donothing)
help_menu.add_command(label="About...", command=donothing)
menubar.add_cascade(label="Help", menu=help_menu)
window.config(menu=menubar)

# ======== Place the device name ================
name_label = Label (window, text = "Arduino MEGA", pady=5, bg="white", font=20)
name_label.place(x=75, y=5)

# ======== Place the status button ================
status_label_1 = Label(window, text='Device Status: ', pady=5)
status_label_1.place (x = 30, y = 155)

# ======== Place the initialize button ================
init_label_1 = Label(window, text='Initial Status: ', pady=5)
init_label_1.place (x = 30, y = 200)

# ======= Place the status label ================
status_label_2 = Label (window, textvariable=connectivity, pady=5)
status_label_2.place(x=150, y=155)

# ======= Place the initialize label ================
init_label_2 = Label (window, textvariable=initialization, pady=5)
init_label_2.place(x=150, y=200)

window.mainloop()
```

PC GUI

The Java code in this section is designed by Zak Tini to create a GUI on a PC operating system that will control the Arduino pins, which in turn, control the PCB relay switch board as shown in Figure 52 above.

```
import javax.swing.*;
import java.awt.*;
import java.awt.event.*;
import java.io.IOException;
import com.fazecast.jSerialComm.*;


public class microfluidicGUI extends Frame{
   static JPanel panel;
   static JPanel question;
   //All pins on arduino MEGA (order is important for device)
   static String[] arduinoPinStorage =
         {"","","","49","42","43","","","38","","39","40","41","","","",
         "46","47","48","54","62","55","44","45","","4","17","1","20","34","35","36",
         "63","56","64","57","65","58","66","59","67","3","18","2","19","5","16"};
   static int apsLength = arduinoPinStorage.length;
   //Pins to be used during device trials -> stored from user input
   String[] secondRound = new String[apsLength];
   static int dimX,dimY;
   //Frame dimensions
   static int frameX = 1280, frameY = 240;
   //declaration of storage variable
   int store;
   Integer storeVal;
   //port name according to device
   //[IMPORTANT]
   static SerialPort port = SerialPort.getCommPort("");
   ///dev/cu.usbmodem141101
   //returns initial index value of button -- maintains positions of all pins
   public static int indexValue(String[] arr1, String a){
      for(int z = 0; z < arr1.length; z++) {
         if (arr1[z].equals(a))
            return z;}
      return 0;}
   public static void catchValues(){
      question = new JPanel(new GridLayout(2, 1));
      JTextField x = new JTextField(10);
      JTextField y = new JTextField(10);
      question.add(x);
```

```
        question.add(y);
        JOptionPane.showMessageDialog(null, question);
        dimX = Integer.parseInt(x.getText());
        dimY = Integer.parseInt(y.getText());
    }

    public microfluidicGUI(String[] arr2, int tester, int arrSize, int x, int y) throws IOException,
InterruptedException{
        //Array of buttons
        JButton[] allButtons = new JButton[arrSize];
        panel = new JPanel(new GridLayout(x, y));
        //Initialize button -- creates new panel with only the saved buttons
        if(tester == 0) {
            JButton testerBtn = new JButton("INIT");
            panel.add(testerBtn);
            allButtons[apsLength] = testerBtn;
        }
        //creates array of buttons to be added
        for(int i = 0; i < arrSize; i++){
            if(i < apsLength) {
                allButtons[i] = new JButton(arr2[i]);
                allButtons[i].setActionCommand(arr2[i]);
            }
            allButtons[i].addActionListener(new ActionListener(){
            public void actionPerformed(ActionEvent e) {
                String choice = e.getActionCommand();
                if(!choice.equals("INIT") && !choice.equals("")){
                    store = indexValue(arduinoPinStorage, choice);
                    storeVal = Integer.parseInt(choice);
                }
                //Accounts for 'empty' buttons
                if(choice.equals("")){
                    ;
                }
                //Creates new interface with only the buttons the user has selected
                else if(choice.equals("INIT") && tester != 1) {
                    try {
                        new microfluidicGUI(secondRound, 1, apsLength, x, y);
                    } catch (IOException | InterruptedException ioException) {
                        ioException.printStackTrace();
                    }
                    microfluidicGUI frame = null;
                    try {
                        frame = new microfluidicGUI(secondRound,  1, apsLength, x, y);
                    } catch (IOException | InterruptedException ioException) {
                        ioException.printStackTrace();
                    }
                    frame.add(panel);
```

```
    frame.pack();
    frame.setVisible(true);
    frame.setTitle("Microfluidic GUI");
    frame.setSize(frameX,frameY);
}
//adds buttons to second interface to allow for device interaction
else if(tester != 1){
    allButtons[store].setBackground(Color.GREEN);
    allButtons[store].setOpaque(true);
    secondRound[store] = choice;
}
//Sends signal to arduino to set specific pins to HIGH
else if(!allButtons[store].getBackground().equals(Color.GREEN)){
    allButtons[store].setBackground(Color.GREEN);
    allButtons[store].setOpaque(true);
    //SET pins to HIGH
    try {
        port.getOutputStream().write(storeVal.byteValue());
    } catch (IOException ioException) {
        ioException.printStackTrace();
    }
    try {
        port.getOutputStream().flush();
    } catch (IOException ioException) {
        ioException.printStackTrace();
    }
    try {
        Thread.sleep(100);
    } catch (InterruptedException interruptedException) {
        interruptedException.printStackTrace();
    }
}
//Sends signal to arduino to set specific pins to LOW
else if(allButtons[store].getBackground().equals(Color.GREEN)){
    allButtons[store].setBackground(Color.RED);
    allButtons[store].setOpaque(true);
    //SET pins to LOW
    try {
        port.getOutputStream().write(storeVal.byteValue());
    } catch (IOException ioException) {
        ioException.printStackTrace();
    }
    try {
        port.getOutputStream().flush();
    } catch (IOException ioException) {
        ioException.printStackTrace();
    }
    try {
```

```
                    Thread.sleep(100);
                } catch (InterruptedException interruptedException) {
                    interruptedException.printStackTrace();
                }
            }
        }
        });
            panel.add(allButtons[i]);
        }
    }
    public static void main(String[] args) throws IOException, InterruptedException {
        //standard reading settings
        port.setComPortParameters(9600, 8 ,1,0);
        port.setComPortTimeouts(SerialPort.TIMEOUT_WRITE_BLOCKING,0,0);
        //checks to make sure port is connected & connects to port
        if(port.openPort()){
            System.out.println("Connected");
        }
        else{
            System.out.println("Error Connecting");
            //return;
        }
        catchValues();
        //apsLength+1 to account for initialize button
        new microfluidicGUI(arduinoPinStorage,  0, apsLength+1, dimX, dimY);
        microfluidicGUI frame = new microfluidicGUI(arduinoPinStorage,  0, apsLength+1, dimX
,dimY);
        frame.add(panel);
        frame.pack();
        frame.setVisible(true);
        frame.setTitle("Select Inputs");
        frame.setSize(frameX,frameY);
    }
}
```

Appendix B: Sandwich Immunoassay Development

The table below is a summary of the series of experiments done to develop a bead-based fluorescent sandwich immunoassay for chromatin detection and immunoprecipitation. In the bolded studies, the absence of chromatin was detected but the presence of chromatin was not. In other words, the negative control fluoresced, and the positive sample did not. These results led to the development of the yellow highlighted study, which is the chromatin detection assay discussed in 4.4.

Table Key**:**
+: Added sequentially, indicates and incubation of 6 hours or overnight at 4°C on rotation
/: Incubated together for 6 hours or overnight at 4°C on rotation
-: No chromatin was added, PBS was used instead, these are the negative controls
G: Invitrogen Dynabeads Protein G Beads (catalog #: 10003D)
br: Active Motif Bridging Antibody for Mouse IgG (catalog #: 53017)
aRNA: Active Motif RNA pol II Antibody (Mouse) (catalog#: 39097)
Ch: Active Motif HeLa Chromatin (catalog #: 53015)
aH3: Active Motif Recombinant Histone H3 Antibody (Rabbit) (catalog #: 91299)
AF405M: Invitrogen Alexa Fluor 405 Goat Anti-Mouse (catalog #: A-31553)
AF405R: Invitrogen Alexa Fluor 405 Goat Anti-Rabbit (catalog #: A-31556)

Diluent for all reagents is 1X PBS – 0.02% Tween
50 ml Preparation: Mix 2.5 ml of Pierce™ 20X PBS Tween™ 20 Buffer (catalog #: 28352) with 47.5 ml of DI water

Samples are washed prior to addition of any Alexa Fluor antibody and before detection to remove any unbound species that would cause interference.

All experiments are listed chronologically.

Table B.1: List of ChIP Assay iterations and conditions.

Experiment	Signal?	Notes
G-br + aRNA/Ch + AF405M		
G-br + aRNA/ - + AF405M	✓	
G-br + aRNA/Ch + aRNA/AF405M		
G-br + aRNA/ - + aRNA/AF405M	✓	
G - PBS		
G-br + aRNA/Ch + aH3 + AF405R		Inconclusive
G-br + aRNA/ - + aH3 + AF405R		Inconclusive
G + aH3/Ch + aRNA + AF405M		
G + aH3/ - + aRNA + AF405M		
G-br + aRNA/Ch/aH3/AF405R		
G-br + aRNA/ - /aH3/AF405R	✓	
G + aRNA/Ch/aH3/AF405M		
G + aRNA/ - /aH3/AF405M	✓	
G-br + Ch + aH3/AF405R	✓	Lower concentration of chromatin Clumped, bright, signal
G-br + - + aH3/AF405R	✓	Evenly dispersed signal
G-br + Ch/aH3/AF405R		
G-br + AF405R		
G-br + - + aH3/AF405R	✓	
G-br + 12.5 µl Ch + aH3/AF405R	✓	
G-br + 25 µl Ch + aH3/AF405R	✓	
G-br + 50 µl Ch + aH3/AF405R	✓	
G-br + AF405R		
G-br + aRNA/Ch + aH3/AF405R	✓	
G-br + aRNA/ - + aH3/AF405R	✓	
G-br + Ch + aRNA/AF405M		
G-br + - + aRNA/AF405M		
G-br + AF405M		
G-br + AF405R		
G + - /aH3/AF405R	✓	
G + Ch/aH3/AF405R		
G-br + aRNA + - /aH3/AF405R		Sample from previous assay
G-br + aRNA + Ch/aH3/AF405R		Sample from previous assay
G/aH3/Ch + aRNA + AF450M		Lower concentration of antibodies
G/Ah3/ - + aRNA + AF450M		Lower concentration of antibodies
G + aH3/Ch/aRNA + AF405M		Lower concentration of antibodies
G + aH3/ - /aRNA + AF405M		Lower concentration of antibodies

References

[1] B. C. Capell and S. L. Berger, "Genome-Wide Epigenetics," *J. Invest. Dermatol.*, vol. 133, no. 6, p. e9, Jun. 2013, doi: 10.1038/jid.2013.173.

[2] J. P. Hamilton, "Epigenetics: Principles and Practice," *Dig. Dis. Basel Switz.*, vol. 29, no. 2, pp. 130–135, Jul. 2011, doi: 10.1159/000323874.

[3] K. R. Stewart-Morgan, N. Petryk, and A. Groth, "Chromatin replication and epigenetic cell memory," *Nat. Cell Biol.*, vol. 22, no. 4, Art. no. 4, Apr. 2020, doi: 10.1038/s41556-020-0487-y.

[4] S. Bhatia, J. Matthews, and P. G. Wells, "Characterization of Epigenetic Histone Activation/Repression Marks in Sequences of Genes by Chromatin Immunoprecipitation-Quantitative Polymerase Chain Reaction (ChIP-qPCR)," in *Developmental Toxicology: Methods and Protocols*, J. M. Hansen and L. M. Winn, Eds. New York, NY: Springer New York, 2019, pp. 389–403. doi: 10.1007/978-1-4939-9182-2_25.

[5] K. Grosselin *et al.*, "High-throughput single-cell ChIP-seq identifies heterogeneity of chromatin states in breast cancer," *Nat. Genet.*, vol. 51, no. 6, Art. no. 6, Jun. 2019, doi: 10.1038/s41588-019-0424-9.

[6] S. J. Clark, H. J. Lee, S. A. Smallwood, G. Kelsey, and W. Reik, "Single-cell epigenomics: powerful new methods for understanding gene regulation and cell identity," *Genome Biol.*, vol. 17, no. 1, p. 72, Apr. 2016, doi: 10.1186/s13059-016-0944-x.

[7] A. Rotem *et al.*, "Single-cell ChIP-seq reveals cell subpopulations defined by chromatin state," *Nat. Biotechnol.*, vol. 33, no. 11, Art. no. 11, Nov. 2015, doi: 10.1038/nbt.3383.

[8] J. Yu, X. J. Loh, Y. Luo, S. Ge, X. Fan, and J. Ruan, "Insights into the epigenetic effects of nanomaterials on cells," *Biomater. Sci.*, vol. 8, no. 3, pp. 763–775, Feb. 2020, doi: 10.1039/C9BM01526D.

[9] "Chromatin," *Genome.gov*. https://www.genome.gov/genetics-glossary/Chromatin (accessed Apr. 14, 2020).

[10] R. A. M. Dirks, H. G. Stunnenberg, and H. Marks, "Genome-wide epigenomic profiling for biomarker discovery," *Clin. Epigenetics*, vol. 8, no. 1, Art. no. 1, Dec. 2016, doi: 10.1186/s13148-016-0284-4.

[11] M. Garber *et al.*, "A High-Throughput Chromatin Immunoprecipitation Approach Reveals Principles of Dynamic Gene Regulation in Mammals," *Mol. Cell*, vol. 47, no. 5, pp. 810–822, Sep. 2012, doi: 10.1016/j.molcel.2012.07.030.

[12] M. V. C. Greenberg and D. Bourc'his, "The diverse roles of DNA methylation in mammalian development and disease," *Nat. Rev. Mol. Cell Biol.*, vol. 20, no. 10, pp. 590–607, Oct. 2019, doi: 10.1038/s41580-019-0159-6.

[13] R. N. Shah *et al.*, "Examining the Roles of H3K4 Methylation States with Systematically Characterized Antibodies," *Mol. Cell*, vol. 72, no. 1, pp. 162-177.e7, Oct. 2018, doi: 10.1016/j.molcel.2018.08.015.

[14] J. Yu, Q. Feng, Y. Ruan, R. Komers, N. Kiviat, and K. Bomsztyk, "Microplate-based platform for combined chromatin and DNA methylation immunoprecipitation assays," *BMC Mol. Biol.*, vol. 12, no. 1, Art. no. 1, Dec. 2011, doi: 10.1186/1471-2199-12-49.

[15] A. T. Grzybowski, R. N. Shah, W. F. Richter, and A. J. Ruthenburg, "Native internally calibrated chromatin immunoprecipitation for quantitative studies of histone post-translational modifications," *Nat. Protoc.*, vol. 14, no. 12, Art. no. 12, Dec. 2019, doi: 10.1038/s41596-019-0218-7.

[16] T. Hattori *et al.*, "Recombinant antibodies to histone post-translational modifications," *Nat. Methods*, vol. 10, no. 10, Art. no. 10, Oct. 2013, doi: 10.1038/nmeth.2605.

[17] T. W. Murphy, Y.-P. Hsieh, S. Ma, Y. Zhu, and C. Lu, "Microfluidic Low-Input Fluidized-Bed Enabled ChIP-seq Device for Automated and Parallel Analysis of Histone Modifications," *Anal. Chem.*, vol. 90, no. 12, pp. 7666–7674, Jun. 2018, doi: 10.1021/acs.analchem.8b01541.

[18] T. J. Stasevich *et al.*, "Regulation of RNA polymerase II activation by histone acetylation in single living cells," *Nature*, vol. 516, no. 7530, Art. no. 7530, Dec. 2014, doi: 10.1038/nature13714.

[19] M. M. Mitchener and T. W. Muir, "Janus Bioparticles: Asymmetric Nucleosomes and Their Preparation Using Chemical Biology Approaches," *Acc. Chem. Res.*, vol. 54, no. 16, pp. 3215–3227, Aug. 2021, doi: 10.1021/acs.accounts.1c00313.

[20] T. O. Tolsma and J. C. Hansen, "Post-translational modifications and chromatin dynamics," *Essays Biochem.*, vol. 63, no. 1, pp. 89–96, Apr. 2019, doi: 10.1042/EBC20180067.

[21] S. M. Gasser, "Open questions: Epigenetics and the role of heterochromatin in development," *BMC Biol.*, vol. 11, p. 21, Mar. 2013, doi: 10.1186/1741-7007-11-21.

[22] N. Iglesias *et al.*, "Native Chromatin Proteomics Reveals a Role for Specific Nucleoporins in Heterochromatin Organization and Maintenance," *Mol. Cell*, vol. 77, no. 1, pp. 51-66.e8, Jan. 2020, doi: 10.1016/j.molcel.2019.10.018.

[23] S. K. Kurdistani, "Histone modifications as markers of cancer prognosis: a cellular view," *Br. J. Cancer*, vol. 97, no. 1, pp. 1–5, Jul. 2007, doi: 10.1038/sj.bjc.6603844.

[24] D. B. Seligson *et al.*, "Global histone modification patterns predict risk of prostate cancer recurrence," *Nature*, vol. 435, no. 7046, pp. 1262–1266, Jun. 2005, doi: 10.1038/nature03672.

[25] M. Shtumpf, K. V. Piroeva, S. P. Agrawal, D. R. Jacob, and V. B. Teif, "NucPosDB: a database of nucleosome positioning in vivo and nucleosomics of cell-free DNA," *Chromosoma*, Jan. 2022, doi: 10.1007/s00412-021-00766-9.

[26] "Revolutionizing the way cancer is diagnosed", Accessed: Mar. 31, 2022. [Online]. Available: http://www.nature.com/articles/d43747-020-00313-y

[27] P. Van den Ackerveken *et al.*, "A novel proteomics approach to epigenetic profiling of circulating nucleosomes," *Sci. Rep.*, vol. 11, no. 1, p. 7256, Dec. 2021, doi: 10.1038/s41598-021-86630-3.

[28] J. Sterling, S. V. Menezes, R. H. Abbassi, and L. Munoz, "Histone lysine demethylases and their functions in cancer," *Int. J. Cancer*, vol. 148, no. 10, pp. 2375–2388, May 2021, doi: 10.1002/ijc.33375.

[29] P. A. Jones and S. B. Baylin, "The fundamental role of epigenetic events in cancer," *Nat. Rev. Genet.*, vol. 3, no. 6, Art. no. 6, Jun. 2002, doi: 10.1038/nrg816.

[30] Q. Mei *et al.*, "Regulation of DNA replication-coupled histone gene expression," *Oncotarget*, vol. 8, no. 55, pp. 95005–95022, Oct. 2017, doi: 10.18632/oncotarget.21887.

[31] E. C. Britt, S. V. John, J. W. Locasale, and J. Fan, "Metabolic regulation of epigenetic remodeling in immune cells," *Curr. Opin. Biotechnol.*, vol. 63, pp. 111–117, Jun. 2020, doi: 10.1016/j.copbio.2019.12.008.

[32] P. Collas, "The Current State of Chromatin Immunoprecipitation," *Mol. Biotechnol.*, vol. 45, no. 1, pp. 87–100, May 2010, doi: 10.1007/s12033-009-9239-8.

[33] T. H. Kim and J. Dekker, "Chromatin Immunoprecipitation (ChIP) Analysis of Protein–DNA Interactions," *Cold Spring Harb. Protoc.*, vol. 2018, no. 5, p. pdb.top082586, May 2018, doi: 10.1101/pdb.top082586.

[34] V. A. Spencer, J.-M. Sun, L. Li, and J. R. Davie, "Chromatin immunoprecipitation: a tool for studying histone acetylation and transcription factor binding," *Methods*, vol. 31, no. 1, pp. 67–75, Sep. 2003, doi: 10.1016/S1046-2023(03)00089-6.

[35] M. J. Bush, G. Chandra, M. J. Bibb, K. C. Findlay, and M. J. Buttner, "Genome-Wide Chromatin Immunoprecipitation Sequencing Analysis Shows that WhiB Is a Transcription Factor That Cocontrols Its Regulon with WhiA To Initiate Developmental Cell Division in *Streptomyces*," *mBio*, vol. 7, no. 2, pp. e00523-16, /mbio/7/2/e00523-16.atom, May 2016, doi: 10.1128/mBio.00523-16.

[36] J. Akhtar *et al.*, "TAF-ChIP: an ultra-low input approach for genome-wide chromatin immunoprecipitation assay," *Life Sci. Alliance*, vol. 2, no. 4, Aug. 2019, doi: 10.26508/lsa.201900318.

[37] M. J. Buck and J. D. Lieb, “ChIP-chip: considerations for the design, analysis, and application of genome-wide chromatin immunoprecipitation experiments,” *Genomics*, vol. 83, no. 3, pp. 349–360, Mar. 2004, doi: 10.1016/j.ygeno.2003.11.004.

[38] T. A. Egelhofer *et al.*, “An assessment of histone-modification antibody quality,” *Nat. Struct. Mol. Biol.*, vol. 18, no. 1, Art. no. 1, Jan. 2011, doi: 10.1038/nsmb.1972.

[39] Z. Wang *et al.*, “An array of 60,000 antibodies for proteome-scale antibody generation and target discovery,” *Sci. Adv.*, vol. 6, no. 11, p. eaax2271, Mar. 2020, doi: 10.1126/sciadv.aax2271.

[40] W. C. Gasper *et al.*, “Fully automated high-throughput chromatin immunoprecipitation for ChIP-seq: Identifying ChIP-quality p300 monoclonal antibodies,” *Sci. Rep.*, vol. 4, no. 1, Art. no. 1, Jun. 2014, doi: 10.1038/srep05152.

[41] L. Coudron *et al.*, “Fully integrated digital microfluidics platform for automated immunoassay; A versatile tool for rapid, specific detection of a wide range of pathogens,” *Biosens. Bioelectron.*, vol. 128, pp. 52–60, Mar. 2019, doi: 10.1016/j.bios.2018.12.014.

[42] B. Teste *et al.*, “Chromatin immunoprecipitation in microfluidic droplets: towards fast and cheap analyses,” *Lab. Chip*, vol. 17, no. 3, pp. 530–537, Jan. 2017, doi: 10.1039/C6LC01535B.

[43] S. Aldridge *et al.*, “AHT-ChIP-seq: a completely automated robotic protocol for high-throughput chromatin immunoprecipitation,” *Genome Biol.*, vol. 14, no. 11, p. R124, Nov. 2013, doi: 10.1186/gb-2013-14-11-r124.

[44] L. Arrigoni *et al.*, “RELACS nuclei barcoding enables high-throughput ChIP-seq,” *Commun. Biol.*, vol. 1, no. 1, Art. no. 1, Dec. 2018, doi: 10.1038/s42003-018-0219-z.

[45] L. Arrigoni, F. Ferrari, J. Weller, C. Bella, U. Bönisch, and T. Manke, “AutoRELACS: Automated Generation And Analysis Of Ultra-parallel ChIP-seq,” *bioRxiv*, p. 2020.03.30.016287, Apr. 2020, doi: 10.1101/2020.03.30.016287.

[46] C. Schmidl, A. F. Rendeiro, N. C. Sheffield, and C. Bock, “ChIPmentation: fast, robust, low-input ChIP-seq for histones and transcription factors,” *Nat. Methods*, vol. 12, no. 10, pp. 963–965, Oct. 2015, doi: 10.1038/nmeth.3542.

[47] S. S. Ivanov *et al.*, “Antibodies Immobilized as Arrays to Profile Protein Post-translational Modifications in Mammalian Cells,” *Mol. Cell. Proteomics*, vol. 3, no. 8, pp. 788–795, Aug. 2004, doi: 10.1074/mcp.M300130-MCP200.

[48] A. Venkataraman *et al.*, “A toolbox of immunoprecipitation-grade monoclonal antibodies to human transcription factors,” *Nat. Methods*, vol. 15, no. 5, Art. no. 5, May 2018, doi: 10.1038/nmeth.4632.

[49] F. C. Wardle and H. Tan, “A ChIP on the shoulder? Chromatin immunoprecipitation and validation strategies for ChIP antibodies,” *F1000Research*, vol. 4, p. 235, Jul. 2015, doi: 10.12688/f1000research.6719.1.

[50] B. L. Kidder, G. Hu, and K. Zhao, “ChIP-Seq: technical considerations for obtaining high-quality data,” *Nat. Immunol.*, vol. 12, no. 10, pp. 918–922, Oct. 2011, doi: 10.1038/ni.2117.

[51] R. A. M. Dirks, P. Thomas, R. C. Jones, H. G. Stunnenberg, and H. Marks, “A plug and play microfluidic platform for standardized sensitive low-input Chromatin Immunoprecipitation,” *bioRxiv*, p. 2020.01.02.893180, Jan. 2020, doi: 10.1101/2020.01.02.893180.

[52] Z. Cao, C. Chen, B. He, K. Tan, and C. Lu, “A microfluidic device for epigenomic profiling using 100 cells,” *Nat. Methods*, vol. 12, no. 10, Art. no. 10, Oct. 2015, doi: 10.1038/nmeth.3488.

[53] N. Dimov *et al.*, “Electrowetting-based Digital Microfluidics Platform for Automated Enzyme-linked Immunosorbent Assay,” *J. Vis. Exp.*, no. 156, p. 60489, Feb. 2020, doi: 10.3791/60489.

[54] S. Momtahen, M. Taajobian, and A. Jahanian, “Drug Discovery Applications: A Customized Digital Microfluidic Biochip Architecture/CAD Flow,” *IEEE Nanotechnol. Mag.*, vol. 13, no. 5, pp. 25–34, Oct. 2019, doi: 10.1109/MNANO.2019.2927773.

[55] L. Chen and R. B. Fair, “Digital microfluidics chip with integrated intra-droplet magnetic bead manipulation,” 2015, doi: 10.1007/s10404-015-1650-9.

[56] A. R. Wu *et al.*, “High throughput automated chromatin immunoprecipitation as a platform for drug screening and antibody validation,” *Lab. Chip*, vol. 12, no. 12, p. 2190, 2012, doi: 10.1039/c2lc21290k.

[57] T. Geng, N. Bao, M. D. Litt, T. G. Glaros, L. Li, and C. Lu, “Histone modification analysis by chromatin immunoprecipitation from a low number of cells on a microfluidic platform,” *Lab. Chip*, vol. 11, no. 17, p. 2842, 2011, doi: 10.1039/c1lc20253g.

[58] Y.-H. Chang, G.-B. Lee, F.-C. Huang, Y.-Y. Chen, and J.-L. Lin, “Integrated polymerase chain reaction chips utilizing digital microfluidics,” *Biomed. Microdevices*, vol. 8, no. 3, pp. 215–225, Sep. 2006, doi: 10.1007/s10544-006-8171-y.

[59] J. Zhai *et al.*, “A digital microfluidic system with 3D microstructures for single-cell culture,” *Microsyst. Nanoeng.*, vol. 6, no. 1, p. 6, Dec. 2020, doi: 10.1038/s41378-019-0109-7.

[60] A. C. Madison *et al.*, “Scalable Device for Automated Microbial Electroporation in a Digital Microfluidic Platform,” *ACS Synth. Biol.*, vol. 6, no. 9, pp. 1701–1709, Sep. 2017, doi: 10.1021/acssynbio.7b00007.

[61] A. H. C. Ng, K. Choi, R. P. Luoma, J. M. Robinson, and A. R. Wheeler, "Digital Microfluidic Magnetic Separation for Particle-Based Immunoassays," *Anal. Chem.*, vol. 84, no. 20, pp. 8805–8812, Oct. 2012, doi: 10.1021/ac3020627.

[62] K. Pandit *et al.*, "An open source toolkit for repurposing Illumina sequencing systems as versatile fluidics and imaging platforms," *Sci. Rep.*, vol. 12, no. 1, p. 5081, Dec. 2022, doi: 10.1038/s41598-022-08740-w.

[63] S. Kalsi, S. Sellars, C. Turner, J. Sutton, and H. Morgan, "A Programmable Digital Microfluidic Assay for the Simultaneous Detection of Multiple Anti-Microbial Resistance Genes," *Micromachines*, vol. 8, no. 4, p. 111, Apr. 2017, doi: 10.3390/mi8040111.

[64] S. Preetam, Bigdeli, Yaas, and R. B. Fair, "ENHANCED BIOMOLECULAR BINDING TO BEADS ON A DIGITAL MICROFLUIDIC DEVICE," *25th Int. Conf. Miniaturized Syst. Fo RChemistry Life Sci.*, pp. 959–960, 2021.

[65] K. A. Bernetski, C. T. Burkhart, K. L. Maki, and M. J. Schertzer, "Characterization of electrowetting, contact angle hysteresis, and adhesion on digital microfluidic devices with inkjet-printed electrodes," *Microfluid. Nanofluidics*, vol. 22, no. 9, p. 96, Sep. 2018, doi: 10.1007/s10404-018-2119-4.

[66] W. C. Nelson and C.-J. 'CJ' Kim, "Droplet Actuation by Electrowetting-on-Dielectric (EWOD): A Review," *J. Adhes. Sci. Technol.*, vol. 26, no. 12–17, pp. 1747–1771, Sep. 2012, doi: 10.1163/156856111X599562.

[67] R. B. Fair, "Digital microfluidics: is a true lab-on-a-chip possible?," *Microfluid. Nanofluidics*, vol. 3, no. 3, pp. 245–281, Apr. 2007, doi: 10.1007/s10404-007-0161-8.

[68] P. G. Murphy, "Selection of a suitable assay," *Clin. Biochem. Rev.*, vol. 29 Suppl 1, pp. S17-22, Aug. 2008.

[69] J. Helbling, K. Kinouchi, P. Trifilieff, P. Sassone-Corsi, and M. Moisan, "Combined Gene Expression and Chromatin Immunoprecipitation From a Single Mouse Hippocampus," *Curr. Protoc.*, vol. 1, no. 2, Feb. 2021, doi: 10.1002/cpz1.33.

[70] I. A. Darwish, "Immunoassay Methods and their Applications in Pharmaceutical Analysis: Basic Methodology and Recent Advances," *Int. J. Biomed. Sci. IJBS*, vol. 2, no. 3, pp. 217–235, Sep. 2006.

[71] N. Parker *et al.*, *Microbiology*. 2016. Accessed: Mar. 31, 2022. [Online]. Available: https://openstax.org/details/books/microbiology

[72] L. M. M. Officer SEPMAG Chief Scientific, "Protein A vs Protein G." https://www.sepmag.eu/blog/protein-a-vs-protein-g (accessed Mar. 31, 2022).

[73] M. Alhajj and A. Farhana, "Enzyme Linked Immunosorbent Assay," in *StatPearls*, Treasure Island (FL): StatPearls Publishing, 2022. Accessed: Mar. 31, 2022. [Online]. Available: http://www.ncbi.nlm.nih.gov/books/NBK555922/

[74] "Basic principles and types of ELISA | Abcam." https://www.abcam.com/kits/elisa-principle (accessed Mar. 31, 2022).

[75] "Sandwich ELISA with Direct Detection - Creative Biolabs." https://www.antibody-creativebiolabs.com/sandwich-elisa-with-direct-detection.htm (accessed Mar. 31, 2022).

[76] S. Vira, E. Mekhedov, G. Humphrey, and P. S. Blank, "Fluorescent-labeled antibodies: Balancing functionality and degree of labeling," *Anal. Biochem.*, vol. 402, no. 2, pp. 146–150, Jul. 2010, doi: 10.1016/j.ab.2010.03.036.

[77] "Fluorescence SpectraViewer." https://www.thermofisher.com/order/fluorescence-spectraviewer (accessed Mar. 31, 2022).

[78] admin, "ET395/25x," Sep. 05, 2021. https://www.chroma.com/products/parts/et395-25x (accessed Mar. 31, 2022).

[79] "420ALP | Omega - Custom Optical Filters." https://www.omegafilters.com/product/3409 (accessed Mar. 31, 2022).

[80] Yaas Bigdeli *et al.*, "Fluorescent detection of nucleosomes using functionalized magnetic beads on a digital microfluidic device," Mar. 2021, vol. 11637. doi: 10.1117/12.2578339.

[81] "Chromatin IP Frequently Asked Questions," *Cell Signaling Technology*. https://www.cellsignal.com/learn-and-support/frequently-asked-questions/chip-faqs (accessed Mar. 31, 2022).

[82] "Ready-to-ChIP Chromatin for Chromatin Immunoprecipitation (Chromatin IP)." https://www.activemotif.com/catalog/20/ready-to-chip-chromatin (accessed Mar. 31, 2022).

[83] Y. Wang *et al.*, "Screening of Peptide Selectively Recognizing Prostate Specific Antigen and its Application in Detecting Total Prostate-Specific Antigen," Social Science Research Network, Rochester, NY, SSRN Scholarly Paper ID 4044447, Mar. 2022. doi: 10.2139/ssrn.4044447.

[84] Yaas Bigdeli *et al.*, "Enhanced fluorescent detection of nucleosomes using functionalized magnetic beads on a digital microfluidic device," Mar. 2022, vol. 11955. doi: 10.1117/12.2620556.

[85] M.-N. Tsaloglou, A. Jacobs, and H. Morgan, "A fluorogenic heterogeneous immunoassay for cardiac muscle troponin cTnI on a digital microfluidic device," *Anal. Bioanal. Chem.*, vol. 406, no. 24, pp. 5967–5976, Sep. 2014, doi: 10.1007/s00216-014-7997-z.

[86] P. Paik, V. K. Pamula, M. G. Pollack, and R. B. Fair, "Electrowetting-based droplet mixers for microfluidic systemsElectronic supplementary information (ESI) available: six mpeg videos showing some mixing schemes used in Fig. 7. See http://www.rsc.org/suppdata/lc/b2/b210825a/," *Lab. Chip*, vol. 3, no. 1, p. 28, 2003, doi: 10.1039/b210825a.

[87] P. Cejas and H. W. Long, “Principles and methods of integrative chromatin analysis in primary tissues and tumors,” *Biochim. Biophys. Acta BBA - Rev. Cancer*, vol. 1873, no. 1, p. 188333, Jan. 2020, doi: 10.1016/j.bbcan.2019.188333.

[88] A. A. Bartlett and R. G. Hunter, “Chromatin Immunoprecipitation Techniques in Neuropsychiatric Research,” in *Psychiatric Disorders: Methods and Protocols*, F. H. Kobeissy, Ed. New York, NY: Springer New York, 2019, pp. 633–645. doi: 10.1007/978-1-4939-9554-7_36.

[89] J. Lamanna *et al.*, “Digital microfluidic isolation of single cells for -Omics,” *Nat. Commun.*, vol. 11, no. 1, p. 5632, Dec. 2020, doi: 10.1038/s41467-020-19394-5.

[90] D. Millington, S. Norton, R. Singh, R. Sista, V. Srinivasan, and V. Pamula, “Digital microfluidics comes of age: high-throughput screening to bedside diagnostic testing for genetic disorders in newborns,” *Expert Rev. Mol. Diagn.*, vol. 18, no. 8, pp. 701–712, Aug. 2018, doi: 10.1080/14737159.2018.1495076.

[91] J. E. Schmitz and Y.-W. Tang, “The GenMark ePlex ® : another weapon in the syndromic arsenal for infection diagnosis,” *Future Microbiol.*, vol. 13, no. 16, pp. 1697–1708, Dec. 2018, doi: 10.2217/fmb-2018-0258.

Biography

Yaas Bigdeli received her Bachelor and Master of Science in Biomedical Engineering from Columbia University in 2014 and 2015, respectively. She plans to continue living and working in Durham, NC. Yaas Bigdeli has published several titles during her time at Duke University, including the "Fluorescent detection of nucleosomes using functionalized magnetic beads on a digital microfluidic device" and the "Enhanced fluorescent detection of nucleosomes using functionalized magnetic beads on a digital microfluidic device" in the SPIE Microfluidics, BioMEMS, and Medical Microsystems conference proceedings. She has contributed, and is a named author, in "Enhanced biomolecular binding to beads on a digital microfluidic device" by Shruti Preetam published in the 25th International Conference on Miniaturized Systems for Chemistry and Life Science proceedings. Finally, she is a contributing author in "Adaptive droplet routing in digital microfluidic biochips using deep reinforcement learning by Tung-Che Liang, published in the proceedings of the 37th International Conference on Machine Learning.